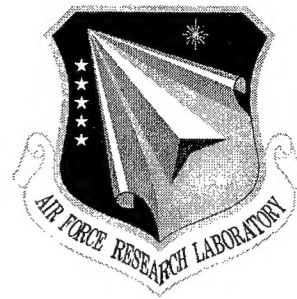


AFRL-IF-RS-TR-2001-199
Final Technical Report
October 2001



NETFLOW: COMPUTER-AIDED DESIGN (CAD) FOR CHEMICAL TRANSPORT IN MICROFABRICATED FLUID INTERCONNECTS

Coventor, Inc.

Sponsored by
Defense Advanced Research Projects Agency
DARPA Order No. E117

APPROVED FOR PUBLIC RELEASE; DISTRIBUTION UNLIMITED.

The views and conclusions contained in this document are those of the authors and should not be interpreted as necessarily representing the official policies, either expressed or implied, of the Defense Advanced Research Projects Agency or the U.S. Government.

20020117 030

AIR FORCE RESEARCH LABORATORY
INFORMATION DIRECTORATE
ROME RESEARCH SITE
ROME, NEW YORK

This report has been reviewed by the Air Force Research Laboratory, Information Directorate, Public Affairs Office (IFOIPA) and is releasable to the National Technical Information Service (NTIS). At NTIS it will be releasable to the general public, including foreign nations.

AFRL-IF-RS-TR-2001-199 has been reviewed and is approved for publication.

APPROVED:



PETER J. ROCCI
Project Engineer

FOR THE DIRECTOR:



MICHAEL L. TALBERT, Technical Advisor
Information Technology Division
Information Directorate

If your address has changed or if you wish to be removed from the Air Force Research Laboratory Rome Research Site mailing list, or if the addressee is no longer employed by your organization, please notify AFRL/IFTD, 525 Brooks Road, Rome, NY 13441-4505. This will assist us in maintaining a current mailing list.

Do not return copies of this report unless contractual obligations or notices on a specific document require that it be returned.

NETFLOW: COMPUTER-AIDED DESIGN (CAD) FOR CHEMICAL
TRANSPORT IN MICROFABRICATED FLUID INTERCONNECTS

John Gilbert and Manish Deshpande

Contractor: Coventor, Inc.

Contract Number: F30602-96-2-0306

Effective Date of Contract: 1 August 1996

Contract Expiration Date: 31 December 1999

Short Title of Work: NetFlow: Computer-Aided Design (CAD)
For Chemical Transport in Microfabricated
Fluid Interconnects

Period of Work Covered: Aug 96 - Dec 99

Principal Investigator: John Gilbert

Phone: (617) 225-0095

AFRL Project Engineer: Peter J. Rocci

Phone: (315) 330-4654

APPROVED FOR PUBLIC RELEASE; DISTRIBUTION
UNLIMITED.

This research was supported by the Defense Advanced Research
Projects Agency of the Department of Defense and was monitored
by Peter J. Rocci, AFRL/IFTD, 525 Brooks Road, Rome, NY.

REPORT DOCUMENTATION PAGE			Form Approved OMB No. 0704-0188	
Public reporting burden for this collection of information is estimated to average 1 hour per response, including the time for reviewing instructions, searching existing data sources, gathering and maintaining the data needed, and completing and reviewing the collection of information. Send comments regarding this burden estimate or any other aspect of this collection of information, including suggestions for reducing this burden, to Washington Headquarters Services, Directorate for Information Operations and Reports, 1215 Jefferson Davis Highway, Suite 1204, Arlington, VA 22202-4302, and to the Office of Management and Budget, Paperwork Reduction Project (0704-0188), Washington, DC 20503.				
1. AGENCY USE ONLY (Leave blank)		2. REPORT DATE OCTOBER 2001		3. REPORT TYPE AND DATES COVERED Final Aug 96 - Dec 99
4. TITLE AND SUBTITLE NETFLOW: COMPUTER-AIDED DESIGN (CAD) FOR CHEMICAL TRANSPORT IN MICROFABRICATED FLUID INTERCONNECTS			5. FUNDING NUMBERS C - F30602-96-2-0306 PE - 63739E PR - E117 TA - 00 WU - 05	
6. AUTHOR(S) John Gilbert and Manish Deshpande				
7. PERFORMING ORGANIZATION NAME(S) AND ADDRESS(ES) Coventor, Inc. 625 Mt Auburn Street Cambridge MA 02138			8. PERFORMING ORGANIZATION REPORT NUMBER N/A	
9. SPONSORING/MONITORING AGENCY NAME(S) AND ADDRESS(ES) Defense Advanced Research Projects Agency Air Force Research Laboratory/IFTD 3701 North Fairfax Drive 525 Brooks Road Arlington VA 22203-1714 Rome New York 13441-4505			10. SPONSORING/MONITORING AGENCY REPORT NUMBER AFRL-IF-RS-TR-2001-199	
11. SUPPLEMENTARY NOTES Air Force Research Laboratory Project Engineer: Peter J. Rocci/IFTD/(315) 330-4654				
12a. DISTRIBUTION AVAILABILITY STATEMENT APPROVED FOR PUBLIC RELEASE; DISTRIBUTION UNLIMITED.			12b. DISTRIBUTION CODE	
13. ABSTRACT (Maximum 200 words) This effort was aimed at developing Computer-Aided Design (CAD) tools for the analysis of microfluidic networks. The main objective was to develop software tools for the analysis of the diverse transport phenomena that are present in these systems - these include pressure driven, electrokinetic and diffusive transport. All original milestones were met and the NetFlow software has been released commercially. All software tools developed under this effort were experimentally validated.				
14. SUBJECT TERMS Fluidics, Computer-Aided Design, CAD, Microsystems, Transport			15. NUMBER OF PAGES 98	
			16. PRICE CODE	
17. SECURITY CLASSIFICATION OF REPORT UNCLASSIFIED	18. SECURITY CLASSIFICATION OF THIS PAGE UNCLASSIFIED	19. SECURITY CLASSIFICATION OF ABSTRACT UNCLASSIFIED	20. LIMITATION OF ABSTRACT UL	

Table of Contents

Research Overview.....	1
Program Summary.....	1
Program Milestones.....	2
NetFlow Introduction.....	3
NetFlow Theory.....	4
Appendix 1: NetFlow Users Guide.....	8
Appendix 2: Research Publications.....	51

1. Research Overview

This report serves as the final summary of our research under the Netflow program as part of the Composite CAD Program. In this report we will discuss the proposed objectives of the Netflow program and the accomplishments over the course of the program.

2. Program Summary

The NetFlow program is aimed at developing Computer-Aided Design (CAD) tools for the analysis of microchemical fluidic networks. The specific aim of the program is to develop software tools for the analysis of the diverse transport phenomena that are present in these systems – these include pressure driven, electrokinetic and diffusive transport. Experimental validation for the software tools developed is an inherent part of this program.

The milestones and deliverables for the program are outlined in the Gantt Chart in Table 1. Variances from the originally proposed milestones are also indicated in the chart.

The overall program summary is as follows:

- All milestones originally set forth in the program have been met. Some of the tasks were completed well ahead of schedule, whereas some others were delayed for various reasons, but we were able to accommodate the delays by faster progress in other areas. Details of each task and results are attached in the appendix.
- Two additional tasks were added in the third year, beyond the scope of the original program – the first is tools for the analysis of non-dilute sample transport, and the second tools for the analysis of pneumatic plug driven flows which is an additional transport mechanism in microchemical networks. These tasks were also completed within the time frame specified.
- The NetFlow software has been released commercially. Three versions of the software have been released in the past two years – each version is an enhancement of the previous one. Tools are available for the analysis of containment (NetFlow-C), transport (NetFlow-T) and for the design of microchemical networks (NetFlow-G). The software is available on Sun, HP, SGI and Windows NT Platforms. The User's Guide and Reference Manuals give much more details about the software and its use. These are attached in the appendix.
- The software allows the analysis of mixed transport mechanisms, including pressure-driven, electrokinetic, pneumatic and diffusive transport. More complex transport mechanisms including the non-dilute sample transport is also incorporated in the software.
- The software tools are in continued development with additional releases planned for the next several years. Current users include both industrial and academic groups.

- NetFlow-G is currently available commercially and allows generator driven creation of shapes for device layout.
- A caged fluorescence experimental setup was developed at PE Applied Biosystems and data was gathered for validating the developed tools. Stanford also collected data at Sandia using the caged fluorescence setup there. Stanford has undertaken the development of their own set up in the past year and the first results are now flowing from their setup.
- NetFlow has found application in helping the design of current and next-generation devices and device components in PE-Applied Biosystems and Stanford, as well as in other research groups.
- Data analysis tools were developed in the program to enable the validation of simulation and experimental results. These tools are available as part of the software.
- Several research publications and presentations have emerged over the course of this program. These include papers at Hilton Head '98, Transducers 99 and the μ conferences, among others. A complete list, including copies of the papers is attached in the appendix.

3. *Program milestones*

Table of Original Deliverables with Current Status and Projections

Original Proposal	●
Completion Date	◆

Contract Quarter	1	2	3	4	5	6	7	8	9	10	11	12
Year 1												
NetFlow-C v 1.0				●	◆							
Test Data for NetFlow-C				●			◆					
Use NetFlow-C in Prototyping				●					◆			
Year 2												
NetFlow-G v1.0 (drop in based)								●	◆			
NetFlow-T v1.0 (transport with pressure flow)								●				
NetFlow-C v2.0 (more validated)								●				
Test Data for Transport Problem								●				
Use NetFlow-G and NetFlow-C in Prototyping.								●	◆			
Year 3												
NetFlow-T, v2.0 (transport in electrokinetics)												●
NetFlow-G, v2.0 (catalog/library support)												●◆
NetFlow-C, v3.0 (containment in electrokinetics)												●
Use NetFlow-G, -C and -T in Prototyping												●◆
Test Data for Transport Problem (electrokinetics)												●

NetFlow

Introduction

The NetFlow module aids the user in the simulation and design of interconnects for chemical transport of species in microchannels. The physical phenomena associated with the transport include:

- Pressure flow
- Diffusion
- Electrophoresis
- Electroosmosis

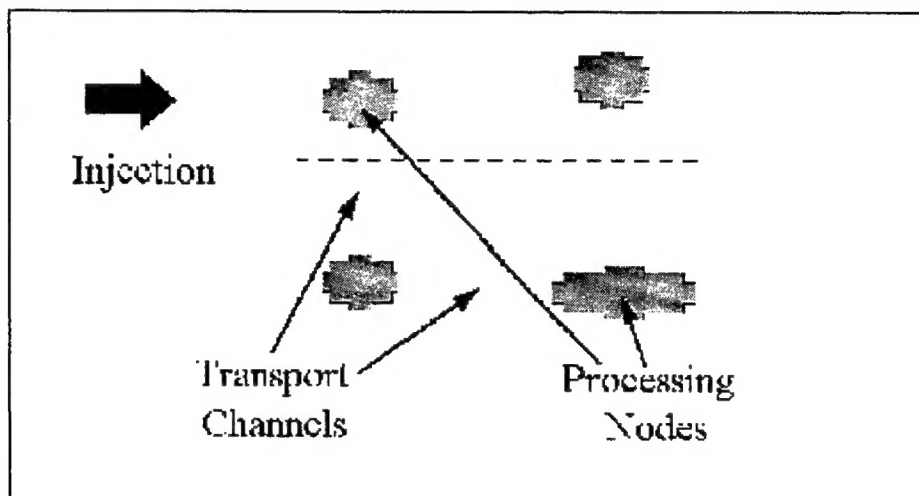
NetFlow can be applied to model these phenomena, either individually or in combination. The equations used to model the flow are the Navier-Stokes equations for the flow, coupled with the mass equation for the species motion and the Poisson equation for the electric field. Electrophoretic effects are modeled through the application of an electrophoretic mobility that represents the force on the charged species due to the electric field. Electroosmotic effects can be modeled by the direct solution of the Poisson-Boltzmann equation for the electrical double layer, or alternatively through the specification of an electroosmotic mobility coefficient for the walls.

The NetFlow module is very useful for designing the “wires” for chemical transport, for designing the containment of a sample in processing nodes, and for making detailed quantitative measurements of microchemical flows to calibrate and validate simulations.

NetFlow Theory

Introduction to NetFlow

The NetFlow module is built on the base MemCFD module in MEMCAD and is specific to the analysis of microfluidic transport channels in chemical and biological analysis systems. On-chip analysis systems consist of active and passive components as shown in the figure. Examples of the former are reaction chambers, switching joints etc., whereas the latter include transport and separation channels.



For a particular system of interest the design analysis generally involves the representation of the device as a system comprising several individual components. The physics of each component is then extracted from detailed computation for that component. Each individual component can thus be represented in the system, yielding a reduced order model for the device. This approach is analogous to the circuit simulation methodology adopted in both mechanical and electrical domains.

Fluidic systems, however, differ in one significant aspect from mechanical and electrical systems. In both mechanical and electrical systems the interconnections between the components can be considered “ideal” —that is, the output of one component can be directly applied as the input to the next. In the fluidic domain, this is not generally true. The interconnects here are channels that transport the chemicals from one processing site to another, often under the effect of diffusion and other related phenomena. As a result, interconnects often have a profound effect on the behavior of the chemical (the “signal” in the system). Analyzing these effects requires modeling of the channels.

In summary, the design problem is as follows: For a given application, the various physical properties that affect the behavior of the device must be extracted in an appropriate parameter space. The properties can then be used in that parameter space to conduct further analyses. NetFlow is the first step in enabling this process.

Governing Equations

The basic equations describing the fluid motion are the Navier-Stokes equations with appropriate electromigratory flux terms to represent the effect of the applied electric field on the carrier and/or the charged species. The effect of the applied field can be divided into two fundamental components, electrophoresis and electroosmosis.

Electrophoresis

The basis for electrophoresis is the differential migration of the charged species ions relative to the carrier molecules under the application of the external field. The differential migration is primarily an effect of the difference in the net charge between the solvent and solute ions, although frictional effects may also have some relevance. The migration velocity of the charged species can be expressed in terms of the applied field strength as

$$V_{ep} = \mu_{ep} E \quad [1]$$

where μ_{ep} is the electrophoretic mobility of the ion in the carrier species. It is important to note that in most cases the carrier does not move under electrophoresis.

Electroosmosis

Electroosmosis, in contrast, is a macroscopic phenomenon involving the pumping of a fluid through a channel under the application of the field. In most cases, walls in microchannels are characterized by the presence of surface charges. The charge may either be due to the property of the wall or by adsorption of the charged species from the buffer. In the presence of an electrolyte, the surface charge density induces the formation of a double layer in the fluid by attracting oppositely charged ions from the electrolyte to the immediate vicinity of the wall. The application of the electric field exerts a force on the fluid that is initially felt only within the double layer. As a result, the fluid in the near vicinity of the wall starts to move. Due to the viscous forces, the fluid in the center of the channel is also accelerated until the net velocity gradient in the radial direction is zero and the whole fluid in the channel moves at a constant velocity.

The determination of the electroosmotic flow field requires the solution of the Navier-Stokes equation. Incorporating the electroosmotic effect as a force the equations become

$$\begin{aligned} \nabla \cdot V_{eo} &= 0 \quad (\text{Continuity}) \\ \frac{D(\rho V_{eo})}{Dt} &= -\nabla P + \nabla \cdot \mu \nabla V_{eo} + \rho_e E \end{aligned} \quad [2]$$

Where V_{eo} is the induced electroosmotic velocity, D/Dt is the material derivative of the momentum, μ is the fluid viscosity and P is the pressure. The last term in the momentum equation represents the electroosmotic force on the fluid. Here ρ_e is the charge density and E is the electric field intensity. The electric field can be determined by the solution of the potential equation

$$E = -\nabla \Phi \quad \nabla^2 \Phi = -(\rho_e / \epsilon) \quad [3]$$

The electric potential Φ can be further decomposed into two components, ϕ , the external applied potential and ζ , the zeta potential at the walls.

$$\Phi = \phi + \zeta \quad [4]$$

Under the assumption that the zeta potential effects are confined to a very small region near the wall, the charge distribution can be assumed to be governed by the zeta potential alone, independent of the external field. This allows the decomposition of Eq. [3] into separate equations for the applied field and the zeta potential

$$\nabla^2 \phi = 0 \quad (\text{Applied potential}) \quad [5a]$$

$$\nabla^2 \zeta = -(\rho_e / \epsilon) \quad (\text{Zeta potential}) \quad [5b]$$

The equation for the zeta potential can be simplified by the Debye-Hückel treatment for the charge density. This is based on the concept of a diffuse double layer, proposed initially by Gouy and Chapman, which assumes that the double layer extends for some finite distance into the fluid. Through the Debye-Hückel approximation the charge density on the walls can be determined through the Boltzmann equation and results in the Poisson-Boltzmann equation for the zeta potential

$$\nabla^2 \zeta = \frac{2n_0 z e}{\epsilon \epsilon_0} \sinh\left(\frac{z e}{k T} \zeta\right) \quad [6]$$

where n_0 is the ionic concentration, Z is the valence of the charged buffer, e is the electron charge, k is the Boltzmann constant and T is the temperature. ϵ_0 is the permittivity of vacuum.

Under further simplification under the assumption that $z e \ll k T$ equation [6] reduces to the form

$$\nabla^2 \zeta = K^2 \zeta \quad [7]$$

where

$$K = (2n_0 z^2 e^2 / \epsilon \epsilon_0 k T)^{\frac{1}{2}}$$

is known as the Debye-Hückel parameter and $1/K$ is termed as the characteristic thickness of the double layer.

The coupled solution of the Eqs. [2], [5a] and [7] yields the flow field under the conditions specified.

The motion of a charged species in the electric field can be determined by coupling the species mass equation [8] with the above equations.

$$\frac{\partial c_i}{\partial t} + (V_{eo} + V_{ep})\nabla c_i = D\nabla^2 c_i \quad [8]$$

The convective transport of the species is through the combined effect of the electroosmotic motion of the carrier fluid and the electrophoretic transport of the species under the effect of the applied electric field.

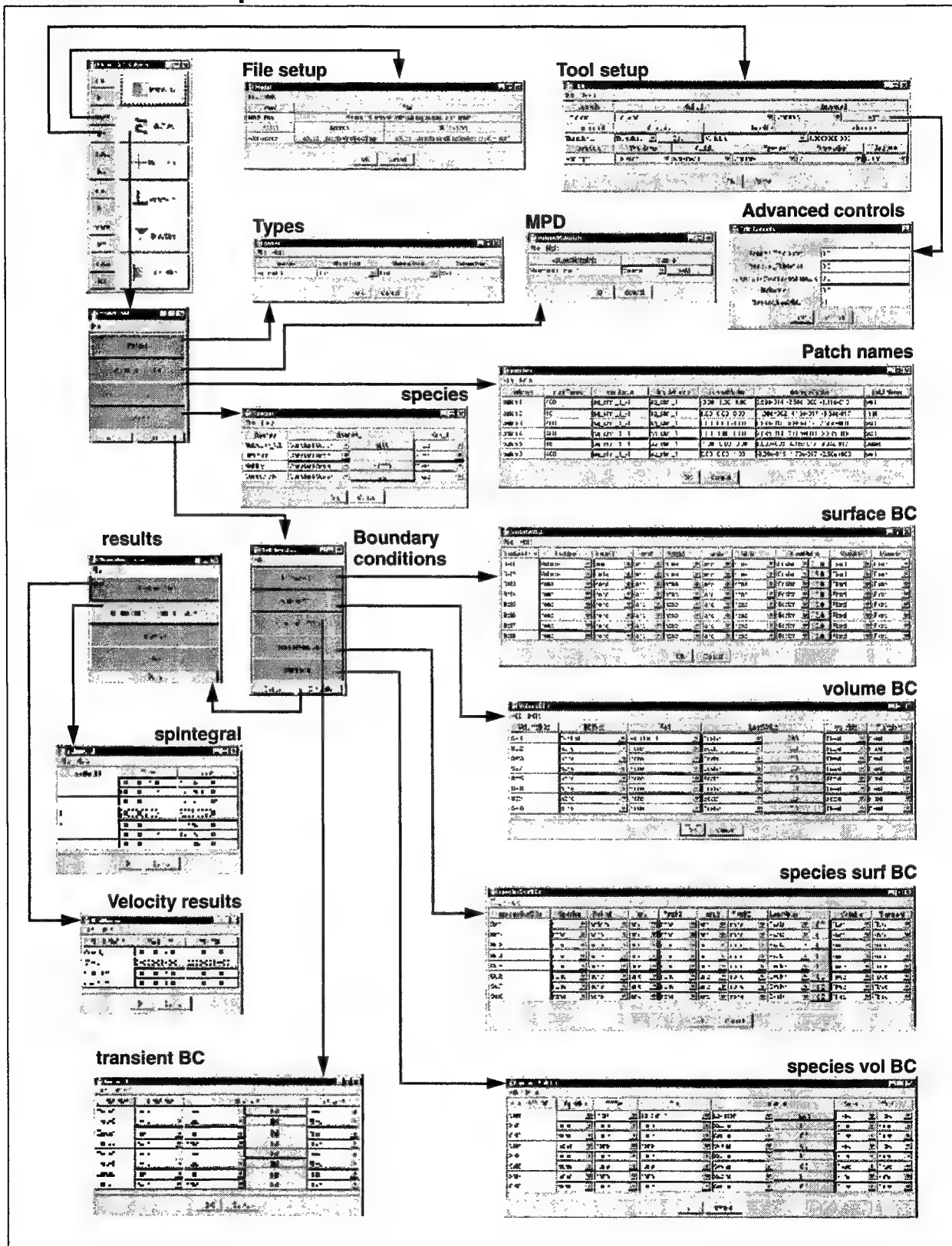
The equations presented in this section are derived under the following assumptions:

- **Dilute Carrier:** The carrier fluid is assumed to be electroneutral everywhere, except within the double layer. The charge distribution is therefore confined to a small region within the double layer.
- **Dilute Solution:** The carrier fluid is assumed to be the predominant species in the mixture. That is, the mass fraction of the charged species is assumed negligible in comparison to the fraction of carrier. This is generally valid in most electrokinetic problems where the species under observation are generally in the millimolar range (corresponding to mass fractions of 10^{-3} and lower). This implication of the dilute assumption is that the solute species does not affect the material properties of the mixture. This allows the species transport equation to be decoupled from the momentum equation.
- **Individual Species do not affect each other:** This assumption is used in describing the flux terms in the above equations, in that the flux of one species does not depend on the fluxes of the other species. This is only true in dilute solutions.
- **No Chemical Reactions:** The charged species are assumed to be fully ionized in the mixture.

As mentioned above, the dilute solution allows the density of the mixture to be assumed constant and equal to the density of the carrier. This reduces the problem to the incompressible form. The decoupling of the species equation from the momentum equation also implies that the species conservation condition is not relevant and can be discarded.

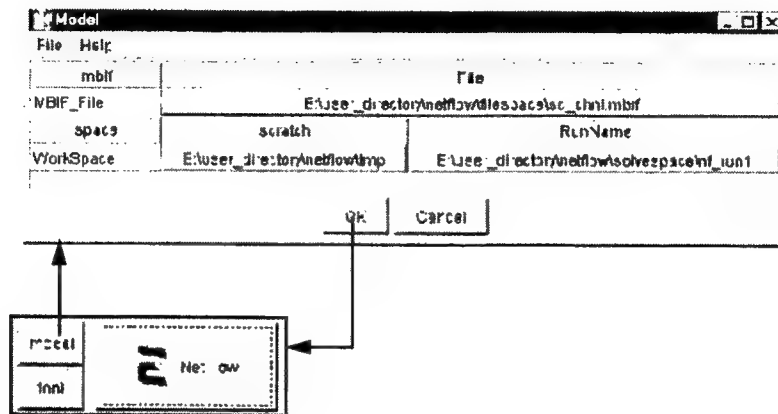
Appendix 1: NetFlow Users Guide

NetFlow window map



NetFlow - Model window

The Model window displays the current mbif files and scratch workspace; the window is the same as viewed with other MEMCAD 4 functions. It is not updated automatically from other windows.



❑ MBIF File

The base model file used for the solver calculations. By convention, the solver always uses the base model mbif, even though mbif files created by NetFlow and other solvers contain all the information needed to compute a solution. The path is not set automatically from other screens.

❑ Scratch workspace

The path used for storing temporary files created during the solution. Any temporary files may be deleted when the solver has completed its task.

❑ Run Name

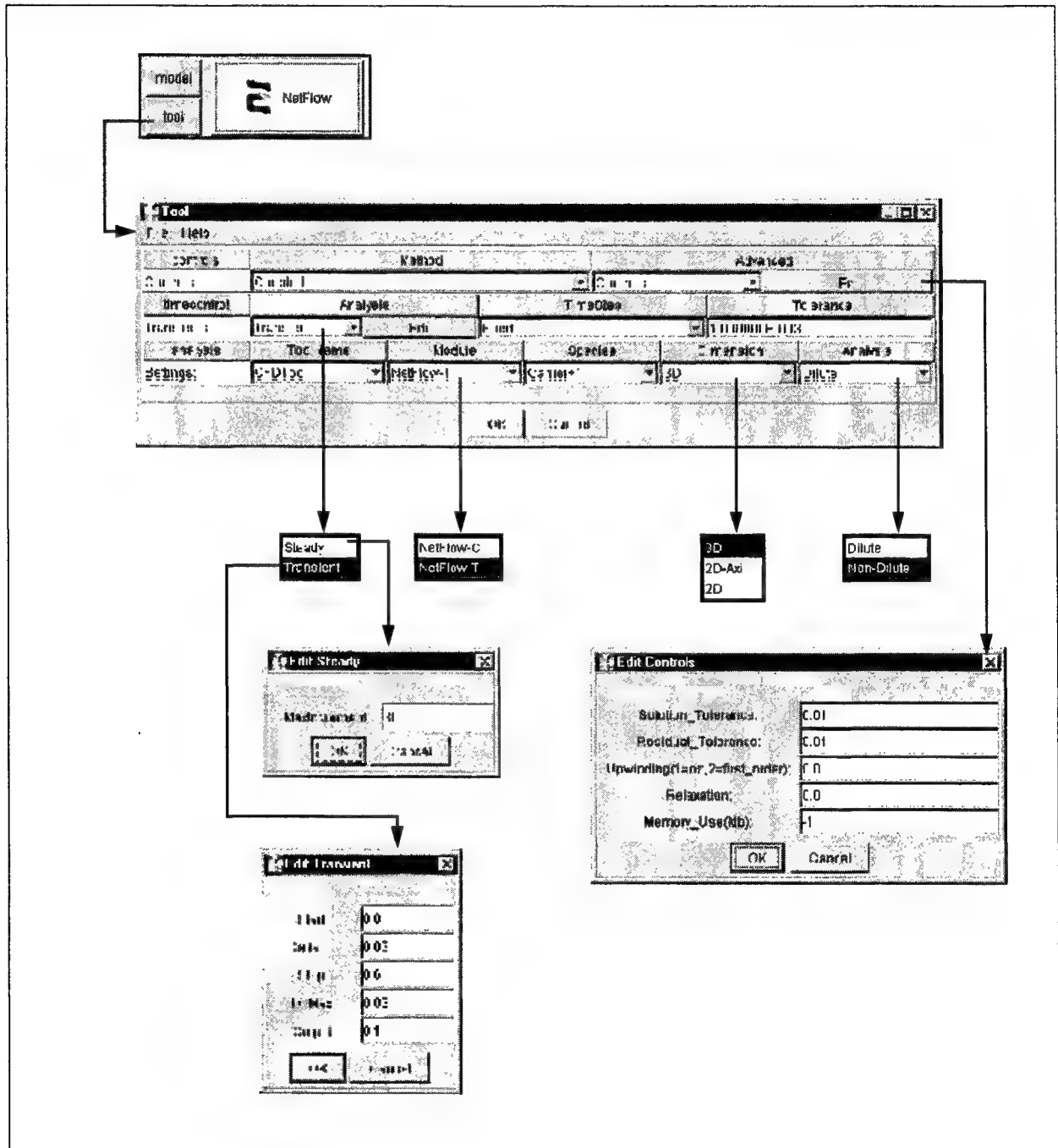
The path used to store the single result mbif file created by NetFlow. The directory name should provide some way of identifying the type of run created.

❑ OK

Close the window and return control to the MEMCAD 4 main menu.

NetFlow - Tool Setup window

The Tool window allows user to set the parameters for running the fluidic solver. Most of the information in the tool window provides the “how” and “what” instructions to NetFlow.



❑ Controls/Method

The Navier-Stokes equations used in the FlumeCAD solvers are non-linear and require an iterative approach to solving problems. The solvers adjust a variety of variables as part of the solution method, allowing them to solve both straightforward problems with single solutions, as well as more complex problems with multiple local minimum or maximum values.

- **Coupled:** The coupled solver is the default choice for FlumeCAD. This iterative solver is recommended for most problems, and can handle steady state and transient flows.
- **Segregated:** The segregated solver solves each degree of freedom in the problem separately and consecutively. Thus, the three momentum equations for flow in the X, Y, and Z directions and the pressure and energy equations are each solved separately. This approach uses less system memory at the expense of a longer solution time. It is recommended for problems containing more than 2500 elements.

❑ Controls/Advanced Controls

Several different tolerances may be set depending on the non-linearity of the flow problem.

- **Solution Tolerance:** Convergence value setting. For large problems, the default value of 0.01 ensures a solution in a reasonable time. For smaller problems this value may be decreased even further.
- **Residual Tolerance:** Similar to the Solution Tolerance; controls the Flux of a particular quantity.
- **Upwinding:** A numerical solution stabilization technique that prevents solver instability. Occasionally, the solver will be unable to complete its calculations due to mesh anomalies. If this occurs, change this value to 1 (second-order stabilization) or 2 (first-order stabilization).
- **Relaxation:** Specifies relaxation factors for the degrees of freedom in the system. The default window setting of 0.0 maintains a 0.05 factor for all degrees of freedom. The number should be changed only to modify the degree of coupling between the system equations. Large factors of 0.2-0.4 can be used for strong coupling, while lower numbers are best for weak coupling. Optimal values are problem-dependent, and can be derived only by trial and error.
- **Memory Use:** The default setting is -1, which allows MEMCAD 4 to allocate memory as required. For large 3D problems, or to avoid unnecessary swapping, the user should set this value if the job is much bigger than the RAM memory. A suggested range is 2/3 to 4/5 of actual RAM.

❑ Transients/Analysis

- **Steady:** Performs a steady state, or time-independent, analysis. The solver will try and converge to an answer within the number of steps given in the Edit Steady window *MaxIncrement* setting.
- **Transient:** This setting sets up the transient simulation. Five time values are set in the Edit Transient window:

Start: Time to start simulation. This value is usually 0.

Delta_T: Time interval for simulation. This is the initial timestep when TimeStep is set to *Variable*, and is the actual timestep when TimeStep is set to *Fixed*. In either case, it should be set to a very small number (roughly 1e-6).

Stop: Time to stop simulation.

DTMax: When TimeStep is set to *Variable*, sets the maximum range for the time step. If set to 0, it is ignored. It should be set to 0, except for complex problems, where it should be set to 1/100 of the total simulation time ($0.01 * (\text{Stop} - \text{Start})$).

Output: Specify time increments at which the mbif files are written. For example, a setting of 0.2 writes an mbif file every 0.2 seconds for the duration of the simulation.

☐ **Transients/TimeStep**

This controls the time step of the overall transient analysis.

- **Variable:** This MEMCAD 4 time stepping control default value is the optimal setting. The solver determines the time step value at any given point in the solution. With a variable setting, the solver can use small time steps at the beginning of the problem, and larger steps near the end when the solution is nearly complete.
- **Fixed:** This time step is used for special problems. An example is when the solver would increase the timestep in the variable mode with steps that are larger than the time in which the effects that are studied occur. In highly viscous flows the actual startup effects of the flow might otherwise be skipped with a variable setting. However, note that compute times may increase dramatically. As an illustration, if the Start time and Stop time in the Transient field is set to 0 and 1 second, and the Delta_T to 1e-6, then in theory it would take the solver 1e6 steps in order to calculate the answer. This setting works well with the *Coupled Method* setting.

☐ **Transients/Tolerance**

Tolerance of a physical time step in the transient analysis. Depending on the mass conservation plot results, the Tolerance value may be increased or decreased from the default setting of 0.001.

☐ **Analysis Settings/Tool name**

- **CFDTool:** The CFDTool is the default fluidics solver. It has been upgraded in MEMCAD 4.6 to work with a Y2K-compatible solver.
- **ViewResult:** Bypass the setup screens and view previous results of a solution. The path to the solution directory is set from the Model window.

☐ **Analysis Settings/Module**

- **NetFlow-C:** This module solves the containment problem. It allows only for the solution of an advection-diffusion equation. Transport is by diffusion only.
- **NetFlow-T:** This module solves the transport problem. It enables the solution of the full Navier-Stokes equations with the appropriate flux terms for the various transport.

☐ **Analysis Settings/Species**

Specifies the number of additional species present in the flow, including the carrier fluid. Choices are *Carrier*, *Carrier+1*, and *Carrier+2* (0, 1, and 2 species present, respectively).

☐ **Analysis Settings/Dimension**

- **3D:** Tells the solver to run a three dimensional solution with dimensions X,Y, and Z.
- **2D-Axi:** Allows the user to run a two dimensional axi-symmetric solution. The model has to be generated in the XY-plane and should be 1 element thick in the Z direction. The X-axis is the axis of symmetry and the Y-axis is the radial coordinate.
- **2D:** allows the user to run a two dimensional solution. The model has to be generated in the XY-plane and should be 1 element thick in the Z direction.

☐ **Analysis Settings/Analysis**

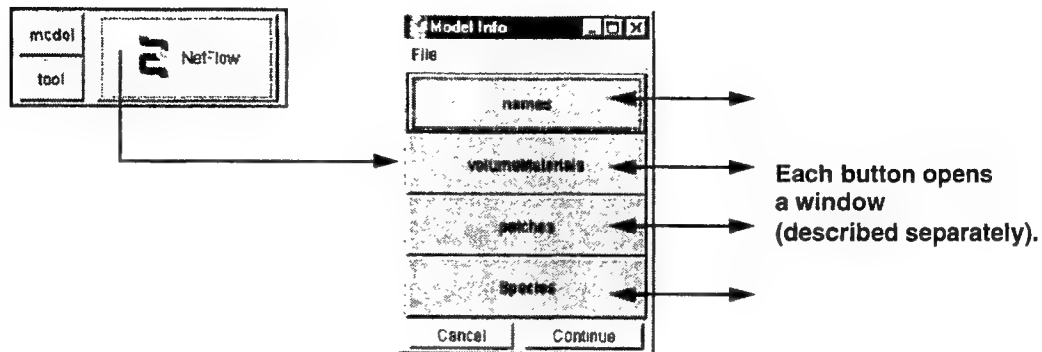
Sets the type of analysis to be performed, depending on the concentration of the fluid. *Dilute* and *Non-Dilute* are the choices.

☐ **OK**

Close Tool window; return control to MEMCAD 4.

NetFlow - Model_Info hierarchical window

This Model_Info window allows access to the names, volumeMaterials, patches, and species windows for setting up the parameters needed by the solver.



❑ names button

Open a names window (see **page F2-113**).

❑ volumeMaterials button

Open a volumeMaterials window (see **page F2-114**).

❑ patches button

Open a patches window (see **page F2-114**).

❑ species button

Opens a species window (see **page F2-115**). Note that this button does not appear if the Tool window is set for a Species=Carrier value.

❑ Continue

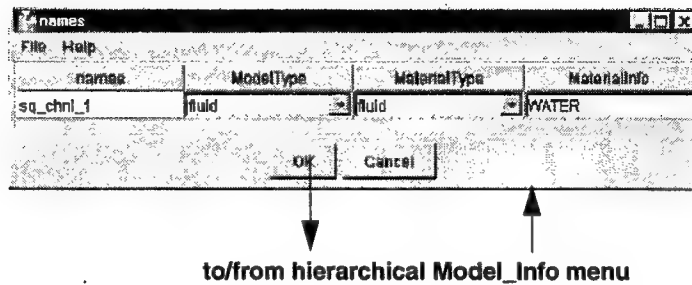
Close the window and open the boundary conditions menu window (see **page F2-118**).

❑ Cancel

Close window and return to MEMCAD 4 main menu.

NetFlow - Model_Info / names window

The names window allows user to specify the Model and Material Types. This information is placed in the mbif file when it is translated.



❑ Model Type

The names window contains a line for each FEM created during the MemBuilder step. User can specify each FEM to be either movable, fixed, or fluid.

- **Movable:** If set to movable, the NetFlow solver treats the part as a solid; this means that the thermal properties of the solid are taken into account.
- **Fluid:** Parts assigned a fluid type have flow velocities, pressures, and temperatures as degrees of freedom. Only one fluid type can be used (such as water or air, but not both). Note that FlumeCAD includes special solvers (BubbleSim and DropSim, both documented in this volume), which are dedicated to solving the gas-liquid-solid phase. Such problems involve surface tension and can be used to study filling of structures, bubble transport, and fluid ejection.
- **Fixed:** A fixed part type will be not enter in to the NetFlow solver calculations, and the thermal properties of the part will not be taken into account.

❑ Material Type

The Material Type setting is not used for the NetFlow solver. See the User Handbook (page U2-50) to learn how to use dielectric material types during Convert Model to obtain patches on the boundaries between solids and fluids.

❑ Material Info

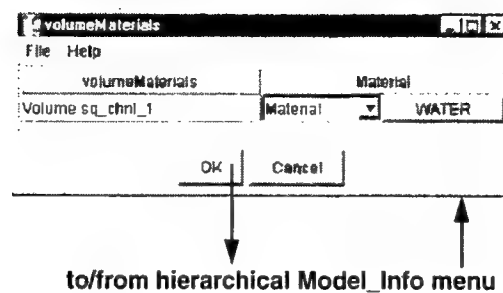
The display-only column lists the current material assignment for the FEM line. The column may display the material assigned during 3D model creation, or reassigned from the Material Property Database, depending on when the window is viewed.

❑ OK

Close window and return to hierarchical window control.

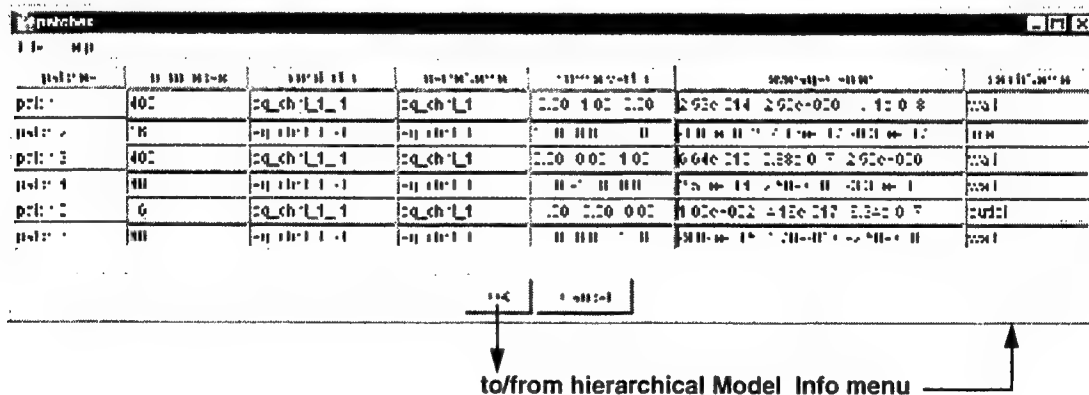
NetFlow - Model_Info / volumeMaterials window

This volumeMaterials window allows user to set the mechanical constants and parameters for the material being modeled for NetFlow. The window is the same as the DeviceCreation / Model Setup volumeMaterials window (see the Reference Manual, page R2-45).



NetFlow - Model_Info / patches window

The patches window allows user to specify names for the patches used in the model. The window is the same as the Device Creation / Model Setup patches window (see the Reference Manual, page R2-46).



NetFlow - Model_Info / species window

The Species window allows user to specify the species characteristics used for the simulation. The species present are in infinitely dilute form, therefore material properties are not needed. The Tool window must have Species set to *Carrier+1* or *Carrier+2* to access this window.

If the Tool window is set for:

Species	Window
Carrier	No species button
Carrier+1	Single column Species window
Carrier+2	Dual column Species window

The Species window displays the following parameters and their settings:

Species	Parameter	Value	Units	Model	Vary_1
Species_1	Molecular_Wt	5000		Constant-Scalar	Fixed
	Diffusion	50		Constant-Scalar	Fixed
	Mobility	16000		Constant-Scalar	Fixed
	Conductivity	0.0		Constant-Scalar	Fixed

Buttons: OK, Cancel

Callout box: Constant-Scalar, Polynomial-T, Polynomial-T,V0, Table-T

Arrow: To Edit windows

□ Species

This view-only window lists the species parameters that user can specify for simulation:

- **Molecular Weight:** scalar measured in atomic mass units.
- **Diffusion:** diffusion constant of the fluid, measured in $\mu\text{m}^2/\text{s}$.
- **Mobility:** mobility of the fluid, measured in $\mu\text{m}^2/\text{V}\cdot\text{s}$.
- **Conductivity:** conductivity of the fluid, measured in $\text{pS}/\mu\text{m}$.

□ Species_1, Species_2

Designate the type of parameter to be specified. An accompanying Edit window (see [page F2-116](#)) stores the parameter fields. Choices include:

- **Constant-Scalar:** Constant with a single value over the entire field.
- **Polynomial-T:** Polynomial function of temperature. Six constant coefficients are allowed to enable the definition of up to a fifth order polynomial.
- **Polynomial-T,V0:** Polynomial function of temperature, with the V_0 term used to define an initial start-up voltage below which electrophoretic effects are absent.
- **Table-T:** Tabular form for defining temperature-property pairs. Linear interpolation is used for intermediate values.

□ Vary_1, Vary_2

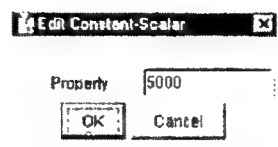
Allows specification of a variable tag for Simulation Manager runs.

NetFlow - Model_Info / species settings / Edit windows

Each LoadValue type selected from the Species window uses its own format for entering parameters. The windows are described in this section.

□ Constant-Scalar

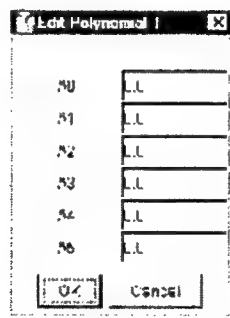
Constant with a single value over the entire field.



The 'Edit Constant-Scalar' dialog box has a title bar with a standard window icon and a close button. Inside, there is a label 'Property' followed by a text input field containing the value '5000'. At the bottom, there are two buttons: 'OK' and 'Cancel'.

□ Polynomial-T

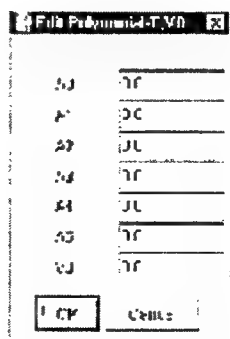
Polynomial function of temperature. Six constant coefficients are allowed to enable the definition of up to a fifth order polynomial.



The 'Edit Polynomial-T' dialog box has a title bar with a standard window icon and a close button. It contains six rows, each with a coefficient label (A0, A1, A2, A3, A4, A5) and a corresponding text input field, all of which currently contain the value '1.1'. At the bottom, there are two buttons: 'OK' and 'Cancel'.

□ Polynomial-T,V0

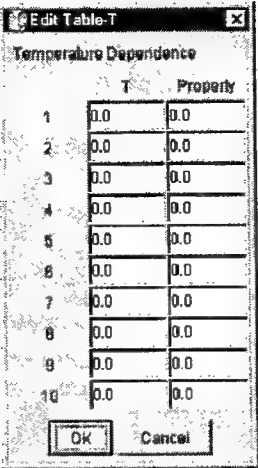
Polynomial function of temperature, with the V_0 term used to define an initial start-up voltage below which electrophoretic effects are absent.



The 'Edit Polynomial-T,V0' dialog box has a title bar with a standard window icon and a close button. It contains seven rows, each with a coefficient label (A0, A1, A2, A3, A4, A5, V0) and a corresponding text input field, all of which currently contain the value '1.1'. At the bottom, there are two buttons: 'OK' and 'Cancel'.

❑ **Table-T**

Tabular form for defining temperature-property pairs. Linear interpolation is used for intermediate values.

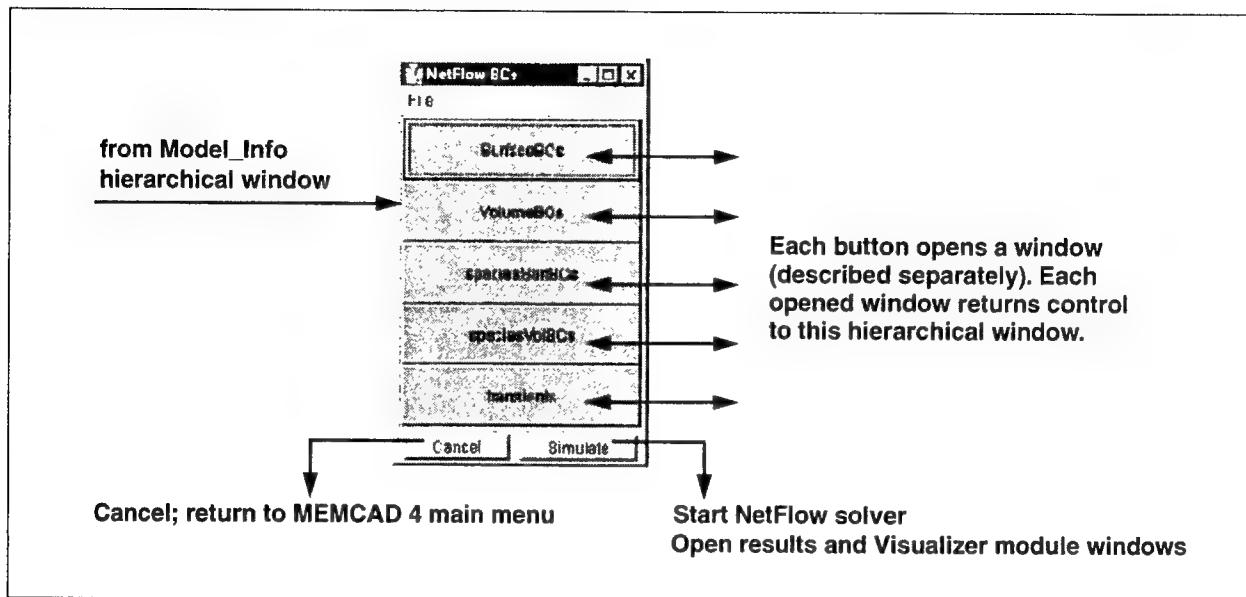


The screenshot shows a dialog box titled "Edit Table-T" with a close button (X) in the top right corner. Below the title bar is the text "Temperature Dependence". The main area contains a table with two columns: "T" and "Property". There are 10 rows, numbered 1 to 10 on the left. Each row contains the value "0.0" in both the "T" and "Property" columns. At the bottom of the dialog box are two buttons: "OK" and "Cancel".

	T	Property
1	0.0	0.0
2	0.0	0.0
3	0.0	0.0
4	0.0	0.0
5	0.0	0.0
6	0.0	0.0
7	0.0	0.0
8	0.0	0.0
9	0.0	0.0
10	0.0	0.0

NetFlow - hierarchical Boundary Conditions menu window

The NetFlow BCs hierarchical boundary conditions menu window allows user to choose windows to specify load conditions for the NetFlow fluidic solver.



□ surfaceBCs

Open window (see **page F2-119**) to set surface boundary conditions, such as velocity and pressure.

□ volumeBCs

Open window (see **page F2-125**) to set boundary conditions that affect an entire volume, such as temperature conditions.

□ transients

Open window (see **page F2-128**) to set conditions for transient calculations.

□ speciesSurfBCs

Open window (see **page F2-128**) to set conditions for species surface boundary conditions.

□ speciesVolBCs

Open window (see **page F2-130**) to set conditions for species volume boundary conditions.

□ Simulate

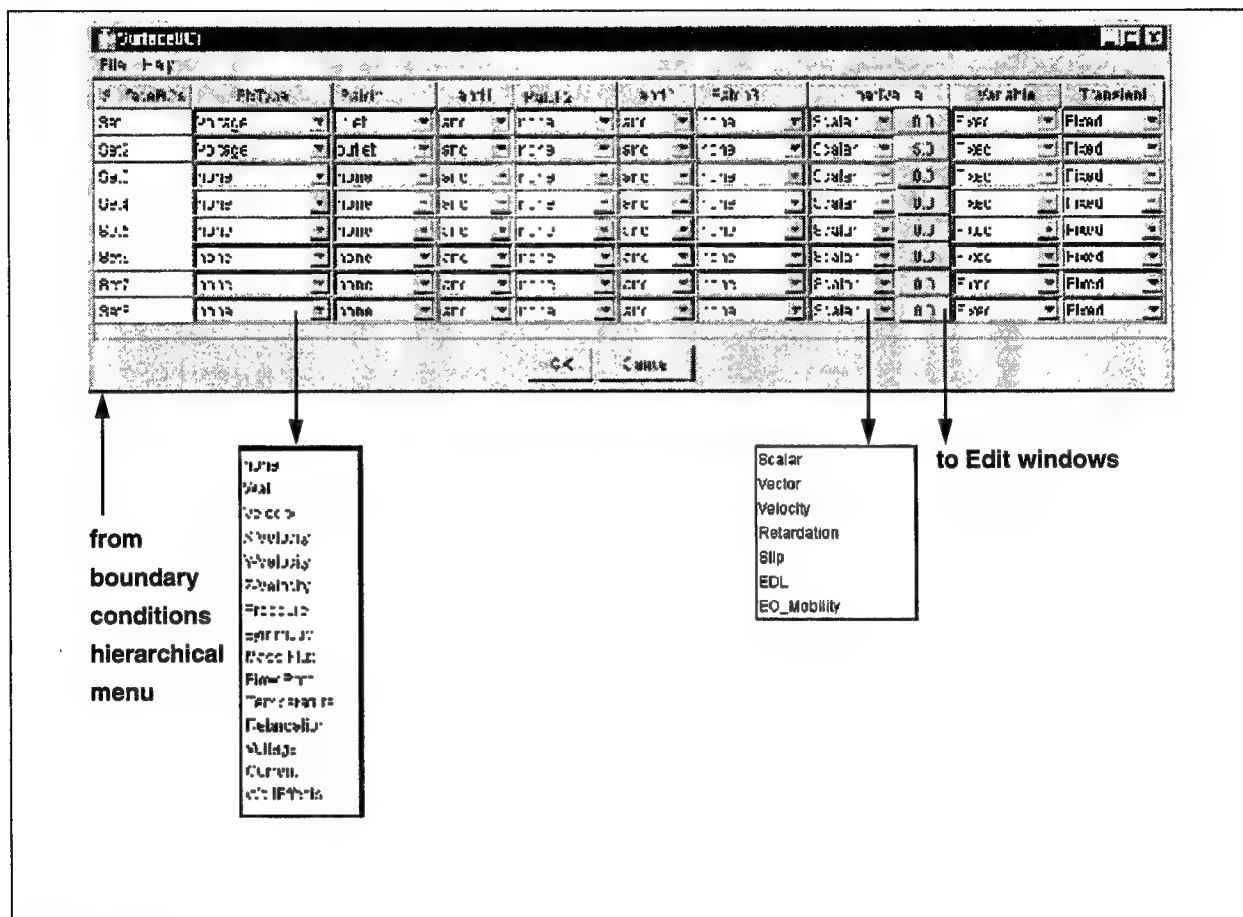
Launch NetFlow solver.

□ Cancel

Do not proceed with NetFlow solver; return to MEMCAD 4 main menu.

NetFlow - NetFlow BCs / surface boundary conditions window

The surfaceBCs window sets patch surface boundary conditions. Fix types and load conditions for these surfaces can be specified in eight Node/Face sets within this window. When setting up conditions, the LoadValue button needs to correspond to the appropriate boundary condition. Not all combinations of boundary conditions and LoadValue are possible.



□ surfaceBCs

This display-only column allows user to define up to eight boundary condition sets for the model.

□ Fix Type

Enables pull-down menu with many load type choices:

- **Wall:** This represents a “no slip” boundary condition at the selected patches. The no-slip boundary condition is an assumption that is made in Newtonian Fluids. Newtonian fluids also form a parabolic velocity profile in steady state. No LoadValue is applied.
- **Velocity:** Possible LoadValues are *Velocity* and *Vector*.
- **X-Velocity:** This option specifies a uniform velocity in the X-direction. The option is very useful when applying symmetric boundary conditions for which the velocity perpendicular to the axis of symmetry is 0. A *Scalar* LoadValue is used.

- **Y-Velocity:** This option specifies a uniform velocity in the Y-direction. The option is very useful when applying symmetric boundary conditions for which the velocity perpendicular to the axis of symmetry is 0. A *Scalar* LoadValue is used.
- **Z-Velocity:** This option specifies a uniform velocity in the Z-direction. The option is very useful when applying symmetric boundary conditions for which the velocity perpendicular to the axis of symmetry is 0. A *Scalar* LoadValue is used.
- **Pressure:** A constant pressure on the selected patch is specified. A *Scalar* LoadValue is used.
- **Symmetry:** The selected patch is a plane of symmetry. It is important that the entire problem, not just the geometry, is symmetric. No LoadValue is applied.
- **Mass Flux:** This option is valid only for the second and third species; a value cannot be provided for the carrier fluid. A *Vector* LoadValue is used.
- **FlowRate:** The flow rate follows the sign convention of all MEMCAD 4 boundary conditions. A positive flow rate is along the normal of the selected patch. Since in MEMCAD 4 the normal always points to the volume, the FlowRate is into the patch when a positive value is specified. A *Scalar* LoadValue is used.
- **Temperature:** Applies a constant temperature on the selected patch. A *Scalar* LoadValue is used.
- **Retardation:** This boundary condition allows application of wall effects such as chemical forces experienced by the species near a wall, slowing down the diffusion and changing the species mobility near the wall. A *Retardation* LoadValue is used.
- **Voltage:** This boundary condition applies a constant potential on the specified patch. Note that a potential difference must be specified; therefore, two Voltage BC specifications are required. A *Scalar* LoadValue is used.
- **Current:** This boundary condition applies a current through the specified patch. A *Scalar* LoadValue is used.
- **Wall Effects:** This boundary condition allows the specification of electroosmotic effects in the flow. *EDL*, *EO_Mobility*, and *Partial_EO* LoadValues can be used. Slip wall effects also can be taken into account with the *Slip* LoadValue.

□ Patch1,2,3

Choose from any of the patch names previously set up.

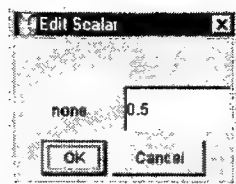
□ and1,2,3

Boolean *or* that defines intersection. Use the Boolean *or* for the Fix Type to apply independently to each of the selected patches. The Boolean *and* is disabled in NetFlow.

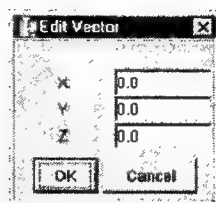
□ Load Value

Choose from several load types. Each type uses a different edit window; the entire set of edit windows is shown as part of the LoadValue explanation.

- **Scalar:** one-dimensional quantity, such as pressure load or temperature.



- **Vector:** Used with the *Velocity* FixType. This defines a uniform velocity profile in the direction of the vector specified on the selected patch.



- **Velocity:** Used with the *Velocity* FixType. This is a quadratic, linear or constant polynomial in all three directions for the velocity on the selected patch. For each velocity U_x , U_y , and U_z a separate polynomial can be given. For example, Poiseuille Flow in a pipe yields the following profile:

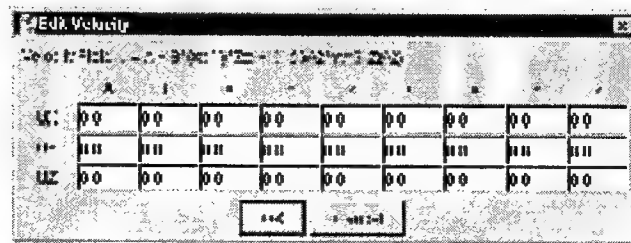
$$U = C \left[1 - \left(\frac{Y}{Y_0} \right)^2 \right]$$

where C is a constant and Y_0 is the pipe radius.

For this example, the Edit Velocity window below requires that only the first U_x line needs to be filled in. The following column values are required for this window:

ColumnA = C , ColumnC = $-C$, Column Y_y^2 = 1. All remaining columns are zero.

The example shown is filled out for the constant $C = 5$.



- **Retardation:** The following fields are provided as input.

Max_distance: The distance over which the wall effects are felt. This can be seen as a Wall-Effect-Boundary layer.

Diffusive: Specifies the diffusive retardation coefficient; i.e., a mechanism for slowing the diffusion of the species in the region within the *Max_distance* parameter.

Convective: Specifies the convective retardation coefficient; i.e., the change in the mobility of the species within the near-wall region.

In both coefficient cases the retardation is applied as a smooth function from a maximum near the wall to a zero retardation value at the specified *Max_distance* value.

- **Slip:** The Mean Free Path and the MAC (Momentum Accommodation Coefficient) are used in the slip equation to study wall effects in microchannels. It is used exclusively with the Wall Effects FixType. The slip velocity at the wall can be expressed as follows:

$$SlipVelocity = \sigma K \left(\frac{\partial U}{\partial n} \right)_{wall}$$

where U is the velocity, n is the direction normal to the velocity, σ is the streamwise momentum accommodation, expressed as follows:

$$\sigma = \frac{2 - \sigma_m}{\sigma_m}$$

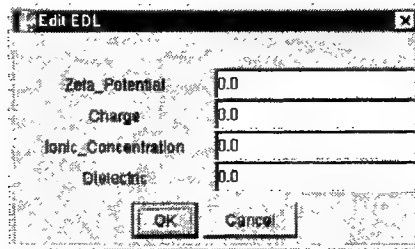
where σ_m is the momentum accommodation coefficient (MAC). Usually, $\sigma_m=1$ but it can vary within the range $0 < \sigma_m < 1$.

K is the Knudsen number, which can be expressed as:

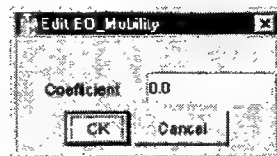
$$K_n = \frac{MeanFreePath}{CharacteristicLength}$$

If this value is smaller than 0.01 the slip effect is neglected.

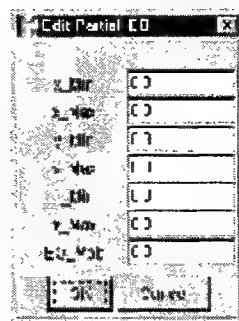
- **EDL:** EDL stands for Electrical Double Layer, which is governed by the Poisson-Boltzmann equation. Four values are needed: *Zeta-Potential*, *Charge*, *Ionic_Concentration*, and *Dielectric* coefficient of the carrier fluid. Setting the EDL LoadValue activates the solution of the Poisson-Boltzmann equation for the double layer to couple in electroosmotic effects. This setting should be used with care, since the resolution of the double layer in most conventional problems requires a very dense mesh near the walls.



- **EO_Mobility:** This setting enables the representation of the electroosmotic effects on the walls through a mobility that defines the velocity achieved by the charged carrier at the edge of the double layer in the electric field. Note that this implies a relaxation of the no-slip wall boundary condition, since the near-wall region is no longer solved. The EO_Mobility is a positive number for a negatively charged wall. (In other words, a positive value will result in flow towards the negative electrode.)



- **Partial_EO:** This setting measures the EO mobility when the surface properties change across the length of a channel. To use this LoadValue with a specific patch, define a volume where the surface changes occur with the first six entries, and enter the new EO mobility for this region with the last entry.



□ Variable

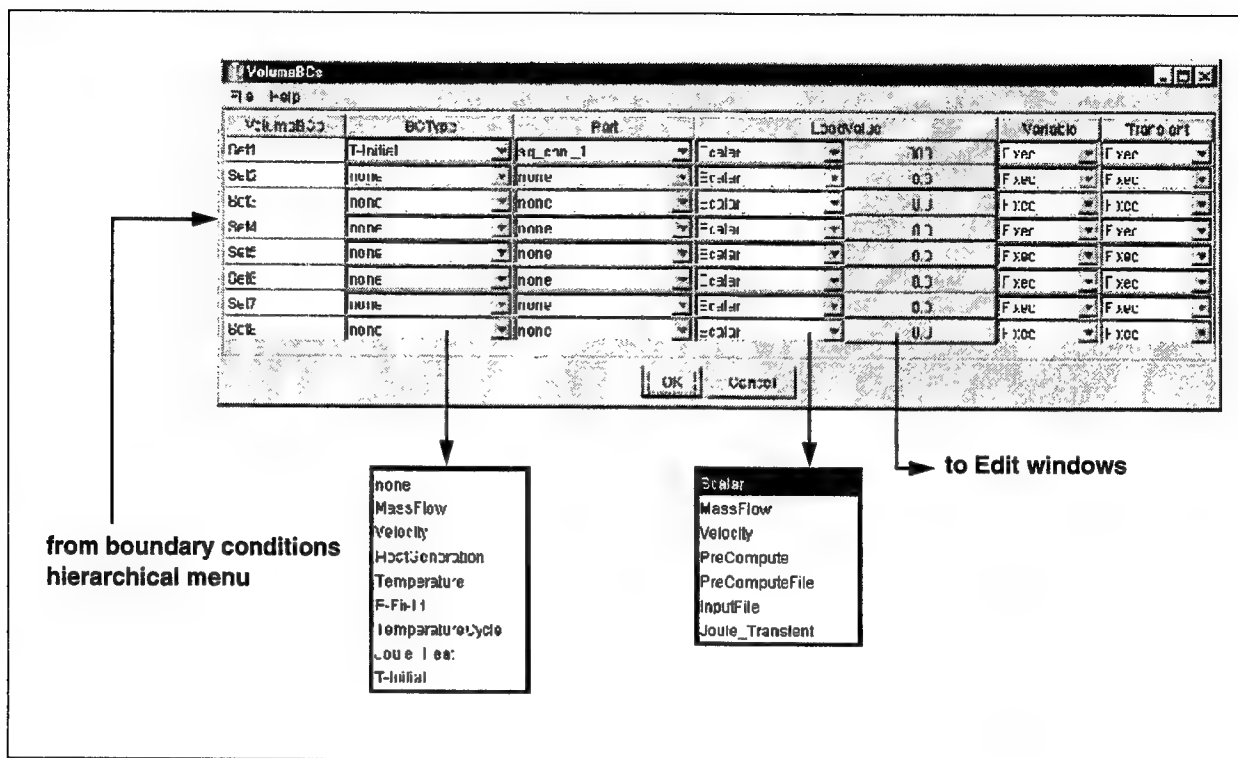
Setting for Simulation Manager. A *Fixed* setting (the default) uses constant Load Values, which are not changed during a Simulation Manager run. When a Load Value is to be a variable modified by a Simulation Manager trajectory, one of eight *NF_BC* variables can be used, corresponding to the lines in the netFlowBC Simulation Manager setup window.

□ Transient

Setting for transients surface boundary condition. A *Fixed* setting (the default) does not apply transients. When a Node Set is to be modified by a transient event, one of two *Transient* variables are available for assignment. The variable is defined in the transients window (see **page F2-128**). With this technique a periodic pressure or input flow can be generated. By setting the Transient variable the input on that node set is coupled to the waves or function defined in the transients window.

NetFlow - NetFlow BCs / volume boundary conditions window

The volumeBCs window sets volume boundary conditions. Types and load conditions for these volumes can be specified in Sets within this window.



□ volumeBCs

This display-only column allows user to define up to eight boundary condition sets for the model.

□ BCType

Enables pull-down menu with several choices:

- **none:** Do not apply a boundary condition to the volume.
- **Mass Flow:** Specify a mass flow in three directions—Mx, My, Mz. The *Mass Flow* LoadValue is used.
- **Velocity:** Apply a velocity to the selected part. A *Vector*, *Velocity*, or *InputFile* LoadValue is used.
- **Heat Generation:** Heat can be generated in a part. The part is usually a solid and not a fluid. A *Scalar* LoadValue is used.
- **Temperature:** Apply a fixed temperature to the selected part. A *Scalar* LoadValue is used.
- **E-Field:** The E-Field in the volume can be read from a pre-computed mbif file. Use the *InputFile* LoadValue and specify the directory path.
- **Temperature Cycle:** Apply a temperature cycle to the part.
- **Joule Heat:** Includes Joule heating effects. Voltage/Current BCs must be set and the carrier should have an electrical conductivity material property defined.
- **T-Initial:** specifies initial temperature conditions.

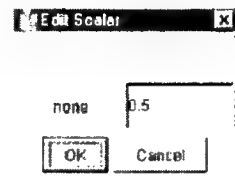
❑ **Part**

Enables pull-down menu with a list of all the parts modeled and stored in the mbif file.

❑ **Load Value**

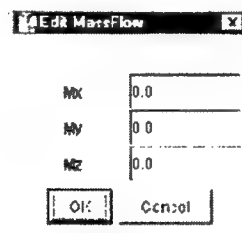
Choose from several load types. Each type uses a different edit window, shown below with the LoadValue description.

- **Scalar:** Used to specify a one-dimensional value, such as Temperature or Heat Generation.



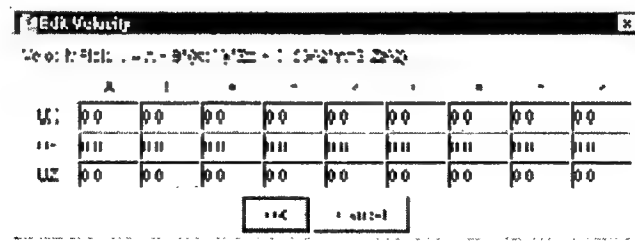
The 'Edit Scalar' dialog box has a title bar with a close button. It contains a label 'none' and a text input field with the value '0.5'. At the bottom are 'OK' and 'Cancel' buttons.

- **Mass Flow:** Used to specify a three-dimensional value for Mass Flow.



The 'Edit MassFlow' dialog box has a title bar with a close button. It contains three labels: 'Mx', 'My', and 'Mz'. Each label is followed by a text input field, all containing the value '0.0'. At the bottom are 'OK' and 'Cancel' buttons.

- **Velocity:** Used with the Velocity BCType. This is a quadratic, linear or constant polynomial in all three directions for the velocity on the selected part. For each velocity U_x , U_y , and U_z a separate polynomial can be given.

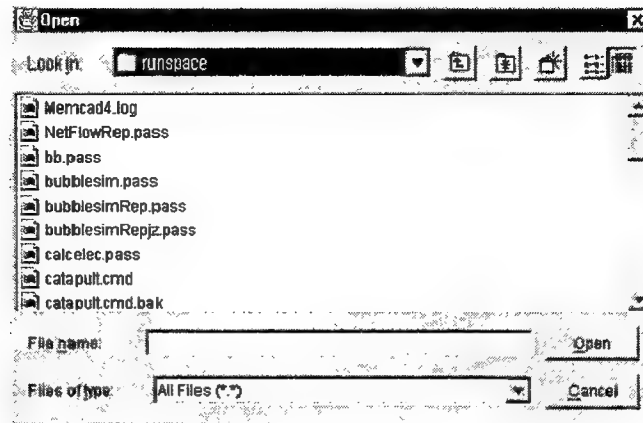


The 'Edit Velocity' dialog box has a title bar with a close button. Below the title bar is a line of text: 'Velocity BCType: - 1 - Quadratic - 2 - Linear - 3 - Constant'. Below this is a table with three rows and nine columns. The rows are labeled 'Ux', 'Uy', and 'Uz'. Each cell in the table contains the value '0.0'. At the bottom are 'OK' and 'Cancel' buttons.

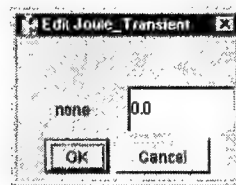
	1	2	3	4	5	6	7	8	9
Ux	0.0	0.0	0.0	0.0	0.0	0.0	0.0	0.0	0.0
Uy	0.0	0.0	0.0	0.0	0.0	0.0	0.0	0.0	0.0
Uz	0.0	0.0	0.0	0.0	0.0	0.0	0.0	0.0	0.0

- **PreCompute:** Decouples the momentum and species equations. The velocity is pre-computed and an advection-diffusion analysis for the species follows. No LoadValue edit window is used.
- **Pre-Compute File:** Specify a result mbif file for the pre-compute values. See *Input File* for window description.

- **Input File:** Specify a result mbif file from another simulation as the source data input initial conditions. The default directory is the directory from which MEMCAD is launched.



- **Joule_Transient:** Specify a scalar value for a joule transient.



□ Variable

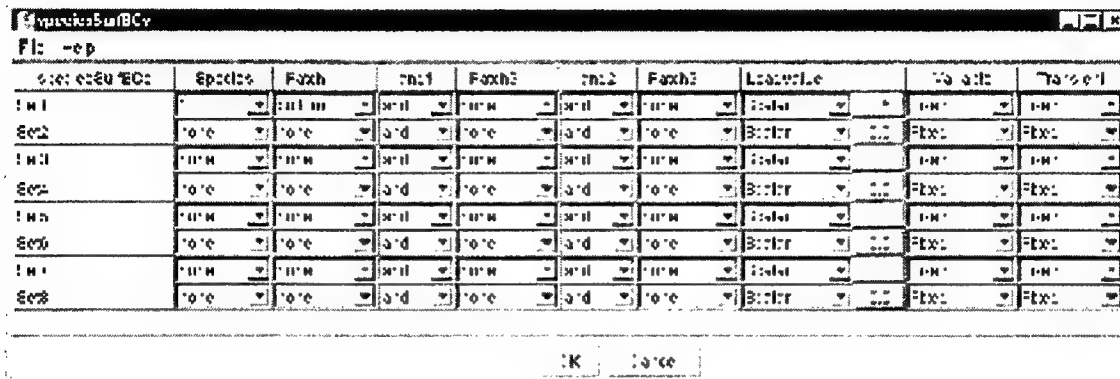
Setting for Simulation Manager. A *Fixed* setting (the default) uses constant Load Values, which are not changed during a Simulation Manager run. When a Load Value is to be a variable modified by a Simulation Manager trajectory, one of eight *NF_BC* variables can be used, corresponding to the lines in the netFlowBC Simulation Manager setup window.

□ Transient

Setting for transients surface boundary condition. A *Fixed* setting (the default) does not apply transients. When a Node Set is to be modified by a transient event, one of two *Transient* variables are available for assignment. The variable is defined in the transients window (see **page F2-128**).

NetFlow - NetFlow BCs / species surface boundary conditions window

The speciesSurfBCs window sets surface boundary conditions for the species. Fix types and load conditions for these surfaces can be specified in eight Node/Face sets within this window. When setting up conditions, the LoadValue button needs to correspond to the appropriate boundary condition. Not all combinations of boundary conditions and LoadValues are possible.



□ speciesSurfBCs

This display-only column allows user to define up to eight boundary condition sets for the model.

□ Species

Can choose either Species 1 or Species 2 for the setting.

□ Patch1,2,3

Choose from any of the patch names previously set up.

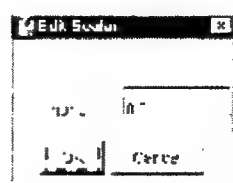
□ and1,2,3

Boolean and/or that defines union or intersection. Use the Boolean *or* for the Fix Type to apply independently to each of the selected patches. Use the Boolean *and* for the Fix Type to apply to the common intersection of the selected patches.

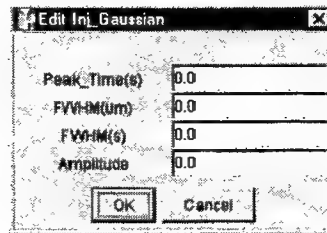
□ Load Value

Choose from several load types. Each type uses a different edit window; the entire set of edit windows is shown as part of the LoadValue explanation.

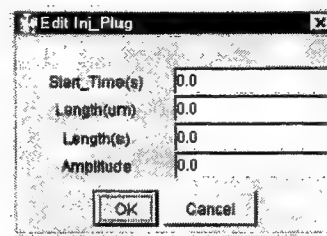
- **Scalar:** a fixed value on a patch.



- **Inj_Gaussian:** the injection of a finite width Gaussian plug through the patch. The Full-Width at Half Max (FWHM) value can be defined in seconds or in microns.



- **Inj_Plug:** the injection of a finite width square plug through the patch. The Length of the plug can be defined in seconds or in microns.



□ Variable

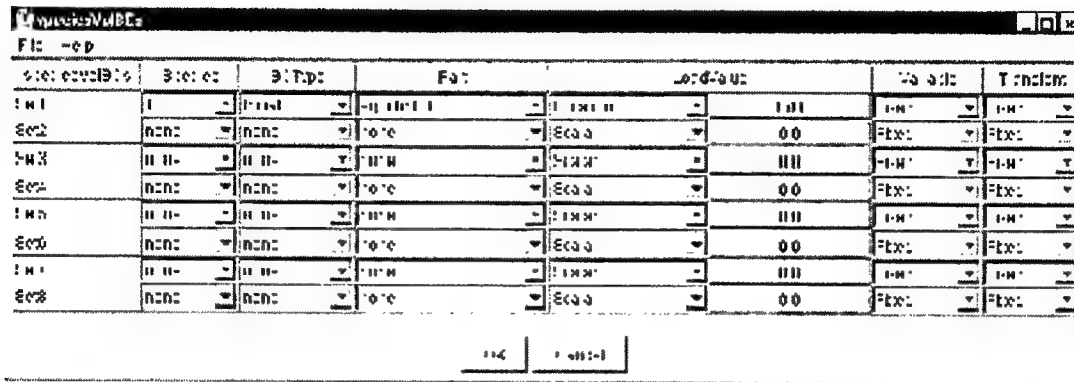
Setting for Simulation Manager. A *Fixed* setting (the default) uses constant Load Values, which are not changed during a Simulation Manager run. When a Load Value is to be a variable modified by a Simulation Manager trajectory, one of eight *NF_BC* variables can be used, corresponding to the lines in the netFlowBC Simulation Manager setup window.

□ Transient

Setting for transients surface boundary condition. A *Fixed* setting (the default) does not apply transients. When a Node Set is to be modified by a transient event, one of two *Transient* variables are available for assignment. The variable is defined in the transients window (see **page F2-128**). With this technique a periodic pressure or input flow can be generated. By setting the Transient variable the input on that node set is coupled to the waves or function defined in the transients window.

NetFlow - NetFlow BCs / species volume boundary conditions window

The speciesVolBCs window sets volume boundary conditions for the species. Types and load conditions for these volumes can be specified in Part sets within this window.



□ speciesVolBCs

This display-only column allows user to define up to eight boundary condition sets for the model.

□ Species

Can choose either Species 1 or Species 2 for the setting.

□ BCType

Enables pull-down menu with several choices:

- **none:** does not apply a boundary condition to the volume.
- **Fixed:** fixes the selected volume.
- **Initial:** This boundary condition is used only for transient flow analysis. A patch needs to be associated and selected in order to pose a numerically correct problem. The selected method enters Mass Fraction into the flow as desired. The transient problem needs a Dirichlet BC for the concentration, which is chosen to be 0 on the selected patch. Thus, the selected patch should be far enough upstream in order for the Mass Fraction not to reach the patch at any time.

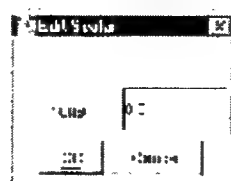
□ Part

Enables pull-down menu with a list of all the parts modeled and stored in the mbif file.

□ Load Value

Choose from several load types. Each type uses a different edit window, shown below with the LoadValue description.

- **Scalar:** Used to specify a one-dimensional value, such as Temperature or Heat Generation.



- **Location:** Confines the concentration, given by the Mass Fraction, to the selected minimum and maximum values of X, Y, and Z. MEMCAD 4 finds all nodes that are within these bounds and applies the Mass Fraction. If the minimum and maximum in any direction are left unchanged (i.e zero), it means that “no filter” (all elements between $-\infty$ and $+\infty$) is applied in this direction. Using this LoadValue can lead to solver uncertainties, due to the sharp edges created by the *Location* setting. The *Gaussian* setting is preferred.

x_Min	0.0
x_Max	40
y_Min	0.0
y_Max	0.0
z_Min	0.0
z_Max	0.0
Amplitude	0.5

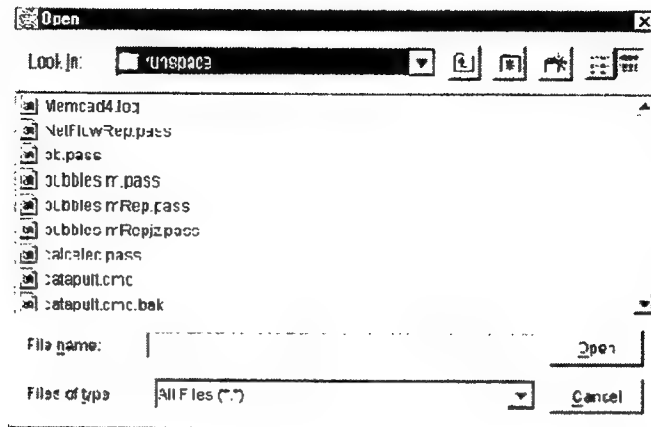
- **Gaussian:** Applies a Gaussian distribution according to the following formula:

$$A \exp \left[\left(\frac{x - x_0}{\sigma_x} \right)^2 \right] \left[\left(\frac{y - y_0}{\sigma_y} \right)^2 \right] \left[\left(\frac{z - z_0}{\sigma_z} \right)^2 \right]$$

where A is the amplitude, and σ is the change in a particular direction. Typically, only one dimension is given a non-zero σ value, which results in a plug of species given a Gaussian distribution in one axial direction. The *Gaussian* setting greatly reduces solver instability, and is the preferred LoadValue for most calculations.

x_0	0.0
y_0	0.0
z_0	0.0
sigma_x	0.0
sigma_y	0.0
sigma_z	0.0
Amplitude	0.5

- **Input File:** Specify a result mbif file from another simulation as the source data input boundary conditions. The default directory is the directory from which MEMCAD is launched.



□ Variable

Setting for Simulation Manager. A *Fixed* setting (the default) uses constant Load Values, which are not changed during a Simulation Manager run. When a Load Value is to be a variable modified by a Simulation Manager trajectory, one of eight *NF_BC* variables can be used, corresponding to the lines in the netFlowBC Simulation Manager setup window.

□ Transient

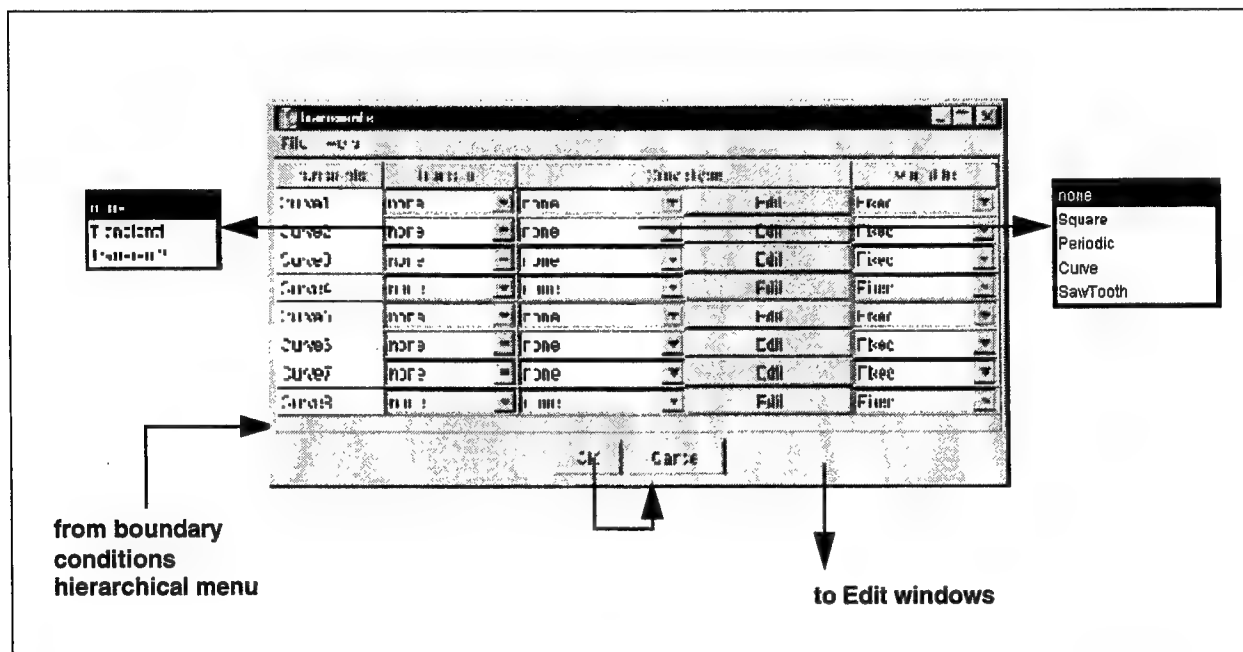
Setting for transients surface boundary condition. A *Fixed* setting (the default) does not apply transients. When a Node Set is to be modified by a transient event, one of two *Transient* variables are available for assignment. The variable is defined in the transients window (see **page F2-134**).

NetFlow - NetFlow BCs / transients boundary conditions window

The transients window enables the user to specify boundary conditions associated with transient calculations. Transient variables can be assigned in the surfaceBC or volumeBC window, and the type of transient response to use for the problem can be specified in this window. Two different transient types can be specified. For any transient analysis, the appropriate parameters should be set up in the NetFlow Tool window.



Transients are restricted to the following boundary condition settings: SurfaceBCs—*Velocity, X,Y,Z Velocity, Pressure, FlowRate Temperature, Heat Flux, Concentration*; VolumeBCs—*Heat Generation*.



□ transients

This display-only column allow user to define up to eight boundary condition transient sets for the model.

□ Transient

This column allows assignment of one of two transient curve variables: *Transient1* or *Transient2*. The equivalent *TransientBC1* and *TransientBC2* variables are assigned in either the surfaceBC or volumeBC window to a desired parameter for transient analysis.

□ Curve Type / Edit

The NetFlow transient capability allows one of four different transient waveforms to be specified for the analysis. The specific waveform characteristics are specified in the Edit window accessed from the Edit button. These Edit windows are further described on **page F2-134**.

- **Square:** Assigns a square wave as the transient curve. The square wave can be controlled by adjusting its period, split (duty cycle), or amplitude.
- **Periodic:** Assigns a periodic curve as the transient. The periodic curve can be controlled by adjusting its period, mean, or amplitude.
- **Curve:** Assigns a table of time step and property values in order to create a customized curve.
- **Sawtooth:** Produces a sawtooth waveform.

□ Variable

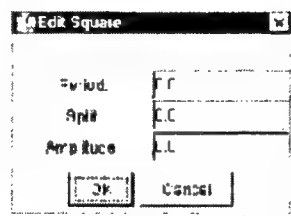
Setting for Simulation Manager. A *Fixed* setting (the default) uses constant Load Values, which are not changed during a Simulation Manager run. When a Load Value is to be a variable modified by a Simulation Manager trajectory, one of two *FluidBC* variables can be used, corresponding to the lines in the fluidBCs Simulation Manager setup window.

NetFlow - NetFlow BCs / transients BC window / Edit CurveType windows

Each transient LoadValue type selected from the Edit CurveType window uses its own format for entering parameters. The windows are described in more detail in this section.

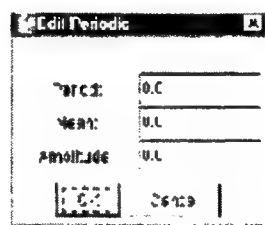
□ Square

The square wave can be controlled by adjusting its period, split (duty cycle), or amplitude. *Period* is the time between the start of two square waves. *Split* is a value between 0 and 1. If Split is 0.5, the square wave is at its maximum for half a period. If the Split is 0.3, then the square wave is at its maximum for 30% of the period. *Amplitude* is the maximum value of the square wave.



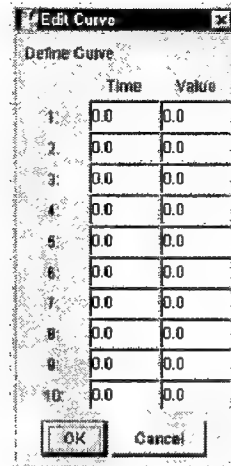
□ Periodic

The periodic wave can be controlled by adjusting its period, mean, or amplitude: *Period* is the time between the start of two periodic waves. *Mean* moves the periodic curve vertically (up or down). *Amplitude* is the maximum value of the periodic wave.



□ Curve

The custom curve is described with a table of time step and property values. Users can enter up to 10 different sets of time and amplitude values to simulate almost any type of transient curve.

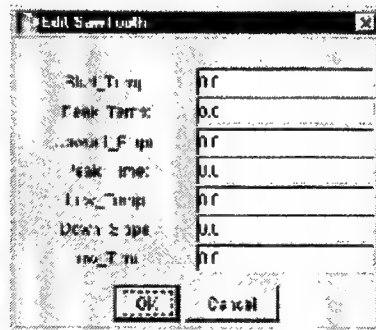


The 'Edit Curve' dialog box contains a table for defining a custom curve. The table has two columns: 'Time' and 'Value'. There are 10 rows, each with a number from 1 to 10 in the first column. All cells in the 'Time' and 'Value' columns are currently empty. At the bottom of the dialog are 'OK' and 'Cancel' buttons.

	Time	Value
1:		
2:		
3:		
4:		
5:		
6:		
7:		
8:		
9:		
10:		

□ Sawtooth

The sawtooth is described with a combination of time and temperature values, along with a slope specification for the sawtooth angle.

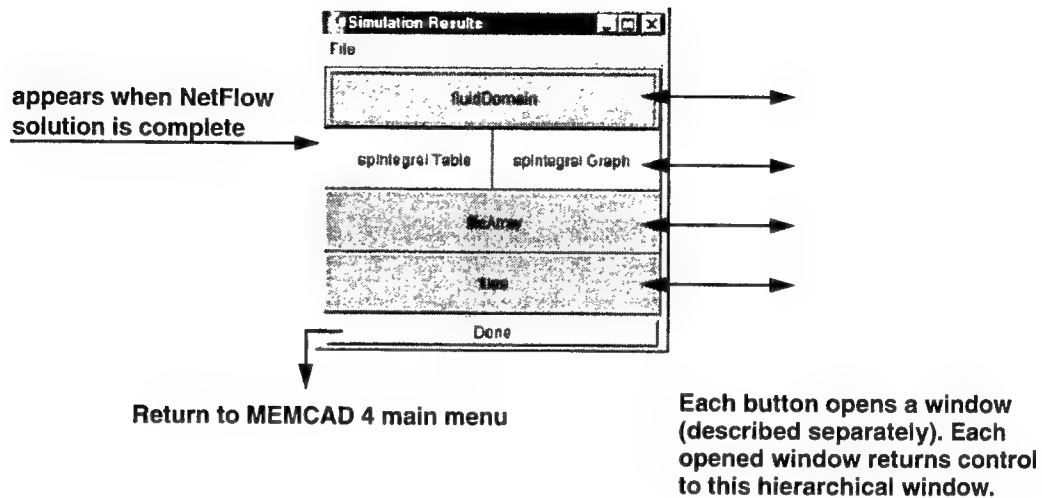


The 'Edit Sawtooth' dialog box contains several input fields for defining a sawtooth wave. The fields are labeled: 'Start Temp', 'Peak Temp', 'Slope Up', 'Peak Time', 'Low Temp', 'Decay Time', and 'Low Temp'. Each field has a corresponding input box. At the bottom of the dialog are 'OK' and 'Cancel' buttons.

Start Temp	0.0
Peak Temp	0.0
Slope Up	0.0
Peak Time	0.0
Low Temp	0.0
Decay Time	0.0
Low Temp	0.0

NetFlow - hierarchical solutions menu window

The fluidic results hierarchical solutions menu window allows user to choose windows to view result tables and mbif file paths used during the computation.



❑ fluidDomain

Open window (see **page F2-137**) to display table of fluid results.

❑ spIntegral/Table

Open window (see **page F2-138**) to display table of spIntegral results.

❑ spIntegral/Graph

Open window (see **page F2-138**) to display graph of spIntegral results.

❑ fileArray

Open window (see **page F2-139**) to display directory paths of all saved mbif files.

❑ files

Open window (see **page F2-139**) to display directory path of solution results.

❑ Done

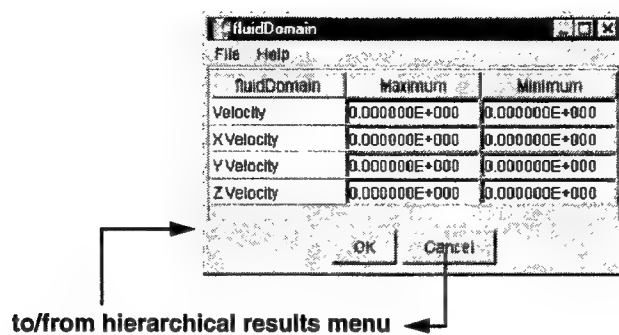
Close window and return control to MEMCAD 4.

❑ File/Print

Enable printing of the individual window results to a single file. The text format file can be used to interface to other programs. The file is located in the directory from which MEMCAD 4 starts.

NetFlow - Results / fluid solution window

This fluidDomain window displays the results from the NetFlow solver.



□ fluidDomain

List the type of velocity for the solver solution. Maximum velocity as well as the individual X,Y, and Z components are displayed.

□ Maximum

The maximum velocity in the channel calculated by the solver. The value shown is an absolute value.

□ Minimum

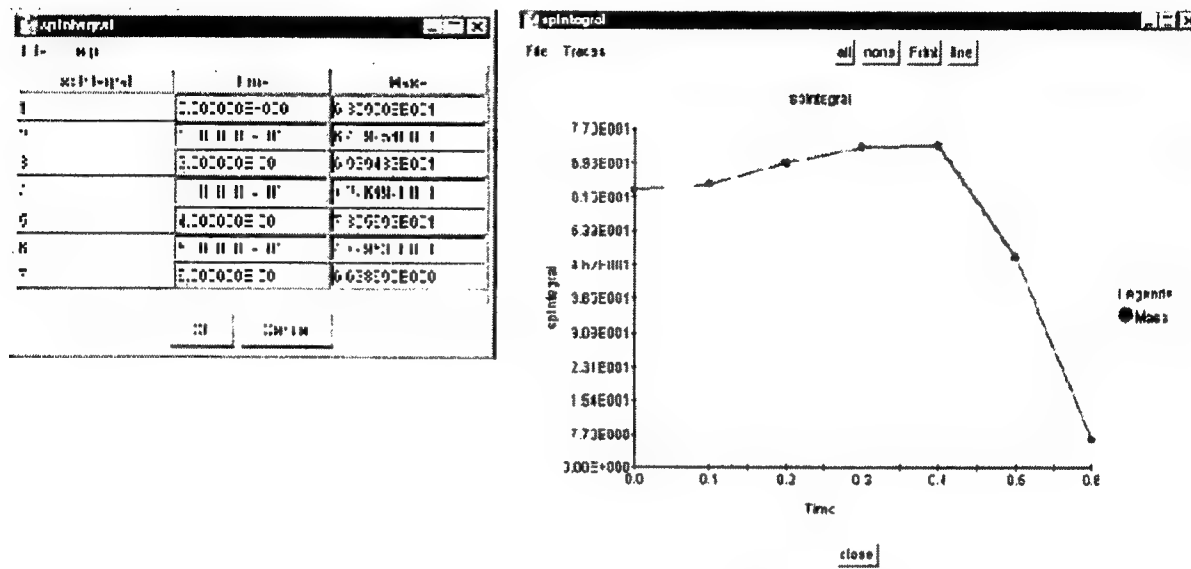
The minimum velocity in the channel calculated by the solver. The sign of the value is derived from the normal vector; a minimum value can represent maximum velocity. If the value in this column represents the maximum velocity for the model, the same value will appear in the Maximum column.

□ OK

Close window.

NetFlow - Results / spIntegral Table and Graph solution windows

These windows display the numerical and graphical species mass results from the simulation. The transient time and output step settings for the table and graph are set in the NetFlow Tool window (see **page F2-109**).



□ spIntegral Time

This column and abscissa in the graph display the output step intervals set in the NetFlow Tool window. In the above example, output mbif files are written every 0.2 seconds, and the mass results are displayed.

□ Mass

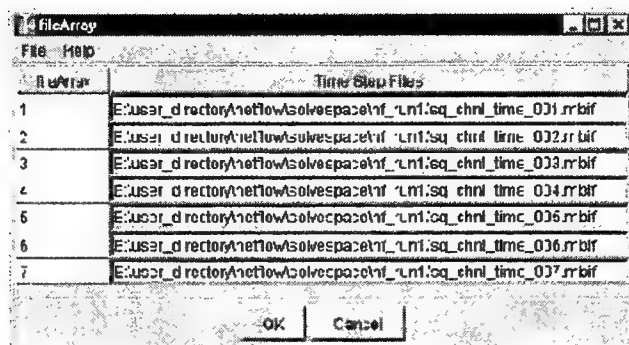
This column and ordinate display the species mass in the carrier fluid.

□ OK

Close window.

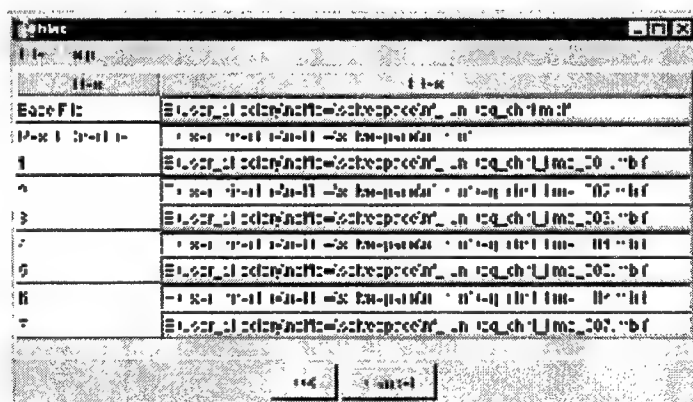
NetFlow - Results / fileArray window

The fileArray window lists the directory paths for each output mbif file written during the simulation. The number of files is determined by the output time step length and total transient simulation run time, as set in the SwitchSimTool window (see [page F2-109](#)).



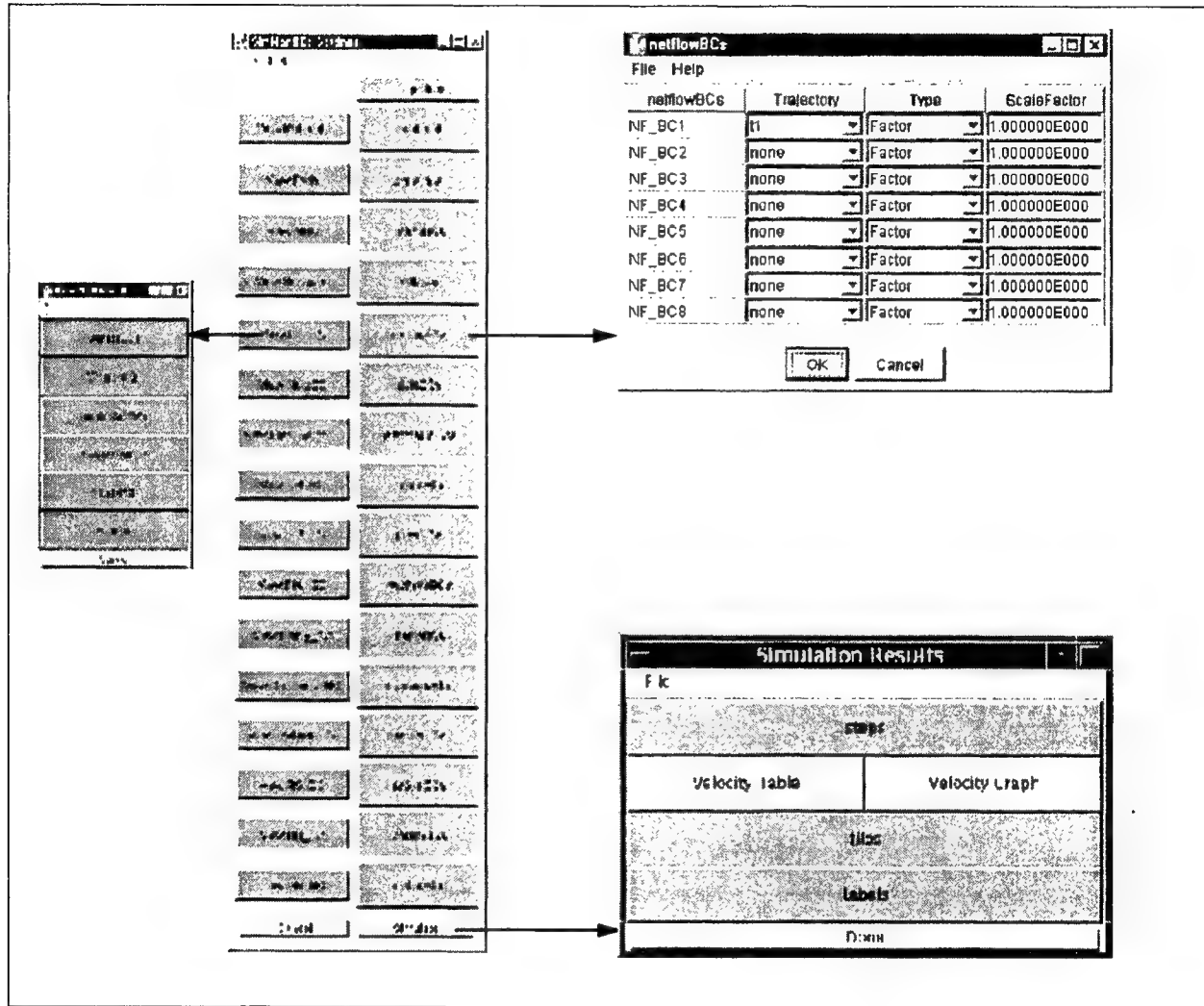
NetFlow - Results / result files window

This files window displays the path to the result mbif file.



Simulation Manager controls for NetFlow

When NetFlow boundary conditions variables are set up, the Simulation Manager can assign a trajectory to the variable and produce a batch run simulation, creating separate mbif files for each trajectory step. This section lists the NetFlow-specific controls accessed from the Simulation Manager. For a complete reference description of general Simulation Manager capability, refer to the Reference Manual, **page R2-94**.



View NF_BC

This gray button provides convenient viewing access for checking the NetFlow boundary condition windows, which are described in detail on pages **page F2-116** through **page F2-135**. The windows are read-only and cannot be modified from this access point.

netFlowBCs

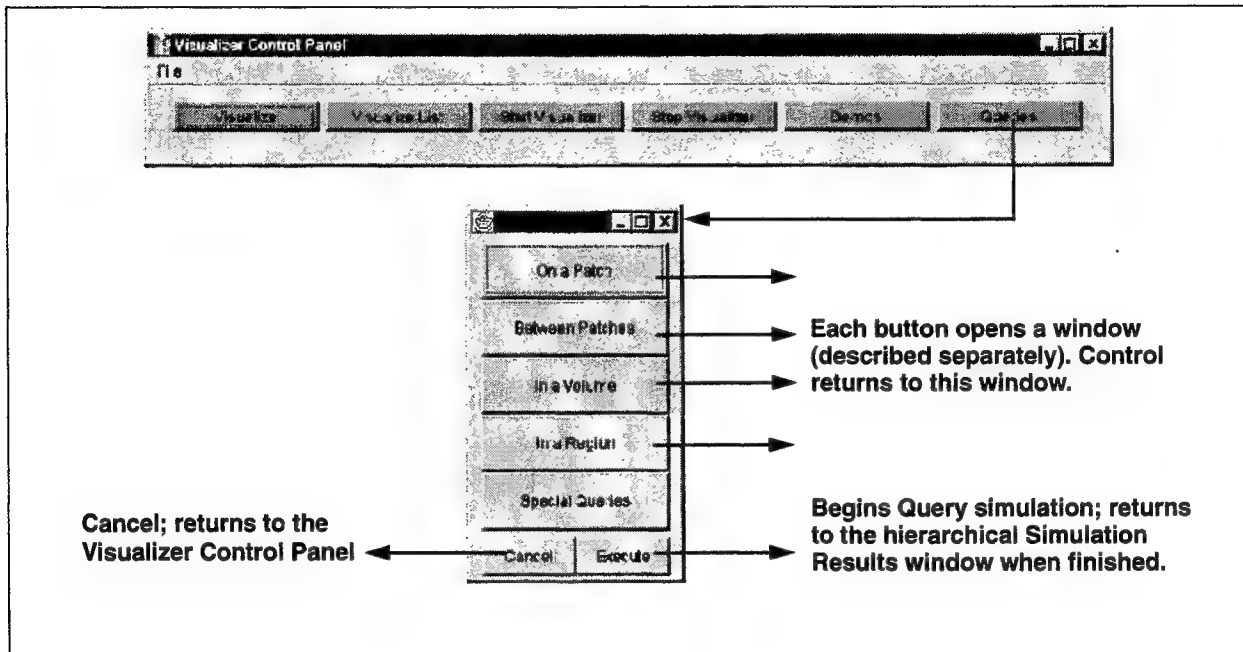
The green button opens a variable assignment window, which allows the user to define up to eight fluid boundary conditions. The variables are assigned in the species, surfaceBC, speciesSurfBCs, volumeBC, and speciesVolBCs windows, and equated in this netFlowBC window to the trajectory type set for the Simulation Manager problem. The functionality of the window is similar to the SimMan/MechBCs window described in the Reference Manual, **page R2-110**.

Simulate

Starts the Simulation Manager calculations. When finished, a hierarchical results window appears, and allows access to a velocity table and accompanying graph.

Visualizer – Query function

Clicking on the Query button on the Visualizer Control Panel opens a set of hierarchical windows. Through these windows, the user can select surface or volume extraction criteria for result values stored in mbif files. An executable then performs the extraction and writes an output file for display or input into another solver.



❑ On a Patch

Opens window that allows user to set query parameters on a patch. See **page F2-142** for further details.

❑ Between Patches

Opens window that allows user to set query parameters between two patches. See **page F2-143** for further details.

❑ In a Volume

Opens window that allows user to set query parameters on a part for a user-defined volume. See **page F2-144** for further details.

❑ In a Region

Opens window that allows user to set query parameters on a part for a point, volume, or an ellipse within a user-defined volume. See **page F2-145** for further details.

❑ Cancel

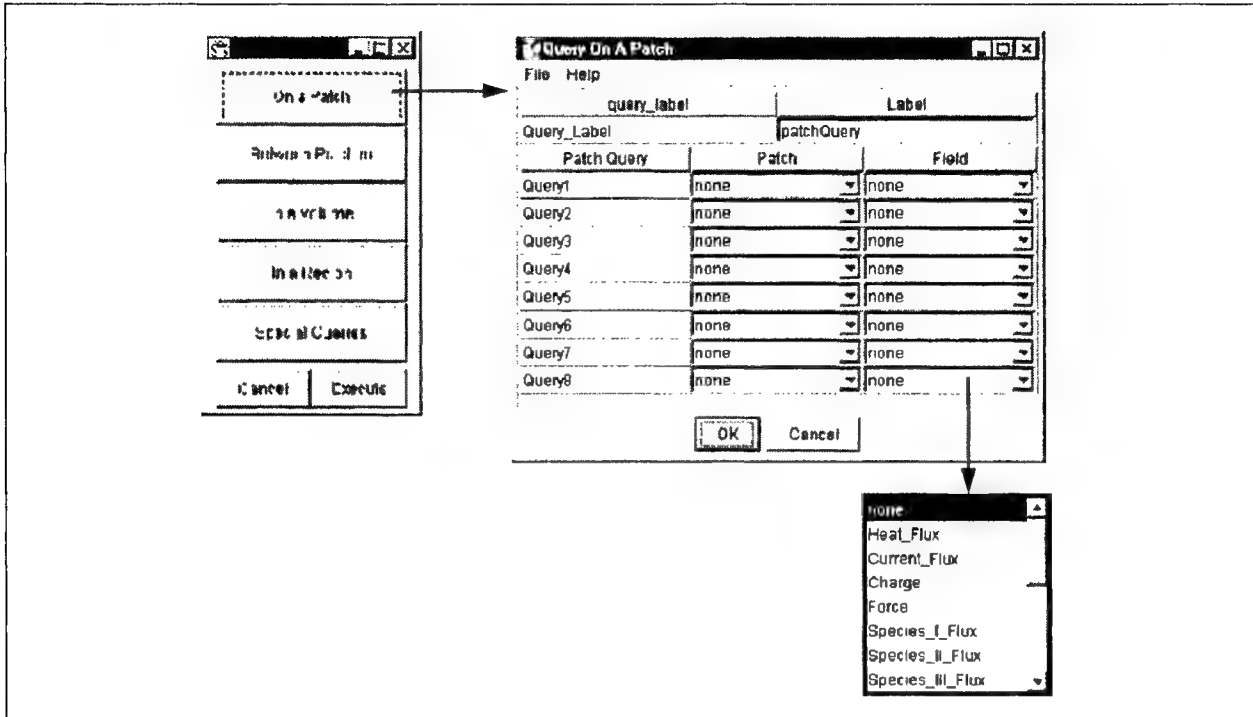
Query is not performed, and control is returned to the Visualizer Control function bar.

❑ Execute

Launches Query solver.

Query – On a Patch

The patch query allows users to extract result values for a specified patch within a MEMCAD model mbif file. Not all field types are applicable; the relevant types are listed below.



□ Label

An editable field that allows user to change the label name. The label will appear in the results window.

□ Patch Query

Indicates the query number. Each set can have a unique patch name and/or field type setting.

□ Patch

User selects a patch name from a pull-down menu.

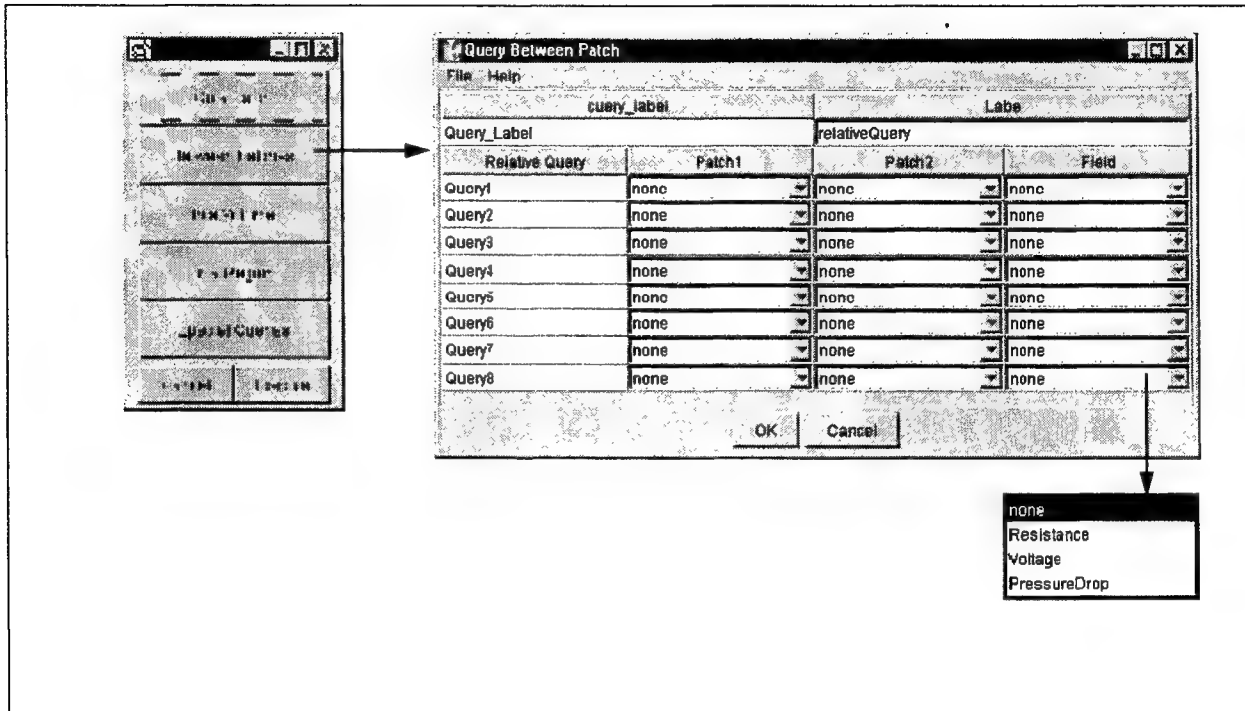
□ Field

User selects a calculation type from a pull-down menu.

- **Heat_Flux:** calculates heat flux through the selected patch.
- **Current_Flux:** calculates current flux through the selected patch.
- **Species_N_Flux:** calculates species flux through a selected patch.
- **AvgVoltage:** calculates average voltage on a patch.
- **Avg, Max, MinTemperature:** calculates average, maximum, or minimum temperature on a patch, respectively.
- **FlowRate:** measures the flow rate through a patch.

Query – Between Patches

The between patches query allows users to extract result values dependent on two patches within a MEMCAD model mbif file.



❑ Label

An editable field that allows user to change the label name. The label will appear in the results window.

❑ Relative Query

Indicates the query number. Each set can have unique patch names and/or field type setting.

❑ Patch1, 2

User selects a patch name from a pull-down menu. Both patch fields must be selected in order to complete the query.

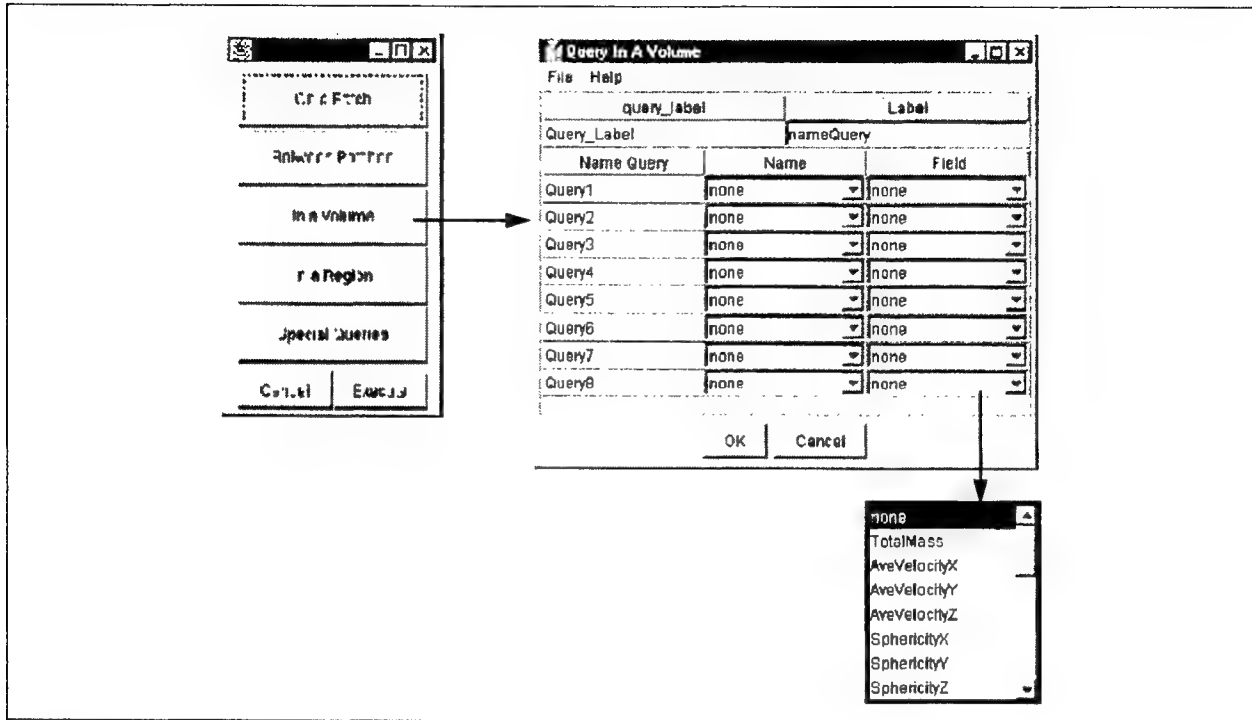
❑ Field

User selects a calculation type from a pull-down menu.

- **Resistance:** calculates resistance between the two selected patches.
- **Voltage:** calculates voltage between the two selected patches.
- **PressureDrop:** measures change in pressure between the two selected patches.

Query – In a Volume

The volume query allows the user to extract result values for a specified volume within a MEMCAD model mbif file. Not all field types are applicable; the relevant types are listed below.



❑ Label

An editable field that allows user to change the label name. The label will appear in the results window.

❑ Name Query

Indicates the query number.

❑ Name

User selects a part name from a pull-down menu. A field calculation type is applied to this name.

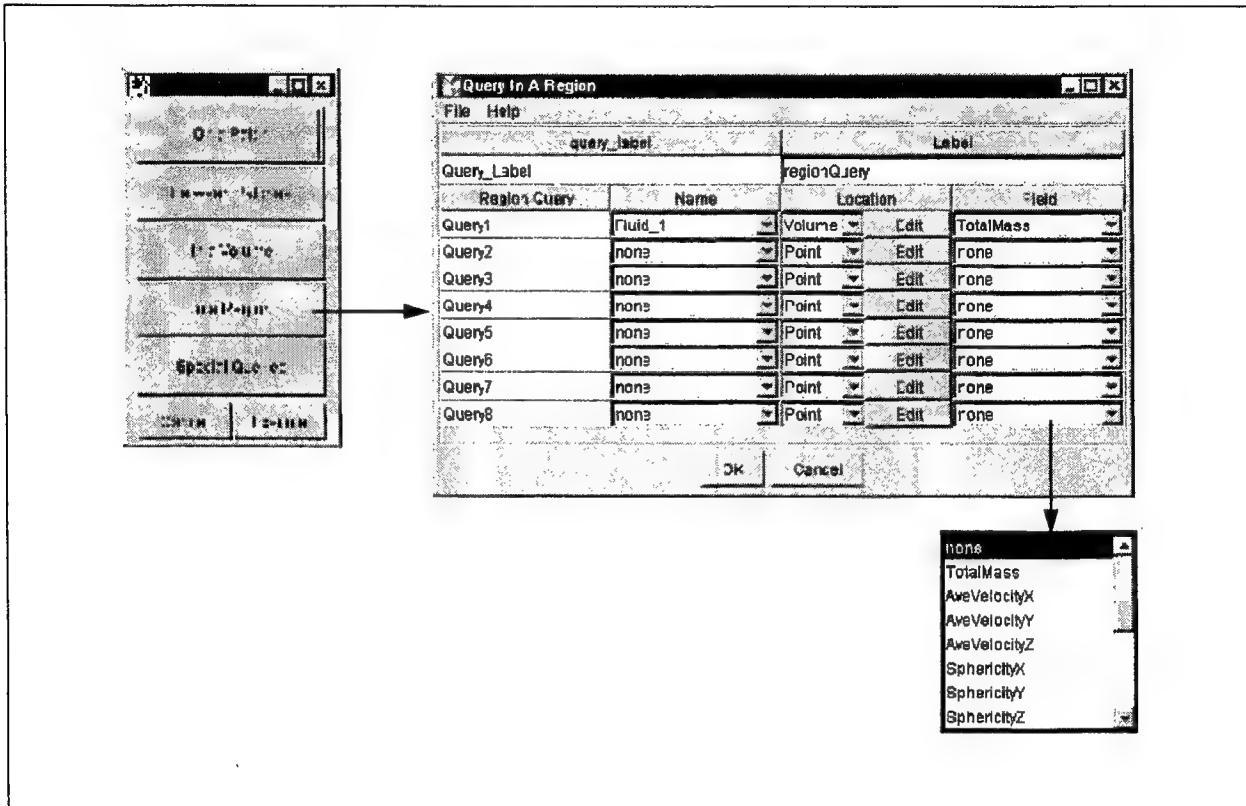
❑ Field

User selects a calculation type from a pull-down menu.

- **Species_N_Integral:** determines the percentage of defined species that passes through a part.
- **Max, MinTemperature:** calculates maximum or minimum temperature on the defined part.

Query – In a Region

The region query allows users to extract result values for a portion of a specified volume within a MEMCAD model. The region can be a point of an inner volume within a specific volume. A point is specified with a single XYZ coordinate defining a location. An inner volume is specified with two XYZ coordinates defining the volume space.



Clicking on the Region Query button opens a setup window.

❑ Label

An editable field that allows user to change the label name. The label will appear in the results window.

❑ Region Query

Indicates the query number.

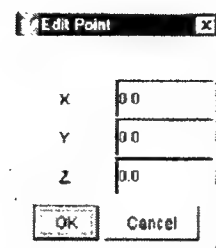
❑ Name

User selects a part name from a pull-down menu.

□ Location

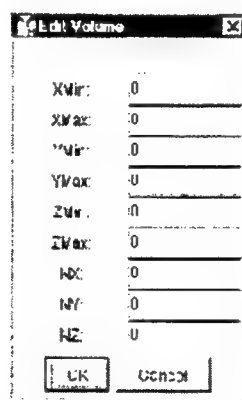
User selects a point, volume, or elliptical region from a pull-down menu to be defined. Each selection opens a window with editable values. The choices are *Point*, *Volume*, or *Ellipse*.

- **Point:** user defines X, Y, and Z-coordinates of the point.



The 'Edit Point' dialog box contains three input fields for X, Y, and Z coordinates, each with a value of 0.0. At the bottom are 'OK' and 'Cancel' buttons.

- **Volume:** user defines volume space and a mesh for query calculation. If any pair of min/max values is left at 0, no filter is applied.



The 'Edit Volume' dialog box contains nine input fields: XMin, XMax, YMin, YMax, ZMin, ZMax, NX, NY, and NZ. Each field has a value of 0. At the bottom are 'OK' and 'Cancel' buttons.

XMin, XMax: defines the X-coordinates for the volume.

YMin, YMax: defines the Y-coordinates for the volume.

ZMin, ZMax: defines the Z-coordinates for the volume.

NX, NY, NZ: Defines number of mesh elements for query calculation in the X, Y, and Z-directions, respectively.



Query mesh

The NX, NY, and NZ mesh elements defined in this window are calculated along with the mesh defined in the solver. To preserve maximum accuracy, keep the query mesh density as close as possible to the solver mesh density.

- **Ellipse:** User defines boundaries of the ellipse and a mesh for query calculation. This is typically used when firing a laser through a channel to determine the amount of species present in a specific volume.

Edit Ellipse	
x0	0.0
y0	0.0
z0	0.0
x_size	0.0
y_size	0.0
z_size	0.0
Nel_x	0.0
Nel_y	0.0
Nel_z	0.0
<input type="button" value="OK"/> <input type="button" value="Cancel"/>	

x0, y0, z0: defines the origin of the ellipse.

x_size, y_size, z_size: the value assigned in each direction is the diameter of the laser where the intensity is greater than or equal to e^{-1} .

Nel_x, Nel_y, Nel_z: Defines the mesh in the x, y, and z-directions. Keep this mesh density consistent with the solver mesh.

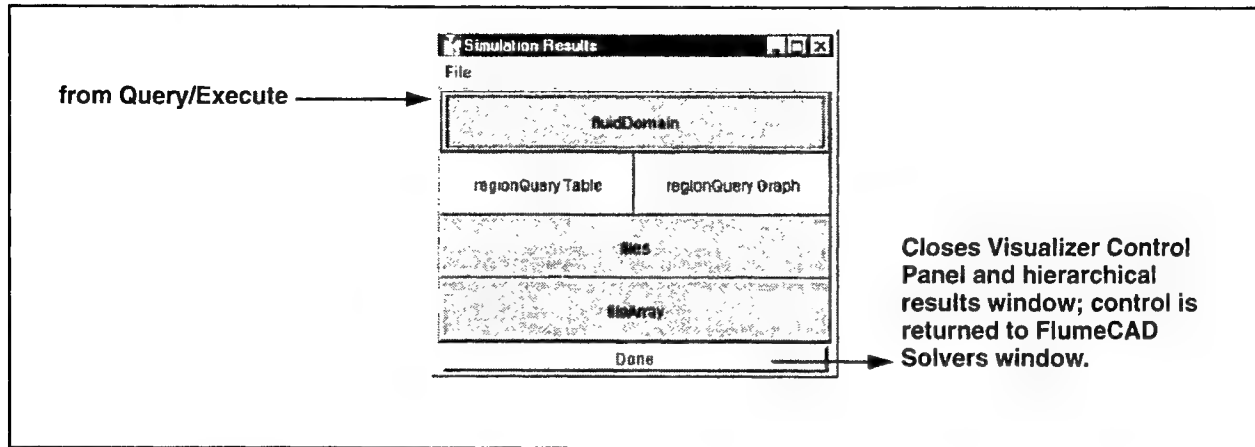
□ Field

User selects a calculation type from a pull-down menu.

- **Species_N_Integral:** calculates the amount of species that exists in the defined volume at each time.

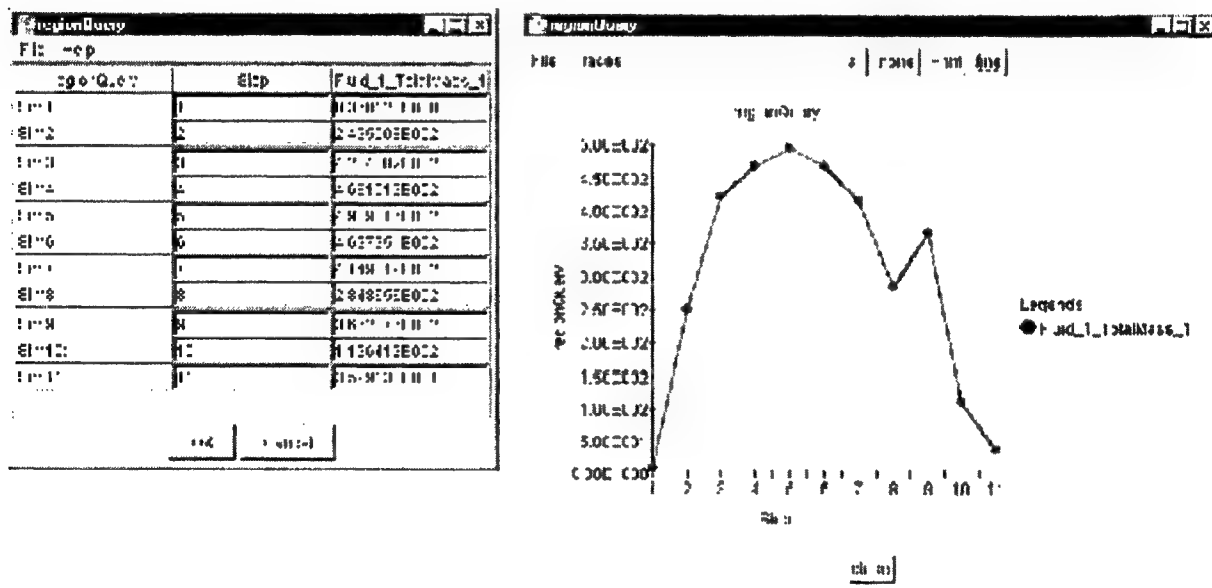
Simulation Results – Query

When the query is complete, a Simulation Results window opens containing both NetFlow and Query results.



regionQuery Table

Opens a window containing a table of results from the *In a Region* query. Here, *regionQuery* is the label (see *Query – In a Region* on page F2-142).



regionQuery Graph

Opens a window containing graphical results from the *In a Region* query. Here, *regionQuery* is the label (see *Query – In a Region* on page F2-142).

Appendix 2: Research Publications

METROLOGY AND SIMULATION OF CHEMICAL TRANSPORT IN MICROCHANNELS

P. M. St. John*, T. Woudenberg, and C. Connell

PE Applied Biosystems
850 Lincoln Centre Drive
Foster City, CA 94404

M. Deshpande and J. R. Gilbert

Microcosm Technologies, Inc.
215 1st St
Cambridge, MA 02142

M. Garguilo and P. Paul

Sandia National Laboratory
Livermore, CA

J. Molho, A. E. Herr, T. W. Kenny, M. G. Mungal

551 Terman
Stanford University
Stanford, CA 94305

ABSTRACT

We are working towards building a CAD tool (NetFlow) for microfluidic systems. To support the development of this tool, diffusion and flow experiments are being performed in microchannels. In this paper, we describe the novel flow visualization approach developed for these experiments and report experimental results and corresponding simulations for fluid transport in microchannels. The experimental approach relies on the use of a caged, charged fluorescent dye which can be activated (uncaged) by a UV laser beam and tracked by fluorescence imaging [1]. In contrast to standard methods for inserting a dye plug in a microchannel, this is the only technique which allows definition of very precise regions at any place along the channel. Specifically, this allows a narrow definition of starting plugs and therefore an improved determination of the flow profile. We have used this technique to study diffusion, pressure-driven flow, and electrokinetic flow in various microchannel geometries.

INTRODUCTION

There is a wide interest in micron-scale integrated chemical/biochemical analysis or synthesis systems, also referred to as lab-on-a-chip. The microfluidic systems being explored today rely on both pressure [2] and electrokinetic effects [3,4] for controlling fluid transport. Complicated relationships between the shape and size of the microchannels and the behavior of multi-component fluids are not completely understood. Researchers are forced to use costly trial and error methods in the design of microfluidic systems.

Discrepancies between experimental measurements and simulations exist because the modeling equations may not fully capture the essential physics and because the experimental parameters used in the simulations are often approximate (e.g. calculation of diffusion constant and mobility in a microchannel). We are attempting to simulate simple flow in specific microchannel geometries and extract parameters which will enable us to predict flow in more complex structures and ultimately allow us to take an active role in the design of microfluidic structures. Flow predictions have direct applications in microcapillary electrophoresis systems where long channels are advantageous for resolved separation of DNA

fragments out to several kilobases but device area must be minimized. Flow predictions are also useful for determining the geometries needed for chemical reactions in microchannels.

EXPERIMENTAL

Silicon microchannel structures were fabricated as "negative" masters using standard photolithography and an STS deep reactive ion etch (DRIE) was used to create raised rectangular structures with dimensions of 50 μm in width, 5 cm in length and 40 – 80 μm in height. An RTV silicone elastomer (Dow Corning) was used to form positive replicas of the silicon structures (Fig. 1) [5]. Scanning electron micrographs (SEMs) show the etched silicon sidewalls and the corresponding elastomer replica (Au sputtered) (Fig. 2). The striae located near the top of the silicon structure was a result of over-etching. The etched silicon region was smooth to an RMS roughness of ~ 7.26 nm, determined by atomic force microscopy. The elastomer SEM shows the reproduction of the features present in

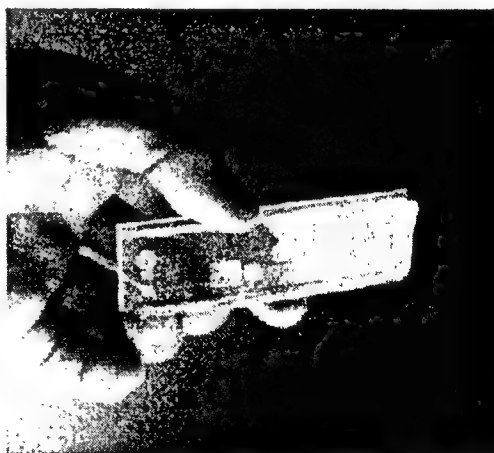


Figure 1. Photograph of the elastomer device with three test microchannels. The circles are the injection wells and the squares are used to study pressure driven flow in a sudden expansion.

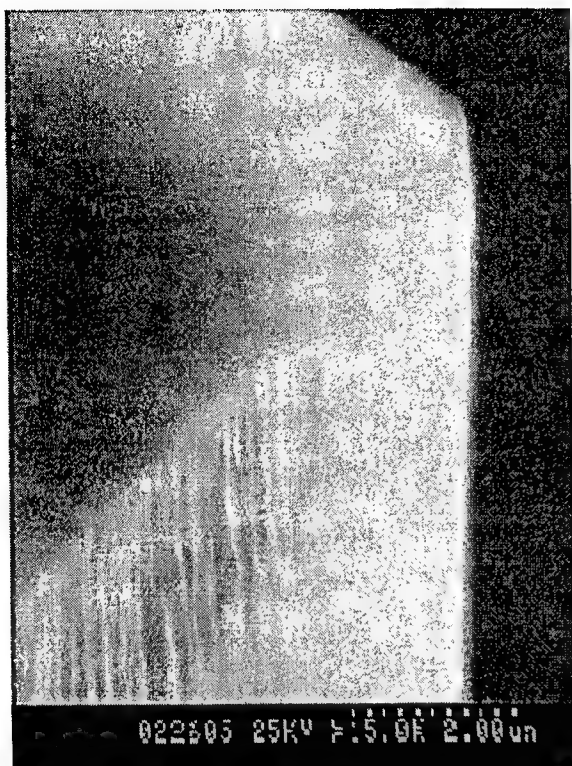


Figure 2a. SEM of the silicon mold

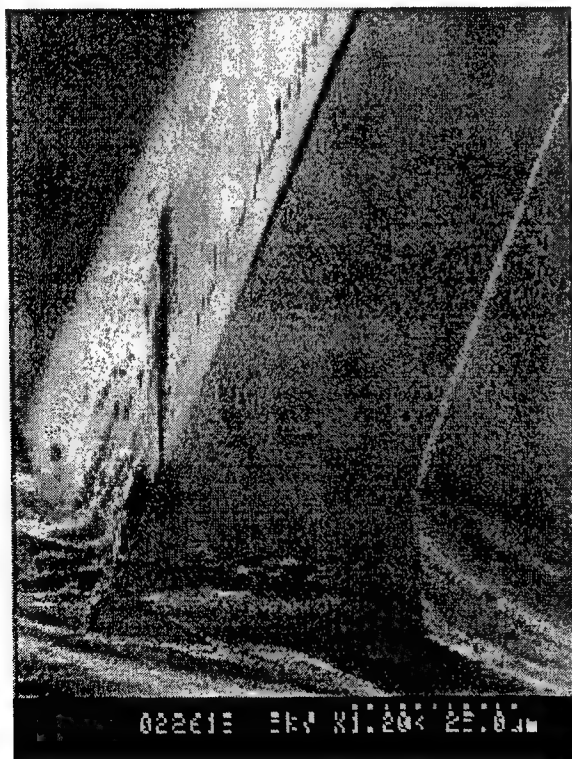


Figure 2b: SEM of the elastomer channel

the silicon. Note the striations which run the length of the channel on the lower portion of the channel wall. This corresponds to the rough overetched region of the silicon mold. The region of the elastomer which replicated the etched silicon

surface had an RMS roughness of ~ 7 nm. The rough edge at the opening of the elastomer channel came from slicing the elastomer structure with a razor blade. The channel was not cleaned prior to metal sputtering and particulates can be seen on the channel floor. The elastomer channels were sealed with either glass microscope slides or elastomer coated glass microscope slides and wells were created in the elastomer using a mechanical hole punch (Figure 1).

Serpentine microchannels in borofloat glass (not shown) were fabricated by Alberta Microelectronics Centre (Alberta, Canada) using standard photolithography and an isotropic wet etch to yield a smooth hemispherical cross-section. A commercially available additive made from a polyacrylamide short chain polymer (ABI DNA Fragment Analysis Reagent 7% w/w) was used (0.1% v/v aqueous) to suppress electroosmotic flow (EOF) [6] in both glass and elastomer structures. Although EOF suppression was verified by observing ion travel under an applied field, the extent of suppression was not quantitated. In this paper, electrophoretic flow refers to negatively charged dye migration towards the positive electrode and electroosmotic flow refers to dye carried toward the negative electrode, despite charge.

The caged fluorophore (fluorescein) was purchased from Molecular Probes and used in micromolar quantities dissolved in either distilled water or Tris-EDTA buffer, pH = 7.4. The dye is negatively charged, both caged and uncaged (fluorescein, -2). When caged, the dye solution is non-fluorescent. Upon photoactivation of a UV light illuminated volume, the protecting group is cleaved and the dye fluoresces. Approximately 0.3 mW average power of 355 nm light from a pulsed Nd:YAG laser (Uniphase) was used for ~ 0.1 s to uncage the fluorophore in a 20 μ m spot. In the electrokinetic experiments, the laser beam was focused using a UV microscope objective which defined a sharp start zone. A continuous wave Microblue diode pumped laser at 473 nm (Uniphase) was used for fluorescence excitation (Figure 3). The Microblue was positioned close to Brewster's angle for glass to minimize laser scatter into the microscope. Pressure driven flow was imaged at Sandia National Laboratories where the experimental setup is similar to that described above with the exceptions that the uncaging region is rectangular in shape and that the uncaging time is much less than one millisecond. Fluorescence images of the molecules diffusing and moving in the local flow were collected using a microscope objective (total magnification = 100 X) and a video rate, interlaced camera. Images were analyzed and flow parameters were extracted for simulations. The evolution of the fluorescent profiles under electrokinetic and pressure-driven flow are shown here by comparing a sequence of timed images to corresponding times from the simulations.

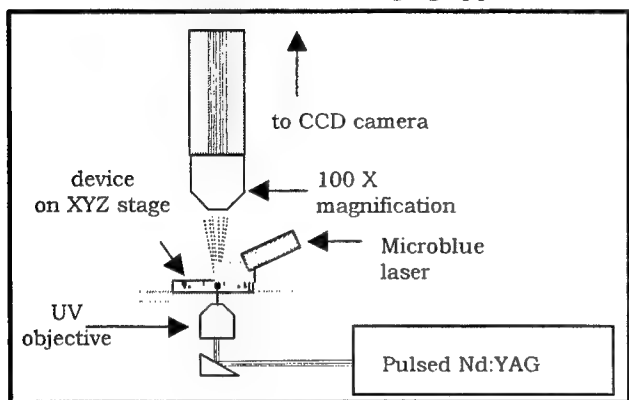
The numerical simulations were performed using the NetFlow module in Memcad [7]. It employs a three-dimensional finite element based tool to solve the Navier-Stokes equations. The electrokinetic effects can be broadly divided into two categories: electrophoresis, involving the transport of a charged species through a carrier due to a differential in the mobility, and electroosmosis, involving the pumping of the carrier fluid due to wall based effects. Electrokinetic effects were incorporated by coupling the Navier-Stokes equations with the Poisson equation for the electric field and with the Poisson-Boltzmann equation for the zeta potential in the electroosmotic cases [8].

The equations are solved here under the assumption of a dilute solution i.e. the carried species does not affect the material properties of the carrier. This allows the equations to be solved in their incompressible form. The finite element meshes were chosen generally to allow for adequate resolution of the

boundary layer and accurate representation of all the experimentally observed fluid physics.

In the design of practical micro-devices, however, accurate coupling of the electrokinetic effects requires the knowledge of several material and physical parameters, such as the diffusivity and the mobility of the solute in the solvent and extent of surface charge on the inner walls of the microchannels. Additionally wall-based effects such as chemical binding sites might exist that affect the flow patterns. Our approach is to extract the required material parameters through quantitative comparison with experimental measurements in simple geometries and use the extracted parameters for simulations and comparisons in more complex geometries.

Schematic of the uncaging apparatus



UV pulse initiates dye



time evolved

Figure 3. Top: Schematic of the experiment. The Nd:YAG laser is used to uncage the dye and a Microblue 473 nm laser is used to excite the fluorescence. Bottom: Illustration of the uncaging process. The starting fluorescent fluid volume is defined by the uncaging laser (either as a spot or as a ribbon).

RESULTS AND DISCUSSION

Figure 4 shows a timed series of pressure-driven flow in microchannels which expand into a large planar reservoir. This figure demonstrates that the simulation qualitatively reproduces the dye dispersion from laminar flow seen during the experiment. The channel width was 100 μm by 40 μm deep. The flow rate was approximately 15 $\mu\text{L/hr}$.

The Reynolds number, Re , in this experiment is typical for bioanalytical systems ($Re = 0.05$) although, it appears low when compared to typical numbers in micropumps ($Re \sim 100$). The images therefore differ from what one might expect to see at higher Reynolds number. The governing equations become linear and harmonic which results in the flow pattern appearing as if it evolved from a point source in Fig. 4. The experiments and simulations in the figure show good agreement which is to be expected for low Reynolds number flows. Similar experiments and simulations were conducted on various other geometrical microchannel shapes and serve to verify the

capabilities of our module in the simulation of pressure-driven flows.

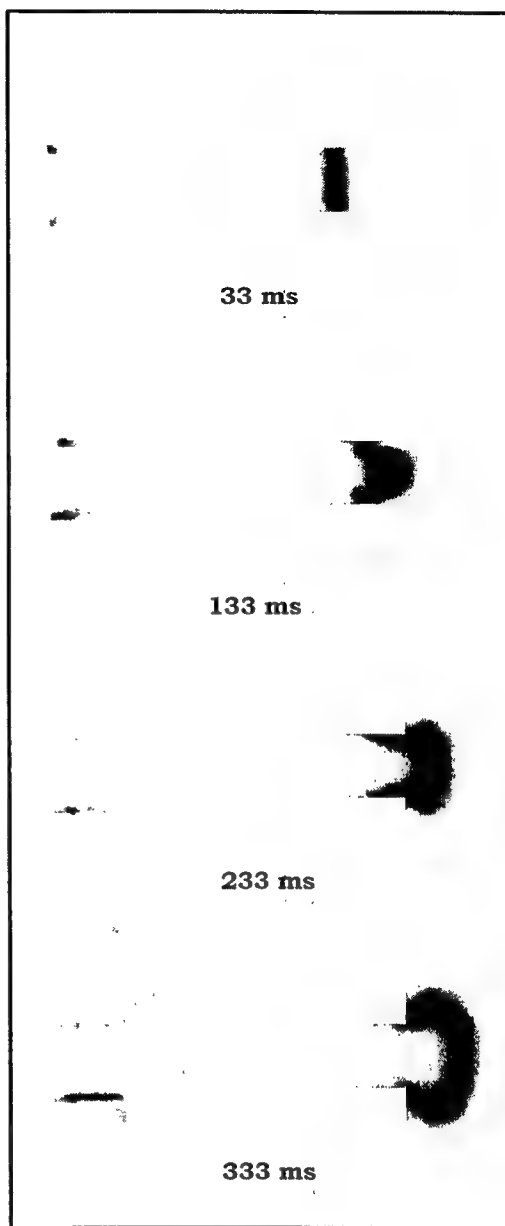


Figure 4. Experimental and simulated pressure-driven flow entering a sudden expansion in an elastomer structure.

Electrokinetic measurements using a range of applied fields and in a number of geometries were compared to simulations of electroosmotic and electrophoretic flow in both elastomer and glass microchannels. Figure 5 shows the simple case of a time-lapse experimental electrophoretic flow at a field strength (E) = 85.8 V/cm in a 50 μm straight elastomer channel with a 0.1% flowable and water soluble polymer added to the dye solution to suppress EOF [6]. For the case of electrophoretic flow where EOF is assumed negligible, the simulated and experimental band shape are similar. The simulated image (right) shows some of the features of the NetFlow software. This image is a 2-D histogram of the integrated experimental fluorescent profile for $t = 0.99$ s. The 2-D histograms provide crucial information regarding the surface forces acting on the flow. The simulation shows an intense

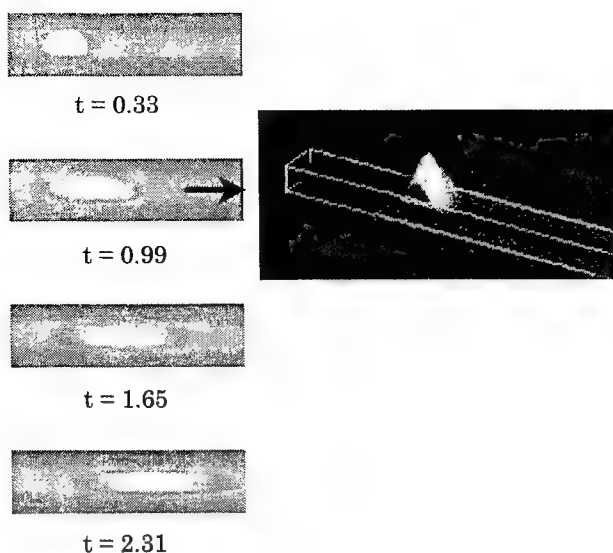


Figure 5. Left: Experimental electrophoretic flow in an elastomer channel, $E = 85.8$ V/cm. Right: Column integration tool from NetFlow used to form 2-D image/histogram corresponding to the fluorescence.

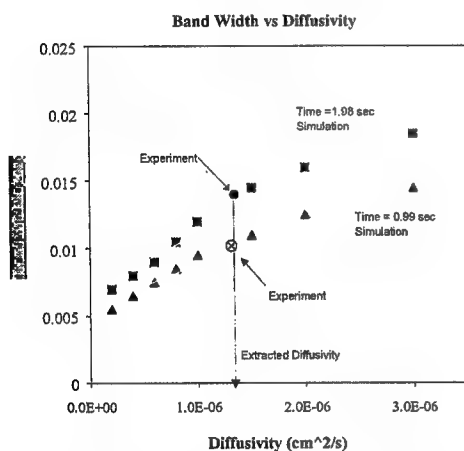


Figure 6. Graph of the simulated band width at two distinct times (squares and triangles) vs. a range of diffusivities. Experimental data (circles) were added to the plot to extract the diffusivity

center region (high mass fraction) and regions of very low intensity along the channel walls, implying that the fluorescent plug may be repelled in this region. The band broadening occurs rapidly because the low mass dye has a high diffusion constant, $\sim 1.3 \times 10^{-6} \text{ cm}^2/\text{s}$. The migration of the band is towards the positive electrode which is expected for electrophoretic flow of a negatively charged species with suppressed EOF.

The simulations can also be used to extract parameters from the experimental data. Figure 6 shows a graph of the simulated band width at two distinct times ($t = 0.99$ s, triangles, and $t = 1.98$ s, squares) as a function of predicted diffusivities. We were able to extract a diffusivity of the uncaged fluorophore in the microchannel, $D = 1.3 \times 10^{-6} \text{ cm}^2/\text{s}$, by comparing the experimental bandwidths (circles) at $t = 1.98$ s and $t = 0.99$ s with the calculated curves. This number seems reasonable considering other reported numbers for diffusivity, $D_{\text{sucrose}} =$

$5.21 \times 10^{-5} \text{ cm}^2/\text{s}$ (at 298 K) [9] (sucrose has 60% the mass of fluorescein) and $D_{\text{fluorescein}}$ was reported to be $3.3 \times 10^{-6} \text{ cm}^2/\text{s}$ by polarography (experimental conditions unknown) [4]. The velocity of the uncaged dye was extracted from the experimental data by plotting the distance versus time for a fluorescent plug moving in an applied field (extracted from experimental images like those shown in Fig. 5). A linear regression was used to obtain the slope or velocity of the line. Velocities at several voltages were obtained in this way and plotted versus the field strength. In the absence of electroosmotic flow, the slope of the line is equal to the electrophoretic mobility (μ). The mobility was estimated to be $2.3 \times 10^{-4} \text{ cm}^2/\text{Vs}$, using the linear region of the graph ($E > 60$ V/cm). The plot shows a non-linear behavior between velocity and field strength for $E < 60$ V/cm. We suspect this is not an interaction between the dye molecules and the solvent because the dye is in such low concentration compared to the solvent. A more likely explanation might be the error associated with obtaining measurements at low field strengths when the diffusion velocity is approximately the same order of magnitude as the convective velocity. The extracted diffusivity and mobility from the elastomer straight channels was used successfully in modeling the plug profile in the glass u-shaped channels implying that these parameters can be used to predict flow in a variety of structures.

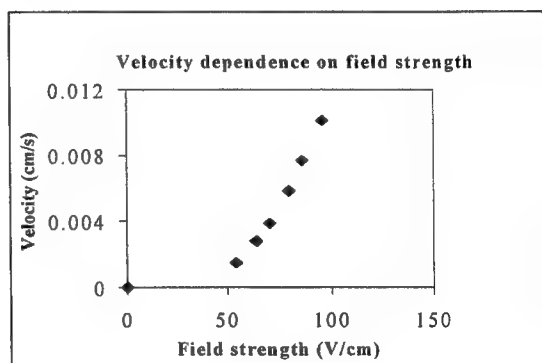


Figure 7. A plot of the velocity vs. field strength used to obtain the mobility of uncaged fluorescein.

Although the field strengths used here are typical for DNA electrophoresis (~ 100 V/cm), the diffusivity of the caged fluorophore in aqueous solution is much higher than that of DNA because of its lower molecular weight ($m.w.$ caged fluorescein = 827 d, $m.w.$ DNA \sim several hundred kd). Therefore, the band profile is dominated by diffusion at these field strengths. In order to predict the loss of resolution from diffusion in DNA separation, a lower diffusivity must be used. We have also examined the flow profile in more complex geometries. Figure 8 compares the experimental to simulated fluorescence profile under electrophoresis in a u-shaped glass microchannel at four different time steps. The images corresponds to $E = 69.5$ V/cm. The inset shows the current density in the same section of the microchannel. As the figure shows, the higher current density on the inner wall of the bend causes the inner region of the band to move faster than the outer region, resulting in an asymmetric profile and eventual band broadening. The greater distance traveled by the species along the outer wall further adds broadening and asymmetry to the band. As it travels past the u-shaped bend the band takes the shape of a parallelogram. In principle, this shape can be corrected by allowing the band to negotiate an equal and opposite turn downstream of this bend.

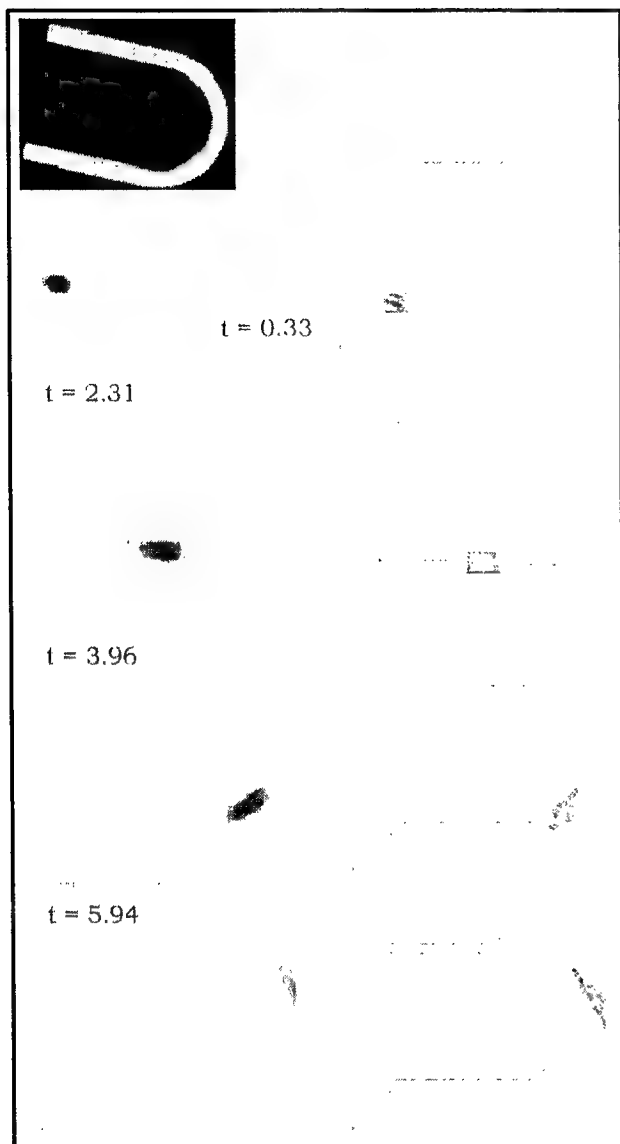


Figure 8. Experimental (left) and simulated (right) electrophoretic flow in a 50 μm diameter glass microchannel (radius of curvature = 0.25 mm), $E = 69.5 \text{ V/cm}$ (inset: current density in channel, the lightest region corresponds to the highest current density).

However, the broadening effects of the bend and the diffusion cannot be corrected.

The simulation at $E = 69.5 \text{ V/cm}$ in Fig. 8 closely matched the experiment. As the field strength was increased further the band was observed to take on a parabolic shape that grew increasingly well-defined with increasing field strength. This behavior is contrary to expectations and is not represented in the numerical models. Consequently, the agreement between experiment and simulations falls off at high voltages. Figure 9 shows the experimental band profile at 0.66 s after uncaging the fluorophore at a range of field strengths, $E = 108 - 125 \text{ V/cm}$. As the field strength increases above $E \sim 100 \text{ V/cm}$, the parabolic profile becomes more pronounced. The increasing parabolic profile with increasing field strength has also been observed in straight microchannels (data not shown) and straight capillaries [10] and is therefore not due to the asymmetry in the field. The simulations in this field range did not match the

experimental data. There are several possible reasons for the observed parabolic shape at high voltages. One possibility is the variation in properties (diffusivity, viscosity, and mobility) across the channel due to joule heating which would cause a temperature gradient in the channel, that becomes more significant at higher voltages. Temperature gradients and their effects on the electrokinetic flow behavior in microchannels have been observed by other researchers [11]. A $1 - 2^\circ \text{C}$ rise in temperature in the channel can cause the mobility (and viscosity

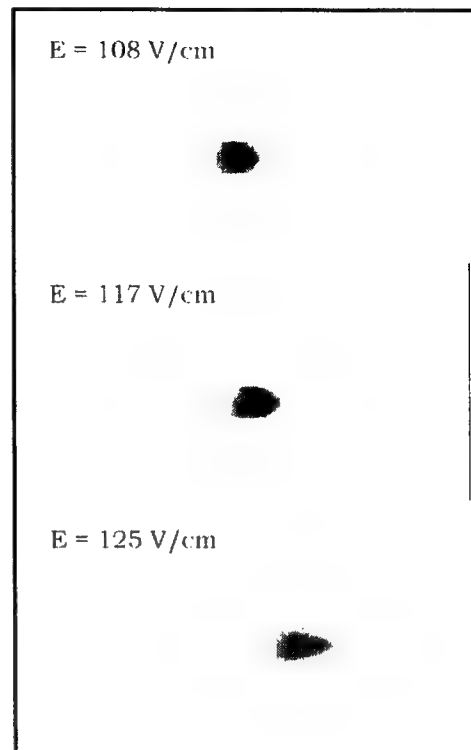


Figure 9. A series of profiles at $t = 0.66 \text{ s}$ after the dye was uncaged at varying field strengths.

of the carrier) to change by 2 – 3%. At higher voltages, where the temperature rise is significant, the change in these material properties may affect the overall flow pattern. A temperature rise may also effect the polymer additive [6], resulting in an incomplete EOF suppression. If EOF is present, then non-uniformities in the zeta potential could induce a pressure gradient and a corresponding parabolic component of the flow. Finally, the parabolic shape may be present at all field strengths but masked by the more rapid decrease in fluorescence at lower field strengths due to diffusion. We are currently exploring these mechanisms to explain the observed deviations from plug-like flow, using both experimental and numerical techniques. An appropriate physical model can then be developed and incorporated into the electrokinetic terms to represent this behavior.

CONCLUSION

We have used a caged fluorophore to image electrokinetic and pressure-driven flow profiles in both glass and elastomer microchannels with varying geometries. Parameters such as diffusivity and mobility were extracted from the experimental data and used in the simulations. This imaging technique has already revealed some interesting and unexpected behavior in these relatively simple fluidic systems. We are looking forward

to using this method to study these behaviors and extract theoretical models or behavioral models suitable for insertion in modeling tools such as NetFlow.

ACKNOWLEDGEMENTS

This work was funded, in part, by DARPA (Grant no. F30602-96-2-0306). We would like to acknowledge EG&G IC Sensors for some of the silicon fabrication, Charles Evans & Associates for AFM data and the use of the Stanford Nanofabrication Facility.

REFERENCES

1. P. Paul, D. Rakestraw, and M. Garguilo, "Imaging of pressure- and electrokinetically -driven flow through open capillaries", *Anal. Chem.*, accepted.
2. J. B. Gravesen, O. S. Jensen, "Microfluidics-a review", *J. Micromech. Microeng.* 3, 168 (1993) and references therein; J. P. Brody and P. Yager, "Low Reynolds number micro-fluidic devices", Solid State Sensors and Actuators Workshop, p. 105, Hilton Head, SC (1996); D. L. Hitt and M. L. Lowe, "Confocal imaging and numerical simulations of converging flows in artificial microvessels", *SPIE*, 2978, 145 (1997); O. Bakajin, J. Chou, S. S. Chan, J. Knight, L. L. Sohn, R. H. Austin, "Nanoscale structures and flows in biotechnology", SPIE, San Jose, CA (1998).
3. C. S. Effenhauser, A. Paulus, A. Manz, and H. M. Widmer, "High speed separation of antisense oligonucleotides on a micromachined capillary electrophoresis device", *Anal. Chem.*, 66, 2949 (1994); S. C. Jacobson, R. Hergenroder, L. B. Koutny, and J. M. Ramsey, "High-speed separations on a microchip", *Anal. Chem.*, 66, 1114 (1994); P. Wilding, J. Pfähler, H. Bau, J. N. Zemel, and L. J. Kricka, "Manipulation and Flow of Biological Fluids in Straight Channels Micromachined in Silicon", *Clinical Chemistry*, 40/1, 43 (1994).
4. A. H. Fan and D. J. Harrison, "Micromachining of capillary electrophoresis injectors and separations on glass chips and evaluation of flow at capillary intersections", *Anal. Chem.*, 66, 177 (1994).
5. C. S. Effenhauser, G. J. M. Bruin, A. Paulus, and M. Ehrat, "Integrated capillary electrophoresis on flexible silicone microdevices: Analysis of DNA restriction fragments and detection of single DNA molecules on microchips", *Anal. Chem.*, 69, 3451 (1997).
6. H. M. Wenz, J. Ziegler, D. M. Demorest, J. Stevens, P. M. Williams, and J. W. Efcavitch (unpublished results); H. M. Wenz, "Capillary electrophoresis as a technique to analyze sequence-induced anomalously migrating DNA fragments", *Nucleic Acids Res.*, 22, 4002 (1994).
7. MEMCAD v4.0, Microcosm Technologies, Inc. (www.memcad.com) (1998).
8. G. M. Mala, D. Li, J. D. Dale, "Heat transfer and fluid flow in microchannels", American Society for Mechanical Engineers, 59, 127 (1996); A. Manz, C. S. Effenhauser, N. Burggraf, D. J. Harrison, K. Seller, and K. Flurl, "Electroosmotic pumping and electrophoretic separations for miniaturized chemical analysis systems", *J. Micromech. Microeng.* 4, 257 (1994); X. C. Qui, L. Hu, J. H. Masliyah, and D. J. Harrison, "Understanding fluid mechanics within electrokinetically pumped microfluidic chips", 1997 *International Conference on Solid-State Sensors and Actuators*, Chicago, IL (1997).
9. P. W. Atkins, "Physical Chemistry", Third Edition (W. H. Freeman and Company, New York 1986).
10. J. I. Molho, A. E. Herr, T. W. Kenny, M. G. Mungal, P. M. St. John, M. G. Garguilo, D. J. Rakestraw, P. H. Paul, M. Deshpande, and J. R. Gilbert, "Fluid transport mechanisms in microfluidic devices", ASME (1998), in preparation.
11. E. Grushka, R. M. McCormick, and J. J. Kirkland, "Effects of temperature gradients on the efficiency of capillary zone electrophoresis separations", *Anal. Chem.* 61, 241 (1989).

Numerical Framework for the Modeling of Electrokinetic Flows

Manish Deshpande^{a1}, Chahid Ghaddar^a, John R. Gilbert^a,
Pamela M. St. John^b, T. Woudenberg^b, C. Connell^b,
Joshua Molho^c, Amy Herr^c, Godfrey Mungal^c, Tom Kenny^c

^aMicrocosm Technologies Inc., Cambridge, MA.

^bPerkin-Elmer Corp., Foster City, CA.

^cStanford University, Stanford CA.

ABSTRACT

This paper presents a numerical framework for design-based analyses of electrokinetic flow in interconnects. Electrokinetic effects, which can be broadly divided into electrophoresis and electroosmosis, are of importance in providing a transport mechanism in microfluidic devices for both pumping and separation. Models for the electrokinetic effects can be derived and coupled to the fluid dynamic equations through appropriate source terms. In the design of practical micro-devices, however, accurate coupling of the electrokinetic effects requires the knowledge of several material and physical parameters, such as the diffusivity and the mobility of the solute in the solvent. Additionally wall-based effects such as chemical binding sites might exist that affect the flow patterns.

In this paper, we address some of these issues by describing a synergistic numerical/experimental process to extract the parameters required. Experiments were conducted to provide the numerical simulations with a mechanism to extract these parameters based on quantitative comparisons with each other. These parameters were then applied in predicting further experiments to validate the process. As part of this research, we have created NetFlow, a tool for micro-fluid analyses. The tool can be validated and applied in existing technologies by first creating test structures to extract representations of the physical phenomena in the device, and then applying them in the design analyses to predict correct behavior.

Keywords : Electrophoresis, Electroosmosis , Numerical Models, Design Analysis, CAD.

1. INTRODUCTION

There is a wide interest in micron-scale integrated chemical/biochemical analysis or synthesis systems, also referred to as lab-on-a-chip. The microfluidic systems being explored today rely on both pressure¹ and electrokinetic effects²⁻⁴ for controlling fluid transport. The design of such systems is hampered by the lack of information required to accurately simulate the systems. The problem is further complicated by the differing solvent/solute combinations that are employed in different applications as well as the actual material and manufacturing process of the system components. Design based analyses of these systems therefore require *a priori* extraction of the material properties. In many cases, however, the material properties, such as the diffusion constant are difficult to extract using purely experimental techniques. On the other hand, a combined experimental/simulation technique is ideally suited for this purpose, and is the focus of this paper.

¹ Further author Information –

Manish Deshpande (correspondence): manish@memcad.com, 215 First Street, Cambridge, MA 02142.
Tel (617) 225-0094 x222, www.memcad.com for information.

Simulation of electrokinetic flows have been reported by several researchers in the literature for both electrophoretic^{5,6} and electroosmotic⁷ flows. In most cases, these simulations have focussed on the numerical problem with well-defined material properties. Using the treatment of electrokinetic flow presented there as a baseline, we demonstrate our attempt at the inverse problem – i.e., the extraction of the parameters required to adequately replicate the experiment. With these parameters in hand, we can then proceed to more complicated design questions that can be answered by simulations. In effect, we demonstrate a mechanism to extract the reduced-order component model for microchannel flow that can then be inserted into the full system model.

2 GOVERNING EQUATIONS

The basic equations describing the fluid motion are the Navier-Stokes equations with appropriate electromigratory flux terms to represent the effect of the applied electric field on the carrier and/or the charged species. The effect of the applied field can be divided into two fundamental components :

Electrophoresis : The basis for electrophoresis is the differential migration of the charged species ions relative to the carrier molecules under the application of the external field. The differential migration is primarily an effect of the difference in the net charge between the solvent and solute ions, although frictional effects may also have some relevance. The migration velocity of the charged species can be expressed in terms of the applied field strength as

$$V_{ep} = \mu_{ep} E \quad [1]$$

where μ_{ep} is the electrophoretic mobility of the ion in the carrier species. It is important to note that in most cases the carrier does not move under electrophoresis.

Electroosmosis : Electroosmosis, in contrast, is a macroscopic phenomenon involving the pumping of a fluid through a channel under the application of the field. In most cases, walls in microchannels are characterized by the presence of surface charges. The charge may either be due to the property of the wall or by adsorption of the charged species from the buffer. In the presence of an electrolyte the surface charge density induces the formation of a double layer in the fluid by attracting oppositely charged ions from the electrolyte to the immediate vicinity of the wall. The application of the electric field exerts a force on the fluid, that is initially felt only within the double layer. As a result the fluid in the near vicinity of the wall starts to move. Due to the viscous forces the fluid in the center of the channel is also accelerated until the net velocity gradient in the radial direction is zero and the whole fluid in the channel moves at a constant velocity.

The determination of the electroosmotic flow field requires the solution of the Navier-Stokes equation. Incorporating the electroosmotic effect as a force the equations become

$$\begin{aligned} \nabla \cdot \mathbf{V}_{eo} &= 0 \quad (\text{Continuity}) \\ \frac{D(\rho \mathbf{V}_{eo})}{Dt} &= -\nabla p + \nabla \cdot \mu \nabla \mathbf{V}_{eo} + \rho_e \mathbf{E} \end{aligned} \quad [2]$$

Where \mathbf{V}_{eo} is the induced electroosmotic velocity. D/Dt is the material derivative of the momentum, μ is the fluid viscosity and p is the pressure.

The last term in the momentum equation represents the electroosmotic force on the fluid. Here ρ_e is the charge density and \mathbf{E} is the electric field intensity. The electric field can be determined by the solution of the potential equation

$$\mathbf{E} = -\nabla \Phi \quad \nabla^2 \Phi = -(\rho_e / \epsilon) \quad [3]$$

The electric potential Φ can be further decomposed into two components, ϕ , the external applied potential and ζ , the zeta potential at the walls.

$$\Phi = \phi + \zeta \quad [4]$$

Under the assumption that the zeta potential effects are confined to a very small region near the wall, the charge distribution can be assumed to be governed by the zeta potential alone, independent of the external field. This allows the decomposition of Eq. [3] into separate equations for the applied field and the zeta potential

$$\nabla^2 \phi = 0 \quad (\text{Applied Potential}) \quad [5a]$$

$$\nabla^2 \zeta = -(\rho_e / \epsilon) \quad (\text{Zeta Potential}) \quad [5b]$$

The equation for the zeta potential can be simplified by the Debye-Hückel⁸ treatment for the charge density. This is based on the concept of a diffuse double layer, proposed initially by Gouy and Chapman⁸, which assumes that the double layer extends for some finite distance into the fluid. Through the Debye-Hückel approximation the charge density on the walls can be determined through the Boltzmann equation and results in the Poisson-Boltzmann equation for the zeta potential

$$\nabla^2 \zeta = \frac{2n_0 z e}{\epsilon \epsilon_0} \sinh\left(\frac{ze}{kT} \zeta\right) \quad [6]$$

where n_0 is the ionic concentration, z is the valence of the charged buffer, e is the electron charge, k is the Boltzmann constant and T is the temperature. ϵ_0 is the permittivity of vacuum.

Under further simplification under the assumption that $ze \ll kT$ equation [6] reduces to the form

$$\nabla^2 \zeta = K^2 \zeta \quad [7]$$

where

$$K = (2n_0 z^2 e^2 / \epsilon \epsilon_0 kT)^{1/2}$$

is known as the Debye-Hückel parameter and " $1/K$ " is termed as the characteristic thickness of the double layer.

The coupled solution of the Eqs (3), (5a) and (7) yields the flow field under the conditions specified.

The motion of a charged species in the electric field can be determined by coupling the species mass equation (8) with the above equations.

$$\frac{\partial c_i}{\partial t} + \left(V_{eo} + V_{ep} \right) \nabla c_i = D \nabla^2 c_i \quad [8]$$

The convective transport of the species is through the combined effect of the electroosmotic motion of the carrier fluid and the electrophoretic transport of the species under the effect of the applied electric field.

The equations presented above are derived under the following assumptions –

Dilute Carrier : The carrier fluid is assumed to be electroneutral everywhere, except within the double layer. The charge distribution is therefore confined to a small region within the double layer.

Dilute Solution : The carrier fluid is assumed to be the predominant species in the mixture. That is, the mass fraction of the charged species is assumed negligible in comparison to the fraction of carrier. This is generally valid in most electrokinetic problems where the species under observation are generally in the millimolar range (corresponding to mass fractions of 10^{-3} and lower). This implication of the dilute assumption is that the solute species does not affect the material properties of the mixture. This allows the species transport equation to be decoupled from the momentum equation.

Individual Species do not affect each other : This assumption is used in describing the flux terms in the above equations, in that the flux of one species does not depend on the fluxes of the other species. This is only true in dilute solutions.

No Chemical Reactions : The charged species are assumed to be fully ionized in the mixture.

As mentioned above the dilute solution allows the density of the mixture to be assumed constant and equal to the density of the carrier. This reduces the problem to the incompressible form. The decoupling of the species equation from the momentum equation also implies that the species conservation condition is not relevant and can be discarded.

3. THE DESIGN PROBLEM

The design analysis for a device of interest generally involves the representation of the device as a system comprising several individual components. The physics of each component is then extracted from detailed computation for that component. The physics of the component can be represented in the system, yielding a reduced order model for the device.

In a microfluidic system the components are traditionally active and passive. Reaction sites, switching chambers etc. form active components, whereas transport and separation channels form passive components. Netflow is about the design of these passive components.

The numerical framework described above enables the computation of the electric and fluid flow fields for a passive component under a specified set of conditions. A design analysis for a practical device, on the other hand, presents several unique challenges. These can be both numerical and physical. Accurate modeling of the device physics requires accurate material property definitions. In general, the carrier fluid is a standard buffer with several additives that are specific to the application under design. The material properties of the carrier fluid can be measured relatively easily. The properties of the solute species such as its diffusivity in the carrier fluid and its electrophoretic mobility are, however, considerably harder to extract. In addition, these properties are often characteristic to specific design conditions.

A second issue is the effect of the chemistry of the channel walls. In microchannels, the walls of the channels often have non-uniform chemistry on them as a result of the manufacturing process, through additives or other reasons. This non-uniform wall chemistry results in flow behavior that cannot be obtained from the above equations without the addition of a model to represent the effect. For example, the presence of chemical binding sites on walls can result in the retardation of the species in the vicinity of the wall. This retardation is highly undesirable since it leads to band broadening, contamination and eventual degradation in the resolution of the detection signal. The effects of the wall chemistry can be represented in a numerical model through retardation terms in the appropriate equations. For example, the affinity between the chemical present on the wall and the charged species can be represented as a retardation force on the charged species. The convection of the charged species is therefore retarded and can be modeled as a variation in the convective velocity that is proportional to its distance from the wall. The exact dependence, however, can only be extracted by quantitative comparison between experiment and simulation. The numerical framework presented in this paper enables extraction of this dependency as well.

In the case of electroosmosis, the accurate solution of the Poisson-Boltzmann equation requires the resolution of the double layer. The thickness of this double layer is as described in eq. [7] above. In general, the double layer thickness is extremely small in comparison to the channel width. For example, under nominal conditions for a 50 micron channel containing water, the double layer thickness is of O(nm). Adequate resolution of scales of this order are not generally tractable and further simplification is necessary. The effect of the potential across the double layer (the zeta potential) is felt as a force on the fluid at the edge of the double layer. The solution to the Poisson-Boltzmann equation can then be reverted to the Smoluchowski equation at the outer edge of the double layer :

$$V_{eo} = \mu_{eo} E \quad [9]$$

Which is analogous to the equation for the electrophoretic velocity, Eq. [1]. The electroosmotic mobility can then also be extracted using an approach similar to the electrophoretic case.

In summary, the design problem is as follows : For a given application, the various physical properties that affect the behavior of the device must be extracted in an appropriate parameter space. The properties can then be used in that parameter space to conduct further analyses. Netflow is the first step in enabling this process.

4. SOLUTION METHODOLOGY

The modeling of electrokinetic effects is incorporated into the NetFlow module in the MEMCAD system. MEMCAD is an integrated design environment consisting of 3D design, modeling and simulation software tools which enable the creation of complex MEMS/MST devices. Inherent in the design process in Memcad is the ability to translate from a layout and process view of the device to a solid model and a suite of simulators to characterize the various physical phenomena present in the device. Netflow, which is a part of the suite, is specific to the analysis of chemical transport in microchannels. It is an ongoing program, and is a result of a collaboration between Microcosm, Perkin-Elmer Corp. and Stanford University.

The numerical solution of the above equations is performed using a three-dimensional finite element based CFD engine. The Memcad interface allows the user to define the geometry from layout and process, or, optionally directly build the model in the solid modeler. Once meshed, the model is available to a suite of solvers for various physical domains, and to the simulation manager to parametrize the dependency in any domain. A schematic of the solution methodology is shown in Fig. 1.

The specific problems presented here are for electrophoretic flow in microchannels. The parameters that need to be extracted are the diffusivity and mobility of the charged species in the channels. The assumption here is that the mobility and diffusivity are independent of the geometry of the channels, and in the electrophoretic case, also independent of the channel wall material. That is, properties extracted from simple structures can be applied to problems in more complex structures, assuming the channel materials and manufacturing processes remain the same.

5. EXPERIMENTAL SETUP

Experimental studies of electrophoretic flow in microchannels were conducted at the Applied Biosystems Division at Perkin-Elmer, and at Stanford. A brief description is provided here. Greater details can be found elsewhere⁹. The elastomer microchannels were fabricated by making positive replicas of raised silicon structures fabricated using photolithography and an STS deep reactive ion etch (DRIE). The elastomer channels were sealed with either glass microscope slides or elastomer coated glass microscope slides.

A commercially available additive made from a polyacrylamide short chain polymer (ABI DNA Fragment Analysis Reagent 7% w/w) was used (0.1% v/v aqueous) to suppress electroosmotic flow¹⁰ (EOF) in both glass and elastomer structures. Although EOF suppression was verified by observing ion travel under an applied field, the extent of suppression was not quantified. In this paper, electrophoretic flow refers to negatively charged dye migration towards the positive electrode and electroosmotic flow refers to dye carried toward the negative electrode, despite charge.

The species tracked was a caged fluorophore (fluorescein) was purchased from Molecular Probes and used in micromolar quantities dissolved in either distilled water or Tris-EDTA buffer, pH = 7.4. The dye is negatively charged, both caged and uncaged (fluorescein, -2). When caged, the dye solution is non-fluorescent. Upon photo-activation of a UV light illuminated volume, the protecting group is cleaved and the dye fluoresces. Fluorescence images of the molecules diffusing and moving in the local flow were collected using a microscope objective (total magnification = 100 X) and a video rate, interlaced camera. Images were analyzed to extract flow parameters by comparing against simulations.

6. RESULTS

Electrokinetic measurements using a range of applied fields and in a number of geometries were compared to simulations of electroosmotic and electrophoretic flow in both elastomer and glass microchannels. Representative results are shown in this section. The field strengths studied ranged from 0 to 150 V/cm. Simulations were conducted for the same conditions and the results were compared to experiment to extract the required material parameters – in this case the diffusivity and mobility of the charged species.

The zero voltage case enables the extraction of diffusivity data, since diffusion is the only transport mechanism present. Note that, as mentioned before, a polymer is added to suppress electroosmotic flow – the bulk carrier is therefore stationary. The mechanism for extraction of the diffusion constant is as follows – a series of runs are conducted for a range of diffusion constants using the Simulation Manager. The results are compared with the experimental observations – in this case the broadening of the band with time – and the diffusion constant is then extracted corresponding to the value that matches experiment.

Time sequence experimental images of flow at zero voltage are shown in Fig. 2. The corresponding simulations for one diffusion constant are also shown in the figure. The initial band shape in the experiment is approximately Gaussian – the initial species distribution in the simulations were also specified to be Gaussian to represent the experiment. The band broadens rapidly because the dye has a high diffusion constant and the initial Gaussian distribution quickly becomes uniform and rectangular. As expected, the simulations also replicate this phenomenon.

Figure 3 shows a graph of the simulated band width at two distinct times ($t = 0.99$ s and $t = 1.98$ s) as a function of predicted diffusivities. The diffusion constant can be extracted from this graph by superimposing the experimentally measured band widths at the same times (shown as the circles in the figure). The diffusion constant extracted is approximately 1.3×10^{-6} cm²/s. As the figure shows the diffusion constant extracted at one time is corroborated by that extracted at a different time. The constant extracted seems reasonable considering other reported numbers for diffusivity, $D_{\text{sucrose}} = 5.21 \times 10^{-5}$ cm²/s (at 298 K)¹¹ (sucrose has 60% the mass of fluorescein) and $D_{\text{fluorescein}}$ was reported to be 3.3×10^{-6} cm²/s by polarography (experimental conditions unknown)³. A point to note is that the curves corresponding to the simulations are extracted from a single Memcad run without user intervention.

To extract the mobility, we chose a field strength (E) of 85.8 V/cm for the comparison. Figure 4 shows the experimental time lapse images for this field strength in similar channels as above. For the case of electrophoretic flow where EOF is assumed negligible, the simulated and experimental band shape are similar. The simulated image (right) shows some of the features of the NetFlow software. This image is a 2-D histogram of the integrated experimental fluorescent profile for $t = 0.99$ s. The 2-D histograms provide crucial information regarding the surface forces acting on the flow. The simulation shows an intense center region (high mass fraction) and regions of very low intensity along the channel walls, implying that the fluorescent plug may be repelled in this region. The band broadening occurs rapidly because the low mass dye has a high diffusion constant, $\sim 1.3 \times 10^{-6}$ cm²/s. The migration of the band is towards the positive electrode which is expected for electrophoretic flow of a negatively charged species with suppressed EOF.

The velocity of the uncaged dye was extracted from the experimental data by plotting the distance versus time for a fluorescent plug moving in an applied field shown in Figure 5 (extracted from experimental images like those shown in Fig. 4). A linear regression was used to obtain the slope or velocity of the line. Velocities at several voltages were obtained in this way and plotted versus the field strength. In the absence of electroosmotic flow, the slope of the line is equal to the electrophoretic mobility (μ). The mobility was estimated to be 2.3×10^{-4} cm²/Vs, using the linear region of the graph ($E > 60$ V/cm). The plot shows a non-linear behavior between velocity and field strength for $E < 60$ V/cm. We suspect this is not an interaction between the dye molecules and the solvent because the dye is in such low concentration compared to the solvent. A more likely explanation might be the error associated with obtaining measurements at low field strengths when the diffusion velocity is approximately the same order of magnitude as the convective velocity.

Although the field strengths used here are typical for DNA electrophoresis (~ 100 V/cm), the diffusivity of the caged fluorophore in aqueous solution is much higher than that of DNA because of its lower molecular weight (m.w. caged fluorescein = 827 d, m.w. DNA \sim several hundred kd). Therefore, the band profile is dominated by diffusion at these field strengths. In order to predict the loss of resolution from diffusion in DNA separation, a lower diffusivity must be used.

The success of this approach is however dependent on the ability to use the extracted parameters to flow in more complex geometries. To demonstrate this we chose u-shaped microchannels using the same buffer and dye combination. Figure 6 4 shows a schematic (top) of the various geometries used in these flow studies. The motivation in using a serpentine structure for DNA separation is that we can separate longer fragments of DNA in nearly the same space required to separate the shorter fragments. The channels were fabricated by etching a series of 50 μ m width, various length serpentine channels into a 4" x 4" borosilicate glass plate which was bonded to a second plate to seal. These channels are trapezoidal in cross-section and require considerable resolution to accurately simulate the flow field. Full 3D computations were conducted. A nominal mesh used in the simulations contained roughly 2000 parabolic finite elements. Initial simulations to verify mesh independence were conducted under nominal conditions and are not presented here.

Figure 7 compares the experimental to simulated fluorescence profile under electrophoresis in a u-shaped glass microchannel at four different time steps. The images corresponds to $E = 69.5$ V/cm. As before, EOF was suppressed by the polymer additive. The higher current density on the inner wall of the bend causes the inner region of the band to move faster than the outer region, resulting in an asymmetric profile and eventual band broadening. The greater distance traveled by the species along the outer wall further adds broadening and asymmetry to the band. As it travels past the u-shaped bend the band takes the shape of a parallelogram. In principle, this shape can be corrected by allowing the band to negotiate an equal and opposite turn downstream of this bend

The simulations for this configuration at the same field strength are also shown in Fig. 7 at the same times as the experiment. The agreement between experiment and simulation is quite good indicating that the diffusivity and mobility extracted from the straight channels are reasonably valid in the more complex curved channels as well.

We have also conducted similar experimental/numerical comparisons for electroosmotic flow to extract an electroosmotic mobility as a function of the field strength. The procedure is similar to the electrophoretic case and is not reproduced here.

The net result of the work presented here is quite encouraging. Using experimental data generated in fairly simple test structures, we are able to generate the parameter required for the numerical analysis of more complex structures. Simple straight channel structures such as those used in the baseline cases are generally easy to manufacture, set up and test experimentally. A test procedure of this nature can also be used to ensure conformity of manufactured structures to some baseline specifications for the device. This is analogous to procedures used in both the MEMS and IC areas.

7. CONCLUSIONS

We have developed Netflow, a CAD tool for chemical transport in microchannels. The tool is built up on the existing framework for MEMCAD, which is a general purpose tool for the design of MEMS and microfluidic systems. Netflow enables the simulation of electrophoretic, electroosmotic, diffusive and pressure-driven flow in microchannels. In its application to practical design problems, however, CAD tools require the knowledge of material and physical parameters, that are generally not known. In this paper, we demonstrate a mechanism to first extract the parameters of interest from simple test structures and then apply them in the analysis of more complex structures. This procedure is analogous to that used in both MEMS and IC design.

The Simulation Manager tool in Memcad allows the computation of the effect of parametric variation in a given problem. This procedure is employed in iterating over a range of values of the parameter of interest, and then comparing with experimental measurements to extract the required parameter value. We have demonstrated this procedure for the extraction of diffusivity and electrophoretic mobility data and have conducted measurements for electroosmotic mobility as well. Using data obtained in straight channels we were able to make reasonably good predictions of flow through curved channels, thereby validating this approach. The next step is to implement this procedure in the design of a practical micro-device.

8. REFERENCES

1. P. Paul, D. Rakestraw, and M. Garguilo, "Imaging of pressure- and electrokinetically -driven flow through open capillaries", *Anal. Chem.*, accepted.
2. J. B. Gravesen, O. S. Jensen, "Microfluidics-a review", *J. Micromech. Microeng.* 3, 168 (1993).
3. A. H. Fan and D. J. Harrison, "Micromachining of capillary electrophoresis injectors and separations on glass chips and evaluation of flow at capillary intersections", *Anal. Chem.*, 66, 177 (1994)
4. A. Manz, C. S. Effenhauser, N. Burggraf, D. J. Harrison, K. Sella, and K. Flurl, "Electroosmotic pumping and electrophoretic separations for miniaturized chemical analysis systems", *J. Micromech. Microeng.* 4, 257 (1994).
5. X. C. Qui, L. Hu, J. H. Masliyah, and D. J. Harrison, "Understanding fluid mechanics within electrokinetically pumped microfluidic chips", *1997 International Conference on Solid-State Sensors and Actuators*, Chicago, IL (1997).
6. G. M. Mala, D. Li, J. D. Dale, "Heat transfer and fluid flow in microchannels", *American Society for Mechanical Engineers*, 59, 127 (1996).
7. N. A. Patankar and H. H. Hu, "Numerical Simulation of Electroosmotic Flow", *Anal. Chem.*, 70, 1870-81 (1998).
8. in Glasstone, "An Introduction to Electrochemistry", Litton Ed., (1942).
9. St. John, P.M. et al, "Metrology and Simulation of Chemical Transport in Microchannels", *Solid State Sensors and Actuators Workshop*, Hilton Head, SC (1998).
10. H. M. Wenz, J. Ziegler, D. M. Demorest, J. Stevens, P. M. Williams, and J. W. Efcavitch (unpublished results); H. M. Wenz, "Capillary electrophoresis as a technique to analyze sequence-induced anomalously migrating DNA fragments", *Nucleic Acids Res.*, 22, 4002 (1994).
11. P. W. Atkins, "Physical Chemistry", Third Edition (W. H. Freeman and Company, New York 1986).

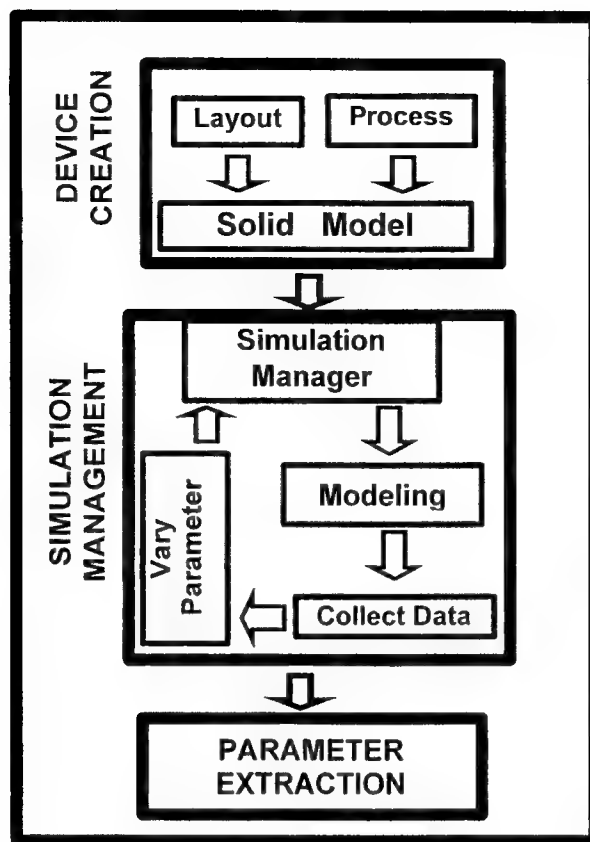


Figure 1 : Schematic of Design Process employed in Material Property Extraction.

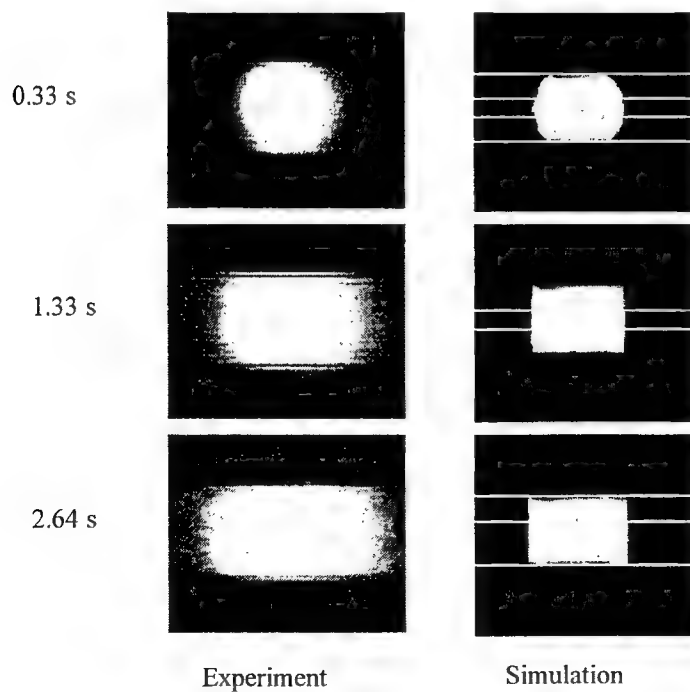


Figure 2: Experimental and Simulation images of zero-voltage flow in elastomer microchannels.

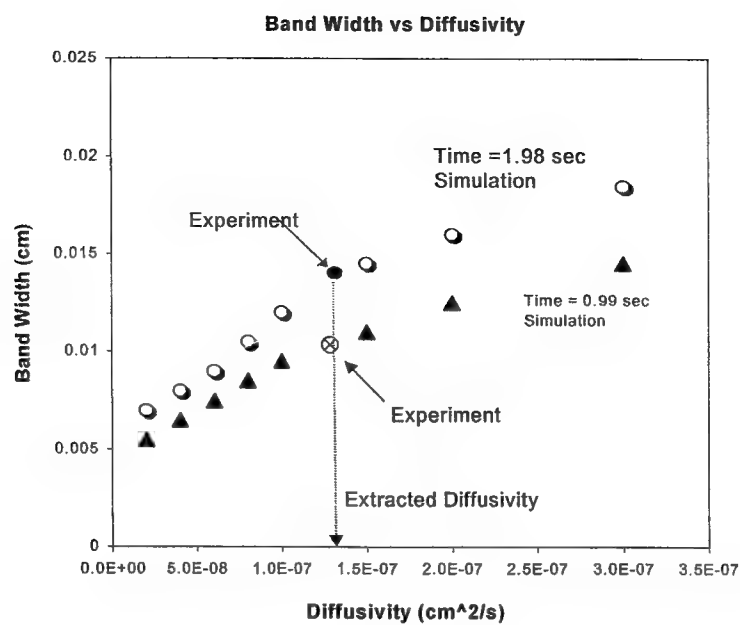


Figure 3 : Graph of the simulated band width at two distinct times ($t = 0.99$ sec, triangles and $t = 1.96$ sec, squares) vs. a range of predicted diffusivities. Circles correspond to experimental values for band width which were used to extract the diffusivity.

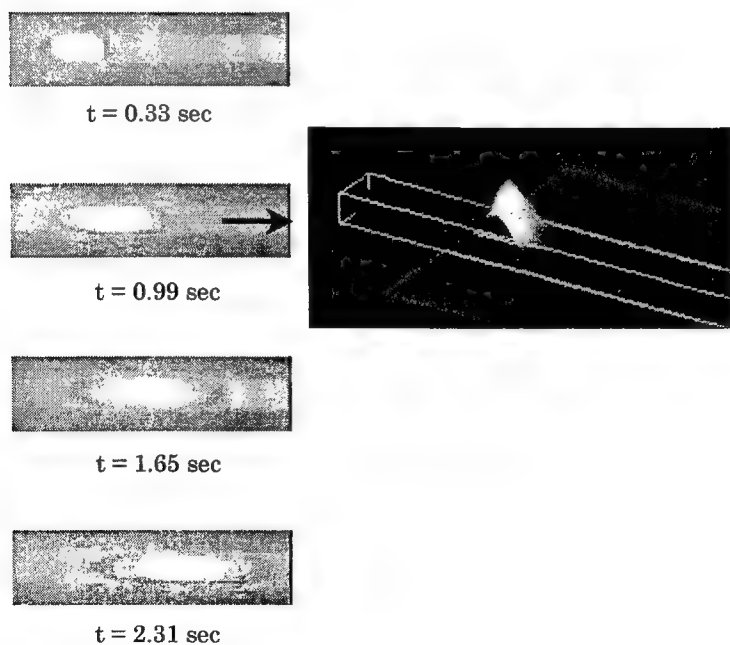


Figure 4 : Left: Experimental electrophoretic flow in an elastomer channel, $E = 85.8$ V/cm. Right: Column integration tool from NetFlow used to form 2-D image/histogram corresponding to the fluorescence.

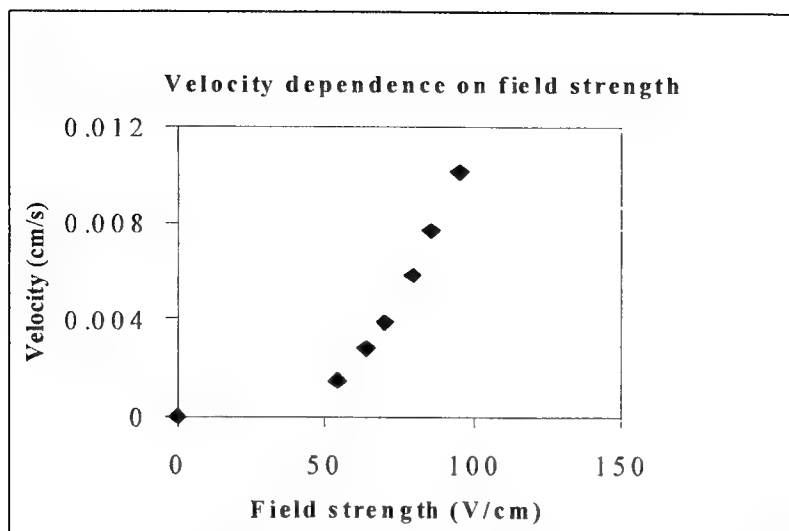


Fig 5. Velocity vs. field strength used to obtain the mobility of uncaged fluorescein

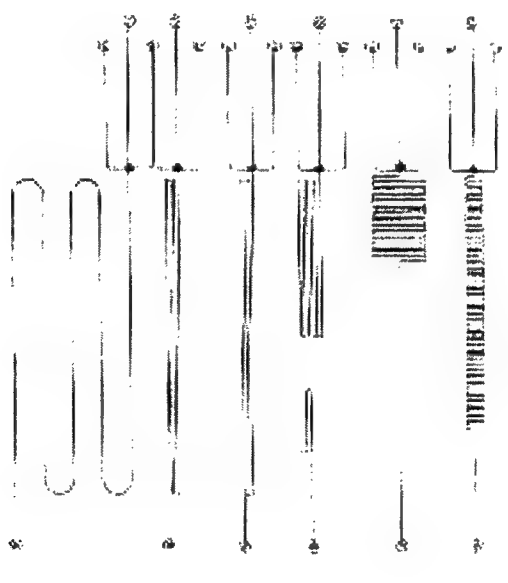


Fig 6. Schematic (scaled to size) of the various glass serpentine channels

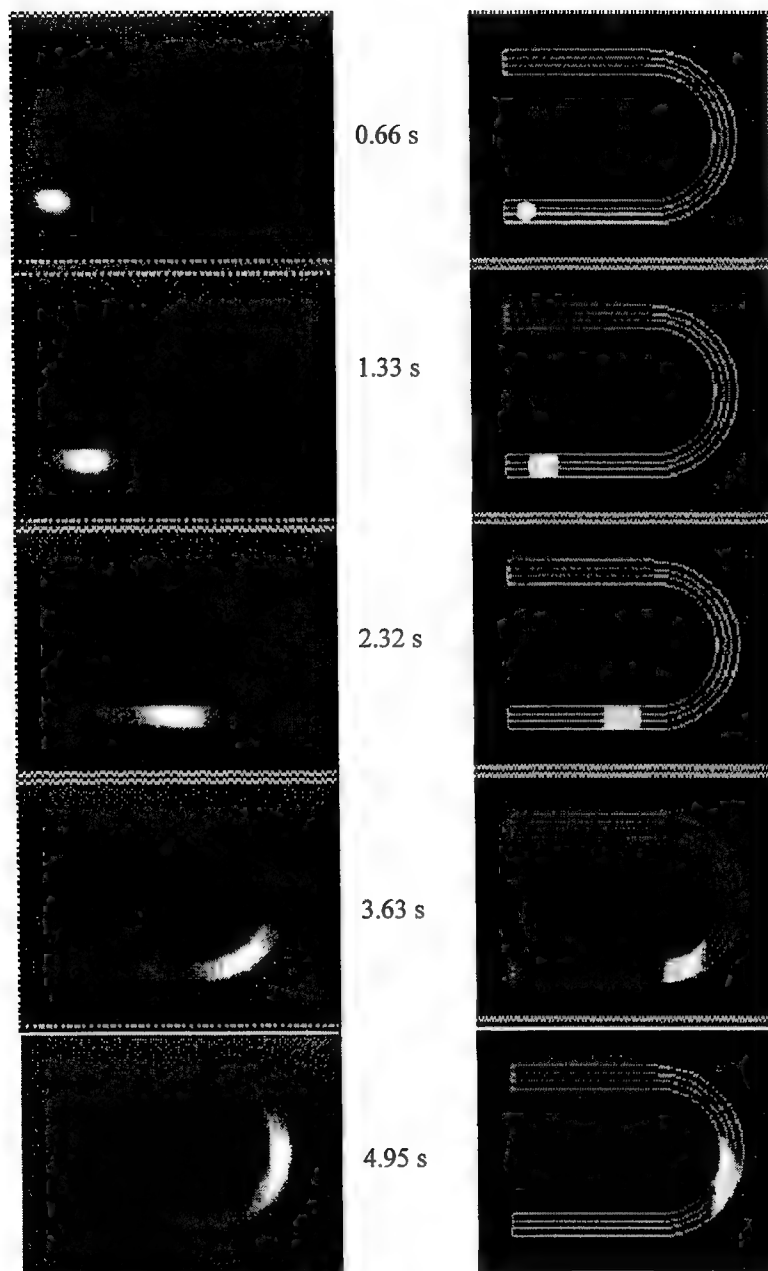


Figure 7: A series of timed images of a fluorescent plug under electrophoretic transport in a curved glass channel. Channel diameter = 50 μ m. Field strength = 76.3 V/cm. All time in seconds.

FLUID TRANSPORT MECHANISMS IN MICROFLUIDIC DEVICES

**Joshua I. Molho, Amy E. Herr,
Thomas W. Kenny, M. Godfrey Mungal**

Stanford University, Mechanical Engineering Department
551 Terman, Stanford, CA 94305-4021
ph: (650) 725-1595, fx: (650) 723-3521
jmolho@stanford.edu

Manish Deshpande, John R. Gilbert

Microcosm Technologies
215 First Street #219
Cambridge, MA 02142
support@memcad.com

Michael G. Garguilo, Phillip H. Paul

Sandia National Laboratories
7011 East Avenue, Livermore, CA 94550
mgarlu@sandia.gov

**Pamela M. St. John,
Timothy M. Woudenberg, Charles Connell**

Perkin-Elmer Applied Biosystems
850 Lincoln Centre Drive, Foster City, CA 94404
StJohnPM@perkin-elmer.com

ABSTRACT

Most microfluidic systems rely on one of two manners of fluid transport: pressure-driven or electrokinetically-driven flow. This investigation focuses on describing these flows in microfabricated channels and small diameter capillary tubes. Flow characterization is accomplished by interrogation of micron-scale fluid regions through a powerful, non-intrusive flow imaging technique. Interesting phenomena have been observed from these detailed examinations. Our results are presented in conjunction with an evaluation of mechanisms that potentially explain observed deviations from the Helmholtz-Smoluchowski equation. In particular, we show that observed perturbations of electrokinetic flow in open capillaries might be caused by induced pressure gradients. We also show how these induced pressure gradients may globally perturb the flow in an electrokinetically-driven microfluidic system.

NOMENCLATURE

Symbol	Definition	Units (SI)
E	electric field	$V m^{-1}$
E_x	axial electric field	$V m^{-1}$
F	Faraday constant ($N_a e$)	$C mol^{-1}$
I_0	Modified Bessel function	
L	length of capillary	m
P	Pressure	Pa
Q	Volumetric flow rate	$m^3 s^{-1}$
R	universal gas constant	$J mol^{-1} K^{-1}$
S	source term	$W m^{-3}$
T	temperature	K
T_0	wall temperature	K
U	electroosmotic or electrophoretic velocity	$m s^{-1}$

U_0	electrophoretic velocity at T_0	$m s^{-1}$
c_0	ion concentration	$mol m^{-3}$
dV	differential volume	m^3
k	thermal conductivity	$W m^{-1} K^{-1}$
r	radial dimension	m
r_0	capillary inner radius	m
u	velocity distribution	$m s^{-1}$
x	axial dimension	m
x_0	axial position of change in wall zeta potential	m
y	distance from planar surface	m
z	charge number	
ϵ	permittivity	$C V^{-1} m^{-1}$
ϕ	electric potential	V
λ_D	Debye length	m
μ	viscosity	Pa s
μ_0	viscosity of water at T_0	Pa s
ρ_E	electric charge density	$C m^{-3}$
ρ	resistivity	ohm m
ζ	zeta potential	V
ζ_{EO}	electroosmotic zeta potential	V
ζ_{EP}	electrophoretic zeta potential	V

INTRODUCTION

Originally emerging from the field of analytical chemistry, micro total analysis systems (μ TAS) have recently enjoyed wide interest. Micro total analysis systems and other

microfluidic systems rely on both pressure and electrokinetic mechanisms for fluid transport. Complicated relationships can arise between the physical characteristics of the microchannels and the behavior of the multi-component fluids flowing through the channels. These relationships have not been systematically studied and are not yet completely understood. In practice, researchers are forced to rely on the use of trial and error in the design of miniaturized fluidic systems.

In this investigation, we employed a caged fluorescence imaging technique in an effort to determine the mechanisms that contribute to the fluid flow in microfluidic systems. Aided with characterizations of relatively simple flows, we endeavor to accurately predict the flow behavior in more complicated flows and geometries.

BACKGROUND

Electrokinetic transport refers to the combination of *electroosmotic* and *electrophoretic* transport. For a historical review of electrokinetic theory, see Burgreen and Nakach (1964). Included below is a brief description of each type of transport.

Electroosmosis

Electroosmosis refers to the *bulk* movement of an aqueous solution past a stationary solid surface, due to an externally applied electric field. Electroosmosis requires the existence of a *charged double-layer* at the solid-liquid interface. This charged double layer results from an attraction between bound surface charges and ions in the passing fluid. In glass capillaries, surface silanol groups become deprotonated and, therefore, are negatively charged. This negatively charged surface attracts positive ions present in the flow. In the situations addressed in this paper, only a very thin layer near the wall has a net charge.

Rice and Whitehead (1965) give a complete analysis of electroosmotic flow in round capillaries; here we quote only a few significant results to which we will refer later. At equilibrium, a Boltzmann distribution of the charges in the solution will exist (Probstein, 1994) with the charge density distribution represented by:

$$\rho_E = zFc_0 \left[\exp\left(\frac{-zF\phi}{RT}\right) - \exp\left(\frac{zF\phi}{RT}\right) \right]. \quad (1)$$

The potential field is determined by solving the Poisson-Boltzmann equation, resulting in the following charge density,

$$\rho_E = \frac{-\varepsilon}{\lambda_D^2} \zeta_{EO} \frac{I_o(r/\lambda_D)}{I_o(r_o/\lambda_D)}. \quad (2)$$

In our experiments, λ_D/r_o is approximately 10^{-4} ; thus the double layer is very thin. The equation of motion for steady, low Reynolds number, incompressible flow is:

$$\mu \nabla^2 \mathbf{u} = -\rho_E \mathbf{E} + \nabla P. \quad (3)$$

In the limit of a small Debye length, λ_D , solving Eq. (3) yields the *Helmholtz-Smoluchowski* equation for the electroosmotic velocity.

$$U = \frac{-\varepsilon \zeta_{EO} E_x}{\mu} \quad (4)$$

The *Helmholtz-Smoluchowski* equation predicts a “plug-like” velocity profile when the Debye length is much less than the capillary diameter. The electroosmotic velocity, U , is approximately 0.1 mm/sec, for $\zeta = 0.1$ V, $E_x = 100$ V/cm, and μ equal to the viscosity of water, (Probstein, 1994).

Electrophoresis

Electrophoresis describes the motion of a charged surface submerged in a fluid under the action of an applied electric field. Considering the case of a charged dye molecule, it can be shown (Probstein, 1994) that the electrophoretic velocity of the dye is again described by the *Helmholtz-Smoluchowski* equation.

$$U = \frac{\varepsilon \zeta_{EP} E_x}{\mu} \quad (5)$$

The electroosmotic zeta potential is a property of the capillary surface while the electrophoretic zeta potential is a property of the charged dye. In general, these two zeta potentials will not be the same.

It is important to note that electroosmosis results in a net mass transfer of the aqueous solution; whereas, electrophoresis causes movement of charged particles or molecules *through a stationary solution*. For a net-neutral solution of charged molecules, electrophoresis will not result in bulk motion of the solvent. Also note that both derivations shown above result in a velocity that is not a function of the radial position; hence, it is termed a “plug-like” flow.

EXPERIMENTAL DETAILS

Two different types of microchannels were used in this investigation. Initially, we used rectangular silicone microchannels. We then began investigating flows within round glass capillaries with an internal diameter of 100 μm . The capillaries were employed in an effort to isolate unexplained flow phenomena observed in our initial silicone microchannel investigation.

To create the silicone channels, *silicon* microchannel molds were fabricated as “negative” masters using standard

photolithography. An STS deep reactive ion etch (DRIE) was used to create raised rectangular structures (inverted channels) with dimensions of 10-200 μm in width, 5 cm in length and 40 μm in height. An RTV silicone (Dow Corning Sylgard 184) was used to form positive replicas of the silicon structures (Effenhauser, et al. 1997). A photograph of a sealed replica is shown in Fig. 1. The elastomer channels were sealed with either glass microscope slides or elastomer coated glass microscope slides.



Figure 1. Photograph of the elastomer device with three test microchannels. The circles are the injection wells and the squares are used to study pressure-driven flow in a sudden expansion.

Our experimental approach utilized caged fluorescent dyes to image the flows. These dyes were activated (uncaged) by a UV laser beam and tracked by fluorescence imaging, see Fig. 2, (Paul et al, 1998). In contrast to standard methods injecting dye, this visualization technique allows definition of narrow, fluorescent regions at virtually any location along the channel. Specifically, this allows for a *precise* definition of a small fluorescent region and therefore an improved determination of the dye profile. Therefore, this caged fluorescence technique has advantages over injection methods that must transport the dye from the location of injection to the region of interest.

The caged fluorophores were purchased from Molecular Probes and used in millimolar quantities. For the pressure-driven studies, a caged fluorescein was dissolved in distilled

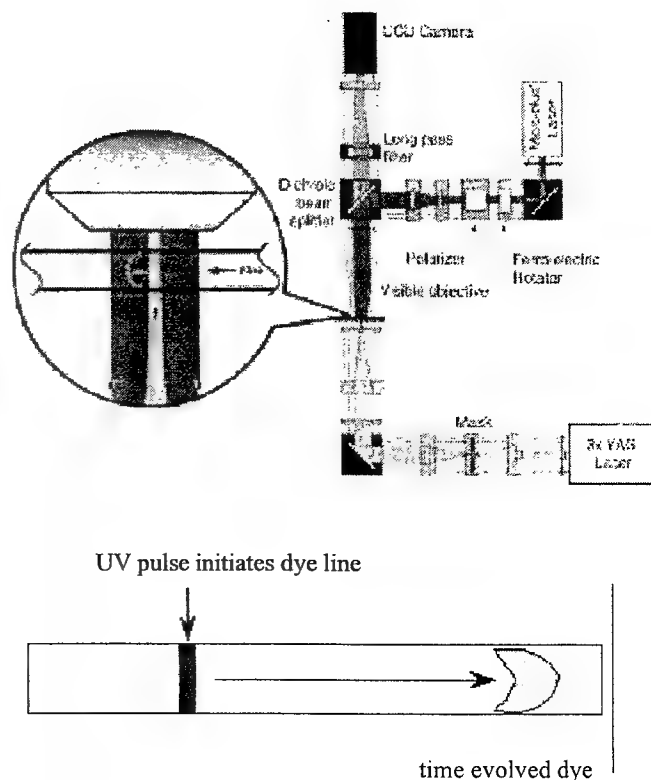


Figure 2. Top: Schematic of the experiment. The Nd:YAG laser is used to uncage the dye and a Microblue 473 nm laser is used to excite the fluorescence. Bottom: Illustration of the uncaging process. The uncaging laser defines the starting fluorescent fluid volume.

water. For the electrokinetic studies, a caged rhodamine was dissolved in Tris-EDTA buffer. The dyes are negatively charged when uncaged and may be either charged or uncharged when caged. When caged, the dye solution is non-fluorescent. Upon photo-activation of a UV light illuminated volume, the protecting group is cleaved and the dye becomes fluorescent. Approximately 100 μJ (per pulse) of 355 nm light from a pulsed Nd:YAG laser uncages the dye. The uncaged region is roughly 20 μm along the length of the channel or capillary and extends across its full width (Fig. 2). The laser beam was focused using a UV microscope objective that defined a sharp start zone. A continuous wave Microblue diode pumped laser at 473 nm (Uniphase) was used for fluorescence excitation after activation (Fig. 2). Fluorescence images of the molecules diffusing and moving in the local flow were collected using a microscope objective and a video rate, interlaced camera (Texas Instruments MC-780PH).

RESULTS

We have investigated transport in microfluidic systems and present experimental studies of pressure-driven and electrokinetic flows. We also present numerical simulations which were performed using the NetFlow module in Memcad (MEMCAD, 1998). The NetFlow module employs a three-dimensional finite element based tool to solve the Navier-Stokes equations. We note that the pressure-driven flow data show good agreement between the preliminary experiments and the simulations. Measurements of the electrokinetic flows, however, reveal deviations from simple theory.

The evolution of a pressure-driven fluorescent profile is compared to a corresponding sequence of simulations in Fig. 3. The agreement is good, but note that there is dye retention near the walls that is not duplicated in the numerical simulations. This dye retention could be due to surface roughness. Atomic force microscopy indicates that the silicone channel has an RMS surface roughness of ~ 7 nm.

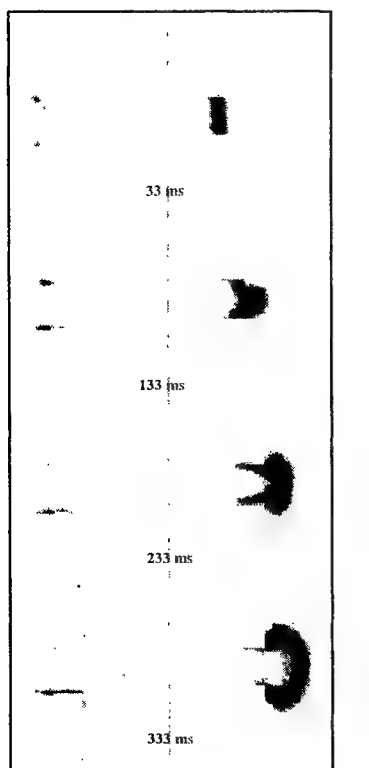


Figure 3. Experimental (left) and simulated (right) pressure-driven flow entering a sudden expansion in an elastomer structure. The channel entering the expansion is rectangular ($100\ \mu\text{m}$ wide and $40\ \mu\text{m}$ deep)

The evolution of an electrokinetically-driven fluorescent profile in a round, fused-silica capillary is shown in Fig. 4. These images reveal that the velocity profile appears to be constant across the channel, in agreement with Eq. (4). Figure 5 shows electrokinetic flow in a DBwax-coated (polyethylene

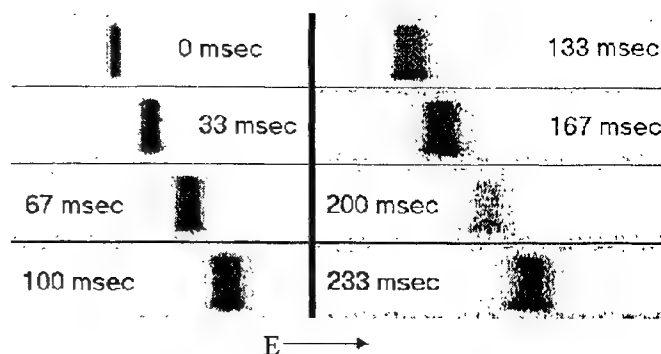


Figure 4. Electrokinetic flow in a $75\ \mu\text{m}$ diameter fused-silica capillary exhibiting a plug-like velocity profile. Applied field strength was 350 volts/cm. The numbers with each image correspond to the time in milliseconds after the uncaging pulse.

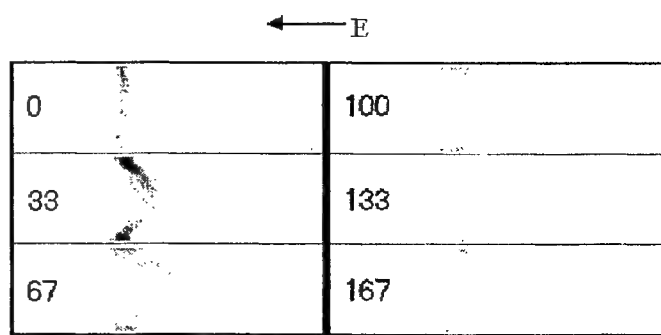


Figure 5. Electrokinetic flow in DBwax-coated (polyethylene glycol), $100\ \mu\text{m}$ diameter fused-silica capillary. The wax-coated capillaries were purchased from J&W Scientific. Applied field strength was 245 volts/cm. The numbers with each image correspond to the time in milliseconds after the uncaging pulse.

glycol) capillary. The wax coating is used to suppress electroosmotic flow, so that the movement of charged particles in the flow is due to electrophoresis only. However, these images show a pronounced parabolic velocity in the direction opposing the electric field. This profile does not agree with Eq. (5), and would be difficult to image without a high-resolution measurement technique such as caged fluorescence imaging. Note that we observed no motion of the dye without application of the electric field, verifying that there was no externally applied pressure gradient. Parabolic components to the electrokinetic velocity profile have previously been observed in capillaries (Paul et al, 1998) and in microchannels (St. John et al, 1998).

DISCUSSION

In Fig. 4, we see that the imaged velocity profiles for electrokinetic flow are in good agreement with Eq. (4). The flow is a combination of electroosmosis and electrophoresis, and the theory outlined above shows that both components yield a flat profile. Figure 5, however, shows significant deviations from a flat profile. This flow suggests a velocity profile similar to that observed in a pressure-driven flow.

In the following sections, we explore two mechanisms that potentially explain this observed departure from plug-like flow: variations in viscosity due to temperature gradients, and induced pressure gradients caused by a non-uniform wall potential (i.e. non-uniform wax coating in the case of Fig. 5).

Variation of viscosity

In this section, we examine the possibility that heat generation within the capillary could cause the electrophoretic velocity profile to deviate from plug-like. To this end, we investigate the temperature, viscosity and corresponding velocity distributions across the capillary.

In cylindrical coordinates, we write the temperature governing equation for our system as:

$$-\frac{1}{r} \frac{d}{dr} \left(kr \frac{dT}{dr} \right) = S = \frac{E_x^2}{\rho} \quad (6)$$

The source term, S , has units of power per unit volume. In this analysis, we assume ρ remains a constant (or at least not a strong function of temperature) based on the experimentally determined fluid-filled capillary resistance and capillary dimensions. This empirically determined resistivity agrees closely with those tabulated in the literature (Masliyah 1994). Integrating twice and applying the boundary conditions of finite temperature at the centerline and a constant wall temperature of T_o , we obtain the temperature distribution

$$T(r) = \frac{E_x^2 r_o^2}{\rho 4k} \left(1 - \frac{r^2}{r_o^2} \right) + T_o \quad (7)$$

As an initial approximation, we assume that the fluid within our capillary has the same thermal properties and viscosity as water. As such, we have chosen to model the viscosity as a function of temperature,

$$\frac{\mu(T)}{\mu_o} = \exp \left[a + b \left(\frac{T_o}{T} \right) + c \left(\frac{T_o}{T} \right)^2 \right] \quad (8)$$

with $T_o = 293.15\text{K}$ and the constants given by $a = -1.94$, $b = -4.80$, and $c = 6.74$, as suggested by Reid (1987).

In order to relate the temperature-dependent viscosity to the electrophoretic velocity profile within the capillary, we return to our analysis of electrophoresis. Utilizing Eq. (5) and neglecting the temperature dependence of ϵ , ζ , or E_x , we arrive at:

$$U(T) = \frac{\epsilon \zeta_{EP} E_x}{\mu(T)} \quad (9)$$

The predicted velocity profiles for both an open capillary and a DBwax-coated capillary each show an expected radial velocity variation of less than 0.2% (Fig. 6). The radial velocity distribution is parabolic in nature, but its magnitude is too small to explain the dye profiles seen in Fig. 5. To obtain a significant radial variation in the electrophoretic velocity, one would need to increase the field strength or the buffer concentration considerably. Our temperature variation model and, hence these conclusions, are in close agreement with those presented by Grushka, et al. (1989).

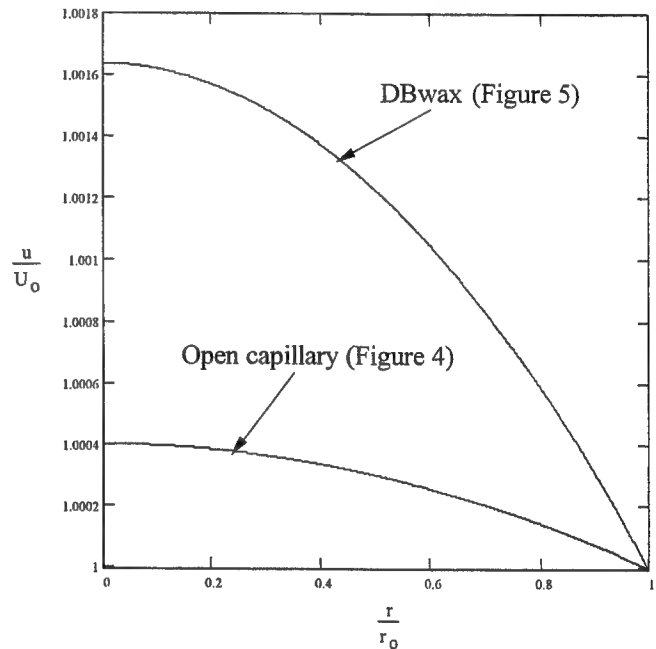


Figure 6. Electrophoretic velocity distribution for an open capillary and a DBwax-coated capillary

From this analysis, we conclude that the viscosity and, therefore, velocity do not vary significantly across the capillary for the prescribed small-bore capillary parameters, buffer concentrations, and field strengths. Therefore, Joule heating induced velocity variation does not appear to be a feasible mechanism for the observed deviations from plug-like flow.

Induced Pressure Gradients

In deriving Eq.(4), the pressure gradient term was neglected because there were no *externally* applied pressure gradients. However, this expression will not be correct if the electrokinetic transport *induces* a pressure gradient. We now explore how the electrokinetic flow could potentially induce

pressure gradients. If we take the divergence of Eq. (3), and apply continuity for the fluid, $(\nabla \cdot \mathbf{u})=0$, we derive the following expression.

$$\nabla^2 P = \mathbf{E} \cdot \nabla \rho_E + (\nabla \cdot \mathbf{E}) \rho_E \quad (10)$$

Equation (10) demonstrates how the pressure field evolves from gradients in the charge density and applied field. Referring to Eq. (2), we see that the first term on the right hand side of Eq. (10) will be non-zero if the wall potential changes in the axial direction. Nonuniformities in the wall potential could exist due to contamination in the capillary, variations in wall coatings, or gradients in the buffer pH. Using classical techniques for solving Poisson's equation (e.g. Green's functions), it should be possible to develop a general solution to Eq. (10) for an arbitrary zeta potential distribution along the wall of a cylindrical capillary. In this paper, a direct method will be used to solve for the pressure field in a capillary with a wall potential as shown in Fig. 7.

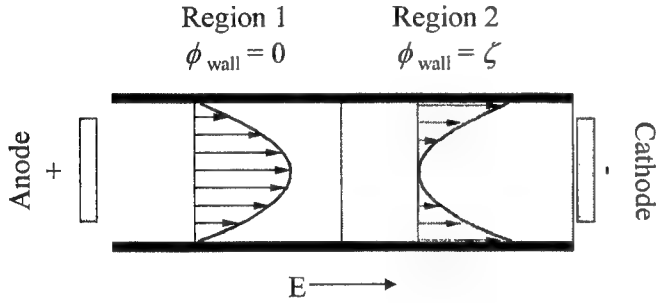


Figure 7. Schematic of capillary with step change in wall potential. The anticipated velocity profiles are also shown.

Let us assume that the fluid velocity is only a function of radial position in both Region 1 and Region 2 shown in Fig. 7. Note that Region 1 describes a section of the capillary with zero wall potential; whereas, Region 2 has a finite wall potential. In other words, we will assume that axial velocity gradients are confined to a vanishingly small region near the discontinuity in wall potential. With this assumption, the volumetric flow rates in regions one and two are shown below.

$$\begin{aligned} Q_1 &= \left(-\frac{\partial P}{\partial x} \right) \frac{\pi r_o^4}{8\mu} \\ Q_2 &= \left(-\frac{\partial P}{\partial x} \right) \frac{\pi r_o^4}{8\mu} + \frac{\varepsilon \zeta E_x}{\mu} \pi r_o^2 \end{aligned} \quad (11)$$

We consider the case where the pressure at either end of the

capillary is a known reference value (i.e. atmospheric pressure). For an incompressible liquid, the volumetric flow rates must be the same in regions 1 and 2. Furthermore, we know that the pressure is continuous and piecewise linear since we assumed that the velocity profile does not vary axially in either region (i.e. the pressure gradient must be constant in both regions). Therefore, we arrive at the following expression for the pressure in the capillary, where x is the axial position and x_o is the axial location of the discontinuity in wall potential.

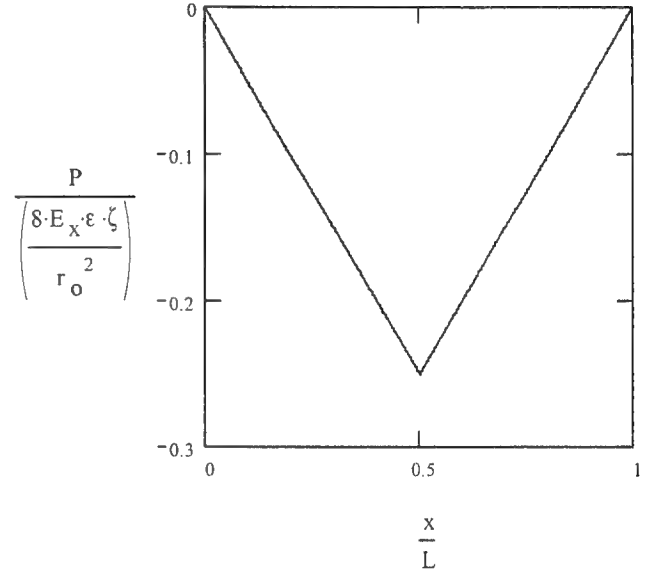


Figure 8. Non-dimensional pressure in a capillary with a step change in wall potential.

$$P(x) = \frac{8E_x \varepsilon \zeta}{r_o^2} \begin{cases} -\frac{x}{L}(L - x_o), & x < x_o \\ -\frac{x_o}{L}(L - x), & x \geq x_o \end{cases} \quad (12)$$

The pressure field corresponding to Fig. 7 is plotted in Fig. 8. We see that the pressure gradient is constant in each section and acts to ensure that the mass flow rates are equal in each region. Figure 9 shows the predicted velocity profiles in regions 1 and 2. The velocity in the first section is due to pressure alone, since the wall potential there is zero. The velocity profile in the second section is simply a superposition of the flat electroosmotic profile and the Poiseuille profile due to the induced pressure gradient. The pressure gradient in each region is readily calculated from Eq. (12). The velocity profiles in Fig. 9 were also shown schematically in Fig. 7.

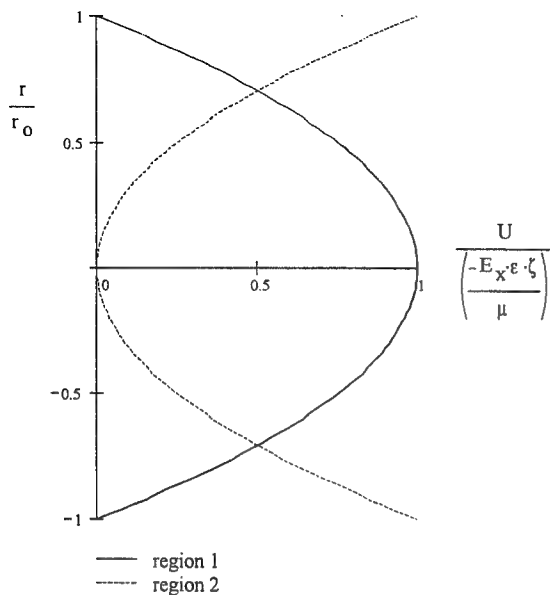


Figure 9. Radial velocity profiles in region 1 and region 2.

To understand the solution qualitatively, one can imagine that the electroosmotic flow in Region 2 “pulls” the flow in Region 1. In other words, the electroosmotic movement of liquid in Region 2 tends to create suction at the interface between the two regions. Hence, the pressure drops at the interface until the mass flow rates in each region are equal. Note that the pressure-driven component subtracts from the electroosmotic flow in Region 2 while only pressure-driven flow is present in Region 1. The analytically calculated velocity profiles also agree qualitatively with the numerical simulation shown in Fig. 10 (MEMCAD, 1998). The simulation confirms that axial gradients in the velocity field are confined to a region less than a single diameter from the wall potential discontinuity.

Superpositions of Eq. (12) can be used to find the pressure field caused by one or many small regions of zero wall potential. This is then a model of a “dirty” silica capillary. Figure 11 demonstrates the nondimensional pressure field in a capillary with three “dirty” regions, each covering 1% of the capillary’s length.

Note that the pressure gradients in the clean regions are identical and that the localized discontinuities in wall potential *perturb the flow everywhere*. Equation (12) can also be superposed to find the pressure field in a coated capillary (zero wall potential) with small “clean” regions where the wall

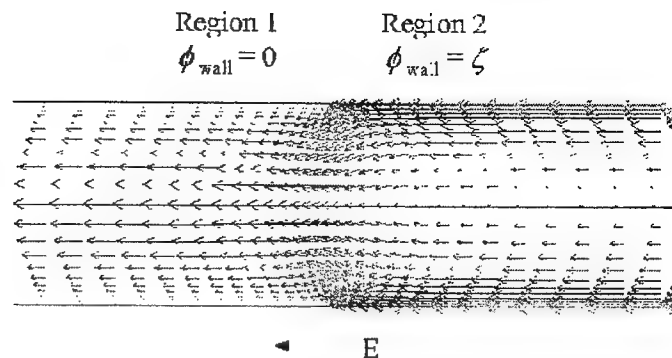


Figure 10. Simulation of flow in a capillary with a step change in wall potential.

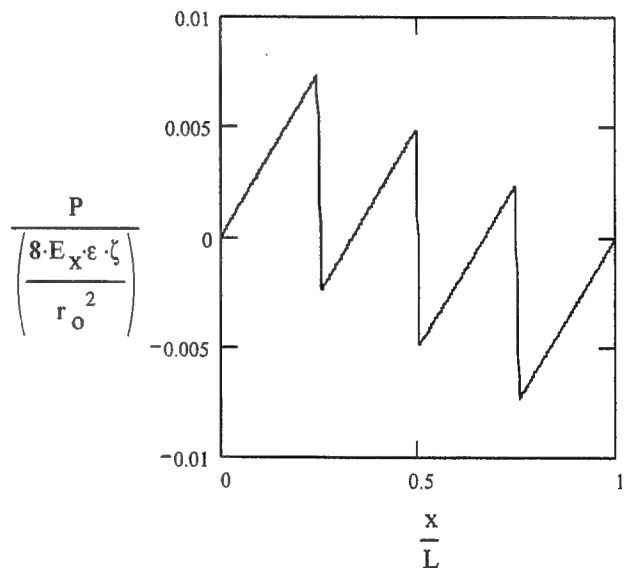


Figure 11. Nondimensional pressure field in a capillary with three “dirty” spots

potential is non-zero. Figure 12 shows the resulting velocity profile in the coated regions, for various amounts of exposed (uncoated) capillary. The induced pressure gradient model presents a rational explanation of the flow imaged in Fig. 5, as it admits a parabolic profile for reasonable variations in wall potential.

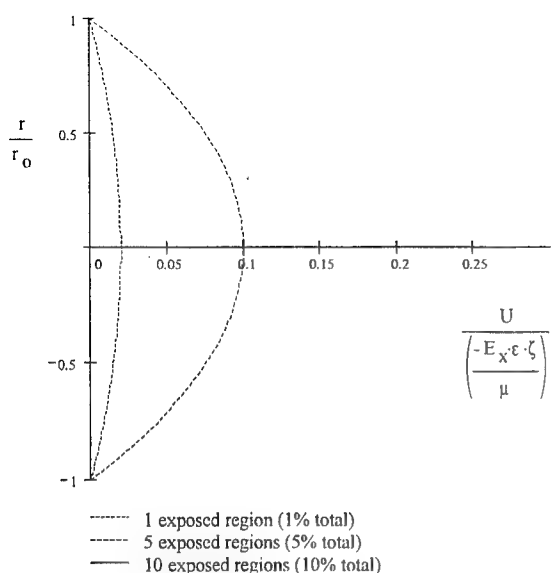


Figure 12. Velocity profile in a coated region of a wax coated capillary with small regions uncoated. The wax coating acts to prevent electroosmotic flow.

CONCLUSIONS

We have imaged pressure-driven and electrokinetically-driven flows in silicone microchannels and silica capillaries using a powerful caged fluorescence technique. The pressure-driven flows agree with theory and numerical simulations. Simple theory predicts that the electrokinetic flows should display uniform (plug-like) velocity profiles. However, in some cases, we observe large parabolic-like components to the electrokinetic velocity profiles.

We explored two mechanisms in an attempt to explain the observed velocity profiles: viscosity variations and induced pressure gradients. We have demonstrated that Joule heating and the subsequent temperature and viscosity gradients do not adequately explain the observed parabolic velocity profile, but that induced pressure gradients are a possible explanation. An important consequence of the induced pressure gradient analysis is that *small regions of non-uniform wall potential create pressure gradients everywhere in the flow*. This conclusion has important implications for those wishing to build lab-on-a-chip devices, since pressure gradients tend to increase the dispersion of sample packets in the flow. We are currently performing experiments that investigate the proposed induced pressure gradient mechanism.

ACKNOWLEDGEMENTS

This work was funded in part by DARPA Composite CAD (Grant no. F30602-96-0306), the National Science Foundation, and Stanford University. The authors would also like to acknowledge assistance from Stanford Professors Juan Santiago and Joel Ferziger.

REFERENCES

1. Burgreen, D., Nakache, F.R., 1964, "Electrokinetic Flow in Ultrafine Capillary Slits." *The Journal of Physical Chemistry*, Vol. 68, No. 5, pp. 1084-1091
2. Effenhauser, C. S., Bruin, G. J. M, Paulus, A., and Ehrat, M., 1997, "Integrated capillary electrophoresis on flexible silicone microdevices: Analysis of DNA restriction fragments and detection of single DNA molecules on microchips," *Anal. Chem.*, Vol. 69, p. 3451.
3. Grushka, E., McCormick, R. M., and Kirkland, J. J., 1989, "Effects of temperature gradients on the efficiency of capillary zone electrophoresis separations," *Anal. Chem.* Vol. 61, p. 241
4. Mala, G. M., Li, D., Dale, J. D., 1996, "Heat transfer and fluid flow in microchannels," *American Society for Mechanical Engineers*, Vol. 59, p.127
5. Manz, A., Effenhauser, C. S., Burggraf, N., Harrison, D. J., Seller, K., and Flurl, K., 1994, "Electroosmotic pumping and electrophoretic separations for miniaturized chemical analysis systems", *J. Micromech. Microeng.*, Vol. 4, p. 257
6. Masliyah, J. H. 1994. *Electrokinetic Transport Phenomena*, Aastra Technical Publications, Alberta.
7. *MEMCAD v4.0*, Microcosm Technologies, Inc. (www.memcad.com) (1998).
8. Paul, P.H., Garguilo, M.G. and Rakestraw, D.J., 1998 "Imaging of Pressure- and Electrokinetically-Driven Flows Through Open Capillaries," *Anal. Chem.*, Vol. 70, pp. 2459-2467.
9. Probstein, R.F., 1994 *Physiochemical Hydrodynamics: An Introduction*. 2nd ed., Wiley and Sons, Inc., New York.
10. Qui, X. C., Hu, L., Masliyah, J. H., and Harrison, D. J., 1997, "Understanding fluid mechanics within electrokinetically pumped microfluidic chips", 1997 *International Conference on Solid-State Sensors and Actuators*, Chicago, IL.
11. Rice, C.L., Whitehead, R., 1965, "Electokinetic Flow in a Narrow Cylindrical Capillary," *The Journal of Physical Chemistry*, Vol. 69, No. 11, pp. 4017-4023.
12. Reid, R.C., Prausnitz, J.M., and Sherwood, T.K., 1987, *The Properties of Gases and Liquids*, 4th ed., McGraw-Hill, New York.
13. St. John, P. M., Deshpande, M., Molho J. I., Garguilo, M. G., et al, 1998, "Metrology and Simulation of Chemical Transport in Microchannels," 1998 *Solid-State Sensor and Actuator Workshop*, Hilton Head Island, SC., pp. 106-111.

CAD Analysis of PCR Well Containment

Manish Deshpande[†], Ken B. Greiner[†], Bart F. Romanowicz[†], John R. Gilbert[†]
Pamela M. St John[‡], Timothy Woudenberg[‡]

[†]Microcosm Technologies, 215 First Street #219, Cambridge, MA 02142, manish@memcad.com

[‡]Perkin-Elmer, Applied Biosystems, 850 Lincoln Center Drive Foster City, CA 94404

Abstract

Design analysis of PCR (Polymerase Chain Reaction) microwells are conducted to observe the contamination between neighboring wells on a PCR chip during the reaction. Thermal effects are incorporated to represent the temperature cycling characteristic of PCR. The analyses are intended to be predictive – and to be applied in the design of high throughput PCR devices. Parametric analyses were conducted to observe the effect of the allowable geometry variations on the contamination of the neighboring wells, and the effect of the variation in the diffusivities of the constituent chemical components. The analyses help in developing a set of curves that can be used to develop a model to represent the behavior of the PCR well. This model can then be implemented in system models for the entire device.

Introduction

There is a wide interest in micron-scale integrated chemical/biochemical analysis or synthesis systems, also referred to as lab-on-a-chip [1-3]. On-chip analysis systems consist of active and passive components. Examples of the former are reaction chambers, switching joints etc., whereas the latter include transport and separation channels. The behavior of these components is generally dependent on a number of parameters, including flow conditions and fluid properties. Researchers are forced to use costly trial-and-error experimental methods to understand and design such microfluidic systems.

CAD analyses, on the other hand, can be a valuable aid in the design of microfluidic systems. Numerical analyses provide significant insight into the fluid mechanics in these systems. They also allow the extraction of material and flow properties that are generally not well documented. Such tools help the designer to explore a much larger space of designs than is easily available from experiment, and do so in a quantitative way which enables the extraction of key parameters for improved or optimal operation of common microchemical system components. Finally numerical analyses enable the extraction of component models for each individual component in a system model of the device.

Several researchers have reported CAD-based analyses of microfluidic components [4-6]. These include components used in injection, transport, as well as mixing and reactions. These authors [7-8] have also reported coupled experimental and numerical analyses for various microfluidic components. The component models can be employed in understanding the behavior of the entire device as a system. The value of the system model in understanding the performance of the system is dependent on the ability of the component models in representing the important physics in the component.

An example of a microfluidic device is shown in Fig. 1. The device is designed for high throughput polymerase chain reactions (μ PCR). The primary components in this device are the microwells and the interconnects between neighboring wells and to the device loading site. The devices are operated by cycling the temperature to control the PCR reaction. The behavior of the device is characterized by the ability of the wells to contain the sample during the reaction with no leakage into the neighboring wells. The containment is affected significantly by the geometry of the interconnects between the wells and the effect of the temperature cycling on the diffusivity of the sample. Good design of the interconnects aims to minimize the contamination of neighboring wells during the reaction.

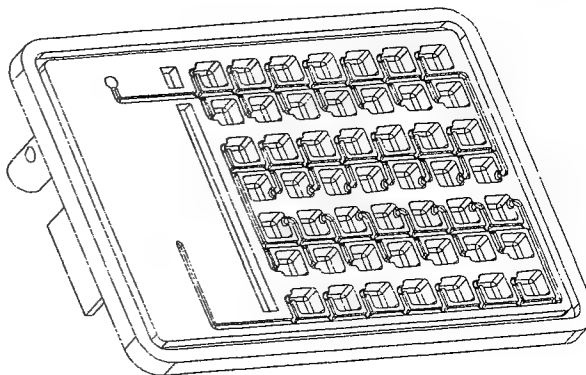


Figure 1: Geometry of Current PCR Chip

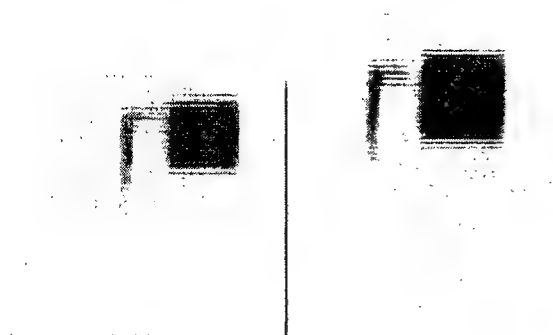


Figure 2: PCR Microwell Configurations – Diagonal (left) and Side-by-side (right)

In general, the entire space of design parameters is fairly difficult to analyze experimentally. Numerical methods on the other hand are a viable mechanism – and are the focus of this paper.

We present here a numerical analysis of the PCR wells during the reaction. The effect of the temperature cycling on the diffusivity is considered in the analysis. The effect of varying the cross sectional area of the interconnects is also presented to demonstrate the potential of numerical methods to effectively analyze the design space for these problems. Finally, we will discuss a mechanism of developing a system model for the device.

Device Geometry

The geometry of the current plastic PCR chip is shown in Figure 1. It consists of an array of 49, 1-microliter wells. The nearest neighbor periodicity in the well layout can have two configurations on the chip, as shown in Figure 2: side-by-side (left) or across the diagonal (right). A possibility for a higher density design may consist of an array of 1024 100 nanoliter wells fabricated from silicon using photolithography and an anodically bonded pyrex glass cover to seal the wells. As in the chip in Figure 1, the wells need to be connected to a microchannel running the length of the chip and column and connecting, via a cross channel, to an inlet port.

The PCR chip shown in figure 1 is loaded with different reagents by drying them down in each well using a dispensing robot [9]. The back is then sealed using a polymer tape and the wells are evacuated and then loaded with sample via the inlet port. The device is temperature cycled on a modified research instrument built for real time detection of the μ PCR reaction. Details of the temperature cycling are shown Fig. 3. At the outset the system is at room temperature (30 °C). The temperature is then raised uniformly at 4 °C/sec from room temperature to 95 °C and held for 10 seconds. It is then lowered at the same rate to 60

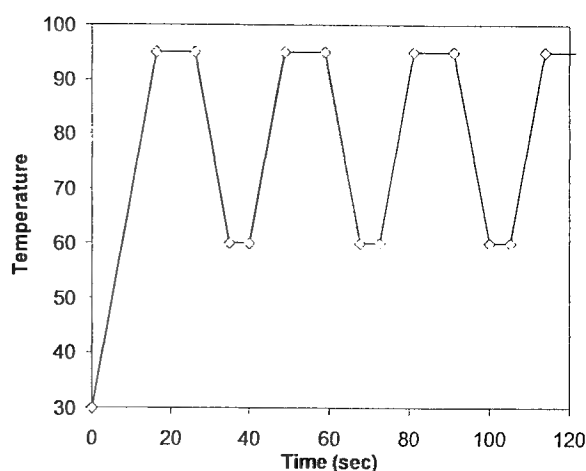


Fig. 3: Temperature Cycling in μ PCR wells.

°C and held for 5 seconds. The process then repeats for a total reaction time of 20 minutes. Note that the cycling shown in Fig. 3 repeats for the specified time. Cycling times, in general, are specific for a given device material, volume of sample, and reagent., The times used here are characteristic for microwells and were used in the simulation.

Numerical Analysis

Predictive CAD analyses for the PCR well configurations were conducted to observe the effect of the temperature cycling on the containment of the sample within the well. The leakage into the nearest neighbor well was also analyzed in the process. The different allowable configurations are also studied as part of the analysis. The numerical analyses were conducted using FlumeCAD. FlumeCAD is an integrated design environment consisting of 3D design, modeling and simulation software tools which enable the creation of complex microfluidic devices. Netflow, which is a part of the suite, is specific to the analysis of chemical transport in microchannels. It is an ongoing program, and is a result of a collaboration between Microcosm, Perkin-Elmer Corp. and Stanford University.

The numerical solution of the above equations is performed using a three-dimensional finite element based CFD engine. The Stokes-Einstein formulation was used to determine the diffusivity variation with temperature. Over the cycle used here the diffusivity varies by a factor of about 3. The FlumeCAD interface allows the user to define the geometry from layout and process, or, from a model built in the solid modeler module. Once meshed, the model is available to a suite of solvers for various physical domains, and to the simulation manager to parametrize the dependency in any domain.

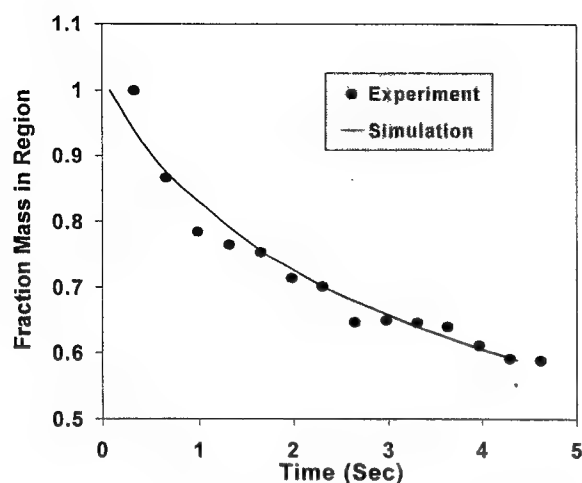


Figure 4: Comparison of Experiment and Simulation for Integrated Mass Leakage out of region.

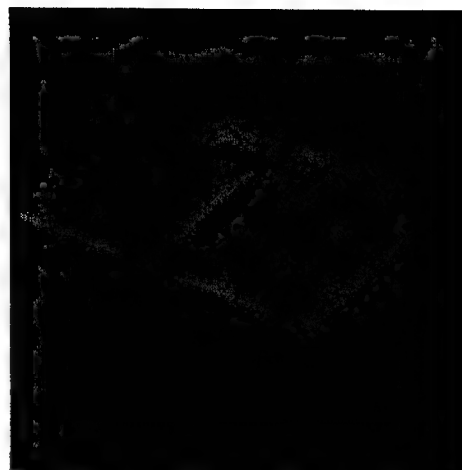


Fig 5: Solid Model of PCR Wells.

Results

Results for the PCR well analysis are discussed in this section. Initially validation of the numerical model is presented, followed by analysis of the different well configurations. Simulations were performed both at ambient temperatures as well as with temperature cycling to compare the difference in containment with temperature cycling in the analysis.

A range of diffusivities is present in the experiment, corresponding to both reactants and products. The lowest diffusivity is $5 \times 10^{-7} \text{ cm}^2/\text{s}$, whereas the highest is $1 \times 10^{-5} \text{ cm}^2/\text{s}$ corresponding to the short chain probe. In the simulations we analyzed diffusivities over this range to ascertain the effect of the various components on the containment in the microwells.

Experimental Validation: To validate our methods, diffusivity experiments were conducted in microchannels to observe the leakage of dye out of a narrow region. The experiments were conducted using fluorescein dye in a straight section of a microchannel (not shown). The comparison between the experiment and simulation, is shown in Fig. 4, and was conducted by digitizing the images and integrating the normalized intensity over a specific region – the integrated intensity corresponds to the amount of dye in the specific region. The agreement between experiment and simulation is good over the entire time sequence, as shown in the figure. This formulation was used to predict the extent of containment during PCR.

PCR Well Simulations: The PCR containment analysis is conducted using the dimensions from the next generation designs. For the purposes of the simulation, detailed analyses were conducted on a reduced configuration,

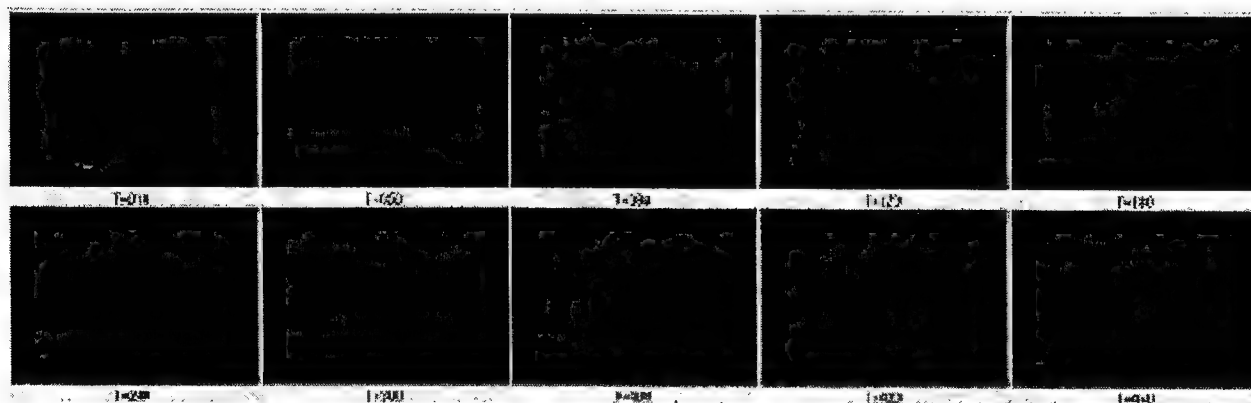


Fig. 6: Species Concentration of Dye in Containment Wells over time. Time increments are in minutes.

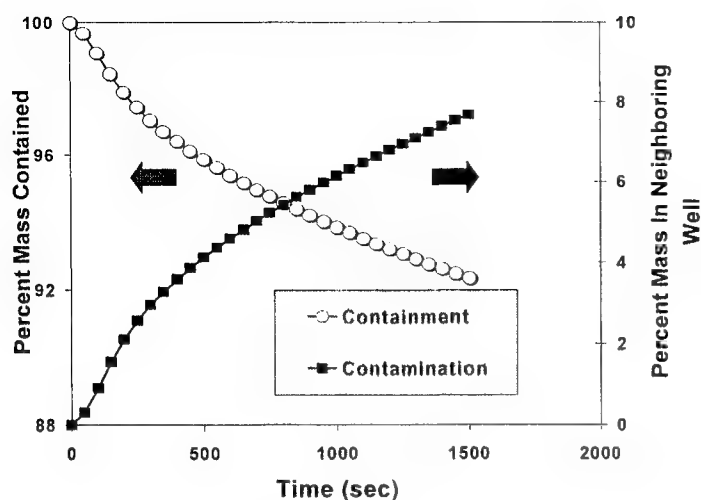


Figure 7: Containment in well during reaction and contamination of Neighboring well.

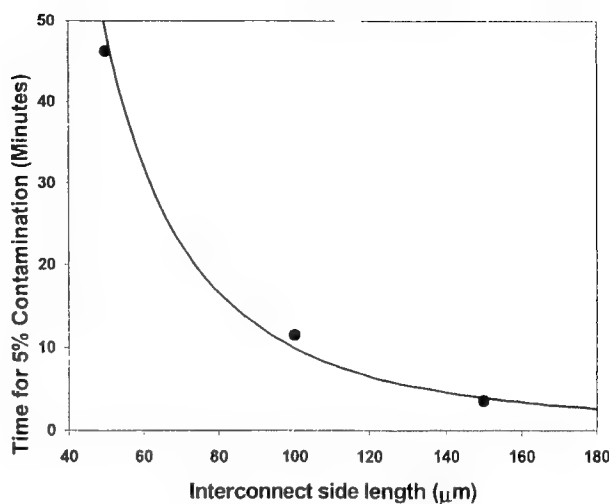


Figure 9: Contamination time as a function of interconnect side length.

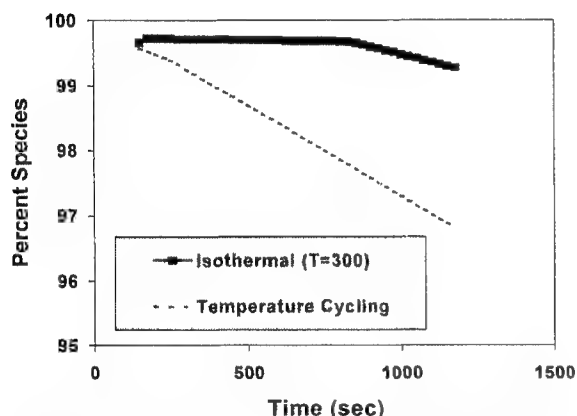


Fig 8: Leakage rate from PCR well with and without temperature cycling

consisting of two nearest neighbor wells. The solid model for this configuration is shown in Fig. 5. This model is adequate to analyze the effects of the temperature cycling and the diffusivity on the containment/contamination characteristics of the design geometry. The problem also becomes considerably more tractable.

Figure 6 shows a simulated timed series of diffusion of material out of a microwell and along an interconnect. The region inside the well is detected during the PCR reaction and therefore, any material which diffuses out of the well in Figure 6 is insignificant providing the material does not diffuse into the neighboring well. Initially, the reactant travels out of the well quickly as it establishes a concentration gradient along the channel. At later times, the solution moves much slower as it diffuses down the channel. Time sequences in the figure are shown for a typical PCR experiment – when allowed to run longer, the species

concentrations were predicted to equalize in the two wells in about 8 hours (not shown). The species concentration contained in the well over time is shown in Figure 7. The concentration entering the neighboring well is also shown in the figure. These curves were computed using a Region-of-Interest (ROI) integration over the wells after the computation. The ROI integral is then analogous to the collected signal in a detection system for the well. A curve such as Fig. 7 is an important asset in the design of these devices since it indicates the allowable reaction times that prevent contamination of reagents (and therefore the reaction) between neighboring wells.

The effect of incorporating the temperature cycling is shown in Figure 8. The leakage rate from the chamber is compared with the results of the simulation at constant temperature. The diffusion constant in the isothermal case was taken to be constant at the room temperature value. A different constant temperature value would yield a shift in the leakage rate, but would still be inaccurate in comparison to the variable temperature results. As the figure shows the temperature cycling and the correspondingly higher diffusivity has a dramatic effect in increasing the leakage rate from the reaction chamber. This figure also serves to highlight the importance of including the relevant physical processes into the computation since the presence of the temperature cycle significantly alters the design analysis for the problem.

Effect of interconnect geometry: The cross sectional area of the interconnect can also have a significant effect on the contamination time between the wells. Computations were conducted using the Simulation Manager in FlumeCAD to analyze the effect of the allowable variations in the design. Results are presented in Fig. 9, showing the contamination time for the different configurations. The contamination time

here was defined as the amount of time required for 5 percent of the species in the first well to enter the neighboring well. As the figure shows, for the highest (150 μm) case, contamination occurs well within the specified reaction time. For a side length of 100 μm as well, contamination occurs at approximately 10.5 minutes, which is within the reaction time. For a 70 μm side length, however, the contamination time increases to over 22 minutes, implying that it is a more appropriate choice for the interconnect cross sectional dimension.

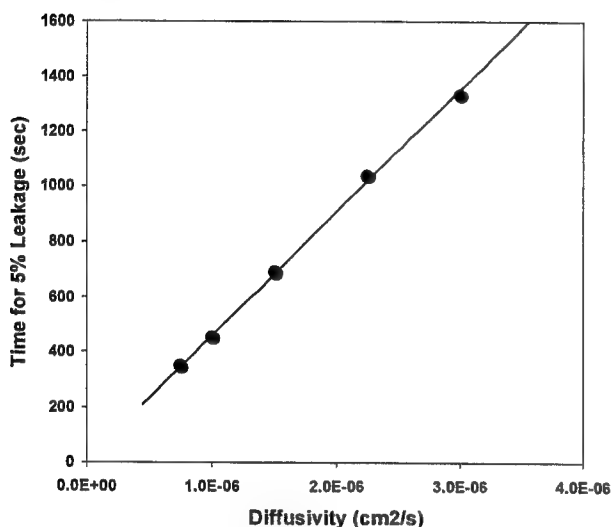


Figure 10: Contamination time as a function of diffusivity.

Effect of Diffusivity: In the course of the PCR reaction the diffusivities observed for the sample, enzyme and product mixture range from about $5\text{e-}7$ cm^2/s to about $1\text{e-}5$ cm^2/s . The rate of contamination is strongly dependent on the diffusivity. However a full reaction analysis for PCR is computationally intensive – and is not entirely required for design analysis. We demonstrate this here, by studying the effect of the diffusivity on the contamination. In general the contamination times lie between that for the highest and the lowest diffusivity – the design can then be tailored for an appropriate specification. The contamination time has a linear dependence on the diffusivity as seen in Figure 10 – appropriate leakage rates for specific diffusivities can then be extracted from this curve.

Curves such as Figures 7-10 describe the behavior of the PCR wells as a component in the overall PCR system. This behavior can be used to develop an appropriate reduced-order model for the wells – this model can be implemented in a system model for the PCR system. The implementation of the system model is the focus of our current research.

Conclusions

Detailed analyses of PCR well configurations were conducted to predict the contamination between neighboring wells during a conventional PCR cycle. Temperature dependent effects from the thermal cycling were incorporated using appropriate diffusion models. The contamination time was computed as the time required for 5 percent sample travel between neighboring wells. The effects of the cross sectional geometry as well as the diffusion constants of the various components in the mixture were analyzed through simulation. The parametric results yielded curves that describe the contamination between wells in terms of the various parameters that affect it. These curves can then be applied in developing optimal designs for the wells, as well as in the development of a model describing the behavior of the PCR well as a function of the various parameters affecting it. This model can then be implemented in a system model for the entire device, and is the focus of our current work.

Acknowledgements

This work was funded by DARPA Composite CAD (Grant no. F30602-96-0306), under the Netflow Program.

References:

- [1] D.J. Harrison, et al, *Science*, **261** (1993) 895-897.
- [2] Luc Bousse, Bob Dubrow and Kathi Ulfelder, *u-TAS '98*, 271.
- [3] N. Chiem and D.J. Harrison, *Anal. Chem.*, **69** (1997), 373.
- [4] X. C. Qui, L. Hu, J. H. Masliyah, and D. J. Harrison, *Solid-State Sensors and Actuators*, Chicago, IL (1997).
- [5] N. A. Patankar and H. H. Hu, *Anal. Chem.*, **70**, (1998).1870-81.
- [6] Sergey V. Ermakov, S.C. Jacobson, and J.M. Ramsey, *u-TAS '98*, 149.
- [7] P.M. St. John, et al, *Solid State Sensors and Actuators Workshop*, Hilton Head, SC (1998).
- [8] M. Deshpande, et al, MEMS '99, Orlando, FL.
- [9] M. Albin, et al, *Solid State Sensor and Actuator Workshop*, 2 June (1996).

ANALYSIS OF MULTICOMPONENT SAMPLE TRANSPORT IN ELECTROKINETIC MICROCHEMICAL SYSTEMS

Manish Deshpande, Ken B. Greiner and John R. Gilbert

Microcosm Technologies, 215 First Street, Cambridge, MA 02142

Phone: (617) 225-0094 Fax: (617) 621-7838 Email: manish@memcad.com

Luc Bousse, Andrea Chow and Anne R. Kopf-Sill

Caliper Technologies, 605 Fairchild Drive, Mountain View, CA 94043

ABSTRACT

Experimental and numerical analyses of multicomponent sample transport are presented in this paper. A novel approach to confining samples of varying electrophoretic mobilities during transport is demonstrated, that uses a plug of high conductivity salt to reduce the local field and thus the local electrophoretic transport. This plug confined transport (PCT) mechanism prevents the separation of analyte mixtures during transport. Experimental measurements and simulation results are presented that show good agreement.

INTRODUCTION

Electrokinetic microfluidic microsystems are powerful analytical tools for many applications, such as nucleic acid analysis, enzyme assays, and immunoassays [1-5]. Such systems have gained considerable importance as components in micron-scale integrated chemical/biochemical analysis or synthesis systems, also referred to as lab-on-a-chip. The basic "unit process" operations in these systems are sample injection, mixing, chemical reaction or modification, separation, and detection. Assembling a system of many "unit process" nodes requires one or more transport mechanisms to move sample and reagents through the "wires" of the system. Many of these systems rely on electrokinetic physics as their transport mechanism, although pressure and pneumatic applications have also been demonstrated. Complicated relationships exist between the microchannel geometries, the conditions under which the devices operate, and the behavior of the multi-component fluids transported in these channels. In the past researchers have been forced to use costly trial and error methods to understand and design such microfluidic systems.

CAD tools can be a valuable aid in the design of microfluidic systems. Numerical analyses provide significant insight into the fluid mechanics in these systems. They allow the extraction of material and flow properties that are generally not well documented, or that vary from application to application or from one manufacturing technology to another. Furthermore such tools help the designer to explore a much larger space of designs than is easily available from

experiment, and do so in a quantitative way which enables the extraction of key parameters for improved or optimal operation of common microchemical system components.

Several researchers have reported CAD-based analyses of microfluidic components [6-9]. These include components used in injection [6-7], transport [8-9], as well as mixing and reactions. These analyses are 2D steady-state analyses with fixed field boundary conditions. Additionally the numerical analyses were conducted for a single species – furthermore the species was assumed not to affect the physical or electrical properties of the carrier during transport. We have developed new tools to enable the removal of these constraints on the numerical analyses. We have presented results for transient field boundary conditions showing a switched injector in a previous paper [10]. In this paper, we extend this work to analyze multicomponent mixtures, comprising of species with varying electrophoretic mobilities. We will also discuss the treatment of high conductivity samples, where the sample conductivity significantly affects the field within the carrier.

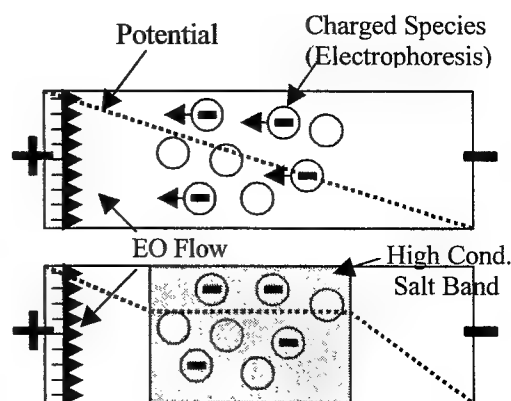


Figure 1 : Schematic of Plug Confined Transport Flow.

Although electrokinetic fluid transport has many significant advantages such as allowing simultaneous control of many wells, it has the potential disadvantage of unwanted separation of components during transport. In this paper we demonstrate a novel approach to confining samples of varying



Figure 2 : On-chip analysis system showing network of interconnected channels.

electrophoretic mobilities during transport, by using a plug of high conductivity salt to reduce the local field and thus the local electrophoretic transport. This plug confined transport (PCT) mechanism prevents separation of the analyte mixtures in circumstances where it is desired to keep all components together, independent of charge. Both experimental and modeling data will be shown to illustrate this concept.

OBJECTIVE

There are two motivations for this research in multicomponent transport. First, is to aid in the development of microchemical components that require mixing or dilution during electrokinetic transport. Second, is to aid in the development of plug confined transport (PCT) systems that use a high conductivity salt plug to transport several analytes of different electrophoretic mobility. This novel approach has been developed at Caliper to prevent the broadening of analyte mixtures during transport between specific sites. A schematic of the operation of PCT is shown in Figure 1. The plug locally increases the conductivity of the medium and therefore reduces the field strength. The reduced field decreases the electrophoretic velocity of the species within the plug, which in turn slows the migration and separation of each species, confining the mixed species band within the plug and reducing its broadening.

EXPERIMENTAL SETUP AND MEASUREMENTS

Figure 2 shows a typical glass microchip used in the validating experiments. Measurements were conducted in a straight section approximately 30 mm in length. The high conductivity salt plug consists of a 90 mM HEPES buffer with 21mM NaCl at a pH of 7. The carrier is a 10 mM HEPES buffer also at a pH of 7. Fluorescein and Rhodamine were used as the markers to observe the motion of the analytes within the high

salt. There is a guard band of high conductivity salt with no dye around the high conductivity salt with dye. Both the rhodamine and the fluorescein are carried along with the electroosmotic flow of the carrier. In addition, the fluorescein also experiences electrophoretic flow due to its charge. The electrophoretic flow is in the opposite direction to the electroosmotic flow.

The fluorescent signal from the dyes is collected at three discrete locations along the channel – 1.1 mm, 13.6 mm and 25.8 mm from the plug creation point.

NUMERICAL FORMULATION

The basic equations describing the fluid motion are the Navier-Stokes equations with appropriate electromigratory flux terms to represent the effect of the applied electric field on the carrier (electroosmosis) and/or the charged species (electrophoresis). The modeling of electrokinetic effects is incorporated into the FlumeCAD system. FlumeCAD is an integrated design environment consisting of 3D design, modeling and simulation software tools, which enable the creation and analysis of complex microfluidic devices. Inherent in the design flow implemented in FlumeCAD is the ability to translate from a layout and process view of the device to a solid model and to continue to a 3D device model allowing simulations that characterize the various physical phenomena present in the device. The numerical solution uses a finite element engine as the back-end solver for the analyses.

RESULTS

In this section both experimental and numerical results are presented. We begin by presenting results for sample mixing and dilution to demonstrate the modeling of multicomponent physics. Results are then presented for separation of two components under electrophoresis – followed finally by the plug confined transport problem – both experimental and numerical results are presented and compared with each other. The effect of the guard band is then analyzed to demonstrate its efficiency in confining the band during transport.

Mixing: The simplest mixing component is a Y shaped channel as shown in Figure 3. This component can be used for mixing two analytes brought in from each arm of the Y – it can also be used for diluting an analyte brought in from one arm with pure carrier. Figure 3 shows experimental images for the latter case for electroosmotic flow of a neutral marker dye (Rhodamine). Control of the field between the inlet ports allows the varying the fraction of the analyte in the downstream mixture – and consequently the dilution of the analyte. Corresponding simulations for

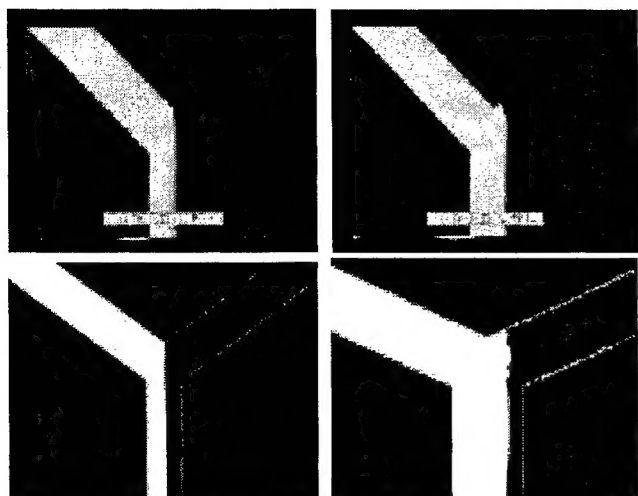


Figure 3 : Experimental (top) and Simulation (bottom) images of Mixing of Analyte and Diluent in Y-channel.

similar cases are also presented in Fig. 4 – showing the computed mass fraction of the analyte. The experiments and simulations show good qualitative agreement with each other, as the figure indicates.

Separation: The separation of two components under the applied field is a special case of the plug confined transport problem – with no high conductivity salt band. Fluorescein and rhodamine were used as the marker dyes in the experiment. Both dyes are transported by the electroosmotic flow in the carrier – in addition, fluorescein, which is charged, also experiences electrophoretic flow. As a result the two species separate. Experimental and simulation results are compared in Figure 4 at two locations along the channel – 1.1 mm and 13.6 mm from the injection point. The simulations demonstrate good agreement with the experimental measurement – both in the position of the band as well as its width. The total integral under the band is not very well predicted,

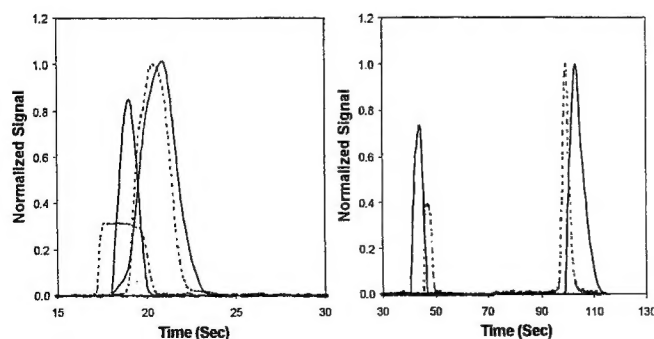


Figure 4: Experimental and Numerical Measurements for Separation of two species (Rhodamine and Fluorescein) . The dashed lines are experiment and solid are simulations.

especially for the rhodamine – this is probably a result of the distortions in the optical system from point to point. The good agreement gives us confidence in our ability to predict the combined electrokinetic transport of several analytes – consequently we now turn to the analysis of plug confined transport (PCT).

Plug confined transport (PCT): Results for the PCT problem are shown in Figures 5-7. Experiments were conducted in similar conditions to those discussed above – however the analyte is now confined in a high concentration salt plug with a conductivity seven times higher than the carrier. The computed potential field along the channel is shown in Figure 5 at different instances in time. The species mass fraction of the high conductivity salt plug is also shown in the figure, along the secondary axis. The presence of the high conductivity salt strongly affects the field as the figure shows – in the region of the plug the field is considerably reduced. This region of low field travels downstream along with the plug. The electrophoresis of the charged species, which is dependent on the local field, is therefore significantly reduced – thus preventing electrophoretic migration of the charged bands out of the plug. Diffusion, however, still exists and is then the primary migration mechanism of the analyte out of the confining band. The guard bands around the sample region act as a diffusion barrier to stop immediate loss of sample. Once the analyte leaks out of the guard band into a region of high field, the overall analyte band broadening increases dramatically through electrophoresis.

The simulated concentrations of fluorescein and rhodamine at one position along the channel are shown in Figure 6. The figure shows a slice plane through the channel at three points in time as the species migrate down the channel. The concentrations at a location 13.6 mm from the injection point are shown in Figure 7 and compared with experimental measurements at the same

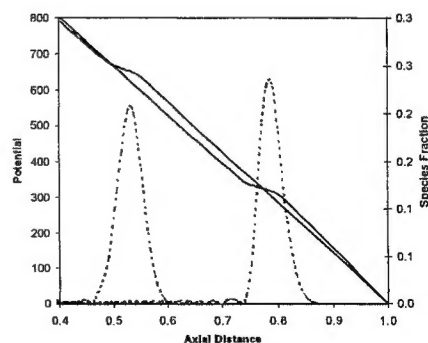


Figure 5: Potential Field and Species position along channel for 7:1 Conductivity

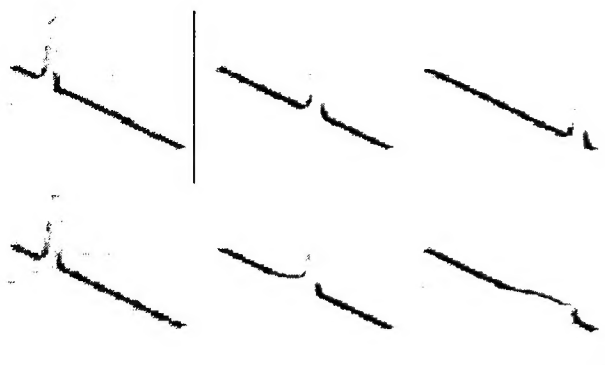


Figure 6: Band Positions of Rhodamine (top) and Fluorescein (bottom) during plug confined transport through channel. Images are at discrete time intervals.

location. The qualitative agreement between experiment and simulation is quite good – the simulations predict the separation of the rhodamine and fluorescein peaks, and the formation of a second trailing fluorescein peak due to the fraction that diffuses out of the edge of the plug and is therefore slowed further by electrophoresis. The effect of the high conductivity salt can be clearly seen by comparing Figs. 4 and 7 for the cases with and without the salt plug at the detection location 13.6 mm away from the injection point. In the case without the high conductivity salt plug the two dyes show considerable separation, with the fluorescein arriving almost 40 seconds after the rhodamine. In contrast, for the plug confined case, both peaks arrive almost simultaneously, showing minimal separation.

CONCLUSIONS

Experimental and numerical analyses of multicomponent sample transport are presented in this paper. The mixing of a sample analyte and pure carrier in a Y-shaped mixer is presented – varying the field in the inlet arms of the mixer can control the dilution of the sample with the carrier. Separation analyses of two components – fluorescein and rhodamine are also presented under both electrophoresis and electroosmosis. The negatively charged fluorescein has a longer time of flight than the neutral rhodamine. Numerical analyses agree quite well with experiment both for position and width of the sample peaks.

A novel approach to confining the samples during transport is studied. This mechanism, plug confined transport (PCT), uses a plug of high conductivity salt to transport analytes of differing electrophoretic mobility. The high conductivity salt reduces the local field and thus the local electrophoretic transport – thus preventing the analytes from separating. This mechanism can be applied in transporting the analytes without separation. Experimental and numerical results presented here agree fairly well in the position of the

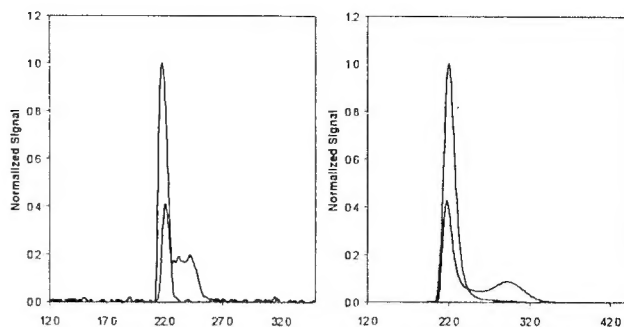


Figure 7: Experiment (left) and Simulation for 7:1 Conductivity Ratio.

components as well as in the eventual diffusion and electrophoresis of the chemicals out of the plug region.

ACKNOWLEDGEMENTS

This work was funded by DARPA ETO, Composite CAD, under the NetFlow (F30602-96-2-0306) and FlumeCAD (F30602-98-2-0151) Programs.

REFERENCES

- [1] D.J. Harrison, et al, "Micromachining a miniaturized capillary electrophoresis-based chemical analysis system on a chip," *Science*, **261** (1993) 895-897.
- [2] S.C. Jacobson, R. Hergenroder, L.B. Koutny, R.J. Warmack and J.M. Ramsey, "Effects of Injection Schemes and Column Geometry on the Performance of Microchip Electrophoresis Devices," *Anal. Chem.*, **66**(1994), 1107.
- [3] Luc Bousse, Bob Dubrow and Kathi Ulfelder, "High Performance DNA Separations in Microchip Electrophoresis Systems," *u-TAS '98*, 271.
- [4] A.T. Woolley and R.A. Mathies, "Ultra High Speed DNA Sequencing using capillary electrophoresis chips," *Anal. Chem.*, **65** (1995), 3676.
- [5] N. Chiem and D.J. Harrison, "Microchip based capillary electrophoresis for immunoassays," *Anal. Chem.*, **69** (1997), 373.
- [6] X. C. Qui, L. Hu, J. H. Masliyah, and D. J. Harrison, "Understanding fluid mechanics within electrokinetically pumped microfluidic chips", *1997 International Conference on Solid-State Sensors and Actuators*, Chicago, IL (1997).
- [7] P.M. St. John, et al, "Metrology and Simulation of Chemical Transport in Microchannels", *Solid State Sensors and Actuators Workshop*, Hilton Head, SC (1998).
- [8] N. A. Patankar and H. H. Hu, "Numerical Simulation of Electroosmotic Flow", *Anal. Chem.*, **70**, (1998), 1870-81.
- [9] Sergey V. Ermakov, S.C. Jacobson, and J.M. Ramsey, "Computer Simulations for Microchip Electrophoresis," *u-TAS '98*, 149.
- [10] M. Deshpande, K. Greiner, J.R. Gilbert, L. Bousse and A. Minalla, "Optimization of Sample Injection Components in Electrokinetic Microfluidic Systems," *Proc. MEMS '99*, Orlando, FL (1999).

***MISSION
OF
AFRL/INFORMATION DIRECTORATE (IF)***

*The advancement and application of Information Systems Science
and Technology to meet Air Force unique requirements for
Information Dominance and its transition to aerospace systems to
meet Air Force needs.*